

University of Crete
Department of Chemistry
Division of Environmental Chemistry



Doctoral Thesis

**Spatial variability of atmospheric pollutants in the
Greater Athens Area using remote sensing techniques**

Myrto Gratsea
M.Sc Environmental Physics

Supervising Professor
Nikos Mihalopoulos

Heraklion, 2022

Advisory & Examination Committee:

1. Nikos Mihalopoulos
Professor, University of Crete

2. Evangelos Gerasopoulos
Research Director, National Observatory of Athens

3. Stelios Kazadzis
Senior researcher, World Radiation Center

4. Andreas Richter
P.D., University of Bremen

5. Mihalis Vrekoussis
Professor, University of Bremen

6. Maria Kanakidou
Professor, University of Crete

7. Spyros Pergantis
Professor, University of Crete

CURRICULUM VITAE

CURRENT POSITION **2008-present**, Research Associate / National Observatory of Athens / Greece

PREVIOUS POSITIONS **2006-2008**, Sales Support / Attica Telecommunications S.A. / Greece
2001-2006, Sales Support / Data Communication Systems Ltd / Greece

ACADEMIC STUDIES **2014-2022**, PhD in Atmospheric Sciences / University of Crete, Chemistry Department / Greece

2011-2013, M.Sc in Environmental Physics / National and Kapodestrian University of Athens, Physics Department / Greece

2003-2009, BSc in Physics / Hellenic Open University, Science and Technology Department / Greece

LANGUAGE KNOWLEDGE **Greek**, mother tongue

English, fluent
First Certificate of Cambridge

French
D.E.L.F. 2nd degree
Certificat de langue Francaise

EXPERIMENTAL EXPERIENCE ◦ Aerosol and trace gase measurements using the MAX-DOAS technique/instrument
◦ Light absorption and scattering measurements using photometers and nephelometers
◦ Particle size distribution measurements using Aerodynamic Particle Sizer (APS)
◦ Ozone measurements using conventional analysers
◦ Irradiance and columnar ozone measurements using Microtops

COMPUTER SKILLS ◦ MATLAB, numeric computing environment and programming language
◦ SCIATRAN, radiative transfer model
◦ LibRadtran, radiative transfer model

**PARTICIPATION
IN RESEARCH
PROJECTS**

- MEDGOLD, Turning climate-related information into added value for traditional Mediterranean Grape, Olive and Durum wheat food systems, Horizon 2020, Research Associate: Investigation and statistical analysis of climatic and meteorological data and trends for the study of climate change impact in agriculture
- MAX3D, ESF-Human Resources Development, Education and Lifelong Learning 2014-2020, Three-dimensional distribution of nitrogen dioxide in the urban environment of Athens, using the MAX-DOAS passive remote sensing technique, Research Associate: Measurements performance, statistical analysis, synergies between air quality data and publication of the results in conferences and journals
- URBANPROOF, Climate Proofing Urban Municipalities, LIFE15 CCA/CY/000086, Research Associate: Investigation and statistical analysis of climatic and meteorological data and trends for the study of climate change impact on urban areas
- ADAPT2CLIMA, Adaptation to Climate change Impacts on the Mediterranean islands' Agriculture, LIFE10 CCA/GR/000928, Research Associate: Investigation and statistical analysis of climatic and meteorological data and trends for the study of climate change impact in agriculture
- EMISSION, Environmental monitoring integrated system using an IoT network, Research Associate: Measurements performance and statistical analysis of air quality data
- ARISTOTELIS, Excellence Research Program GSRT (2015-2017) "Environment, Space and Geodynamics/Seismology 2015-2017", Research Associate: aerosol optical properties analysis and investigation of their impact on solar radiation
- KRIPIS-THESPIA I, National Strategic Reference Framework, Developmental proposals for research Institutes, 2014-2015, Research Associate: Development and application of statistical method for the separation of the anthropogenic and the natural component of suspended particles
- CHARADMExp, Characterization of Aerosol mixtures of Dust and Marine origin, 2014, Role: Ground base actinometric measurements
- XENIOS, Climate change impacts on the touristic development of sensitive areas in the Greek territory. Case study: Messinia-Integrated Tourism Areas, 2011-2013, Research Associate: in situ aerosol measurements and data process
- CITYZEN, megaCITY - Zoom for the ENvironment, FP7 - Collaborative Project, Small or medium-scale focused research project, ENV.2007.1.1.2.1. Megacities and regional hot-spots air quality and climate, 2008-2011, Research Associate: Databases creation and maintenance, time series analyses
- ACI-UV, Aerosol and Cloud Influence on global surface UV irradiance retrieved from satellite sensors, 2010-2013, Research Associate: Satellite and ground based data process, algorithm development
- THERMOPOLIS 2009 Campaign, European Space Agency (ESA), 2009-2010. Study of "urban heat island" phenomenon in Athens, Research Associate: Ground baseD actinometric measurements

SCIENTIFIC PUBLICATIONS

- ‘Five years of spatially resolved ground-based MAX-DOAS measurements of nitrogen dioxide in the urban area of Athens, synergies with in situ measurements and model simulations’
M. Gratsea, E. Athanasopoulou, A. Kakouri, A. Richter, A. Seyler, E. Gerasopoulos
Atmosphere, 12, 1634, doi:10.3390/atmos12121634, 2021
- ‘An improved TROPOMI tropospheric NO₂ research product over Europe’
S. Liu, P. Valks, G. Pinardi, J. Xu, K.L. Chan, A. Argyrouli, R. Lutz, S. Beirle, E. Khorsandi, F. Baier, V. Huijnen, A. Bais, S. Donner, S. Dorner, M. Gratsea, F. Hendrick, D. Karagiozidis, K. Lange, A.J.M. PETERS, J. Remmers, A. Richter, M. Van Roozendaal, T. Wagner, M. Wenig, D.G. Loyola
Atmospheric Measurement Techniques, 14, 7297-7327, 2021, doi:10.5194/amt-14-7297-2021
- ‘Evaluation of the LOTOS-EUROS NO₂ simulations using ground-based measurements and S5P/TROPOMI observations over Greece’
I. Skoulidou, M.E. Koukouli, A. Manders, A. Segers, D. Karagiozidis, M. Gratsea, D. Balis, A. Bais, E. Gerasopoulos, T. Stavrakou, J. van Geffen, H. Eskes, A. Richter
Atmospheric Chemistry and Physics, 21, 5269–5288, 2021, doi: 10.5194/acp-21-5269-2021
- ‘Retrieval and evaluation of tropospheric aerosol extinction profiles using MAX-DOAS measurements over Athens, Greece’
M. Gratsea, T. Bösch, P. Kokkalis, A. Richter, M. Vrekoussis, S. Kazadzis, A. Tsekeri, A. Papayannis, M. Mylonaki, V. Amiridis, N. Mihalopoulos, E. Gerasopoulos
Atmospheric Measurement Techniques, 14, 749-767, 2021, doi:10.5194/amt-14-749-2021
- ‘Ground-based validation of the Copernicus Sentinel-5p TROPOMI NO₂ measurements with the NDACC ZSL-DOAS, MAX-DOAS and Pandora global networks’
T. Verhoelst, S. Compernelle, G. Pinardi, J.C. Lambert, H.J. Eskes, K.U. Eichmann, A.M. Fjæraa, J. Granville, S. Niemeijer, A. Cede, M. Tiefengraber, F. Hendrick, A. Pazmiño, A. Bais, A. Bazureau, K.F. Boersma, K. Bogner, A. Dehn, S. Donner, A. Elokhov, M. Gebetsberger, F. Goutail, M. Grutter de la Mora, A. Gruzdev, M. Gratsea, G.H. Hansen, H. Irie, N. Jepsen, Y. Kanaya, D. Karagiozidis, R. Kivi, K. Kreher, P.F. Levelt, C. Liu, M. Müller, M. Navarro Comas, A.J.M. PETERS, J.P. Pommereau, T. Portafaix, O. Puentedura, R. Querel, J. Remmers, A. Richter, J. Rimmer, C. Rivera Cárdenas, L. Saavedra de Miguel, V.P. Sinyakov, K. Strong, M. Van Roozendaal, J.P. Veefkind, T. Wagner, F. Wittrock, M. Yela González, C. Zehner
Atmospheric Measurement Techniques, 14, 481-510, 2021, doi:10.5194/amt-14-481-2021
- ‘Adverse results of the economic crisis: A study on the emergence of enhanced formaldehyde (HCHO) levels seen from satellites over Greek urban cities’
I. Zyrichidou, D. Balis, M.E. Koukouli, T. Drosoglou, A. Bais, M. Gratsea, E. Gerasopoulos, N. Liora, A. Poupkou, C. Giannaros, D. Melas, I. De Smedt, M. Van Roozendaal, R.J. Van der A, K.F. Boersma, P. Valks, A. Richter
Atmospheric Research, 224, 42-51, 2019, doi:10.1016/j.atmosres.2019.03.017
- ‘GARLiC and LIRIC: Strengths and limitations for the characterization of dust and marine particles along with their mixtures’
A. Tsekeri, A. Lopatin, V. Amiridis, E. Marinou, J. Igloffstein, N. Siomos, S. Solomos, P. Kokkalis, R. Engelmann, H. Baars, M. Gratsea, P. Raptis, I. Biniotoglou, N. Mihalopoulos, N. Kalivitis, G. Kouvarakis, N. Bartsotas, G. Kallos, S. Basart, D. Schuettemeyer, U. Wandinger, A. Ansmann, A. Chaikovsky, O. Dubovik
Atmospheric Measurement Techniques, 10(12), 4995-5016, 2017, doi:10.5194/amt-10-4995-2017

- ‘The combined effect of reduced fossil fuel consumption and increasing biomass combustion on Athens’ air quality, as inferred from long term CO measurements’
M. Gratsea, E. Liakakou, N. Mihalopoulos, A. Adamopoulos, E. Tsilibari, E. Gerasopoulos
 Science of the Total Environment, 592, 115-123, 2017, doi:10.1016/j.scitoenv.2017.03.045

 - ‘Slant Column MAX-DOAS measurements of nitrogen dioxide, formaldehyde, glyoxal and oxygen dimer in the urban environment of Athens’
M. Gratsea, M. Vrekoussis, A. Richter, F. Wittrock, A. Schönhardt, J. Burrows, S. Kazadzis, N. Mihalopoulos, E. Gerasopoulos
 Atmospheric Environment, Volume 135, 118-131, 2016, doi: 10.1016/j.atmosenv.2016.03.048

 - ‘Fire risk, atmospheric chemistry and radiative forcing assessment of wildfires in eastern Mediterranean’
 E. Athanasopoulou, D. Rieger, C. Walter, H. Vogel, A. Karali, M. Hatzaki, E. Gerasopoulos, B. Vogel, C. Giannakopoulos, M. Gratsea, A. Roussos
 Atmospheric Environment, Volume 95, 113-125, 2014,
<https://doi.org/10.1016/j.atmosenv.2014.05.077>
-

CONFERENCE PUBLICATIONS

- ‘An improved TROPOMI Tropospheric NO₂ Research Product over Europe’
 ESA Atmospheric Science Conference 2021 (22-26 November 2021, online)
 P. Valks, S. Liu, S. Seo, G. Pinardi, J. Xu, K.L. Chan, A. Argyrouli, R. Lutz, S. Beirle, E. Khorsanidi, F. Baier, V. Huijnen, A. Bais, S. Donner, S. Dorner, M. Gratsea, F. Hendrick, D. Karagkiozidis, K. Lange, A.J.M. PETERS, J. Remmers, A. Richter, M. Van Roozendaal, T. Wagner, M. Wenig, D.G. Loyola

- ‘Long-term MAX-DOAS NO₂ measurements over Athens and association with urban sources’
 15th International Conference on Meteorology, Climatology and Atmospheric Physics (26-29 September 2021, Ioannina, Greece)
 M. Gratsea, E. Athanasopoulou, A. Kakouri, A. Richter, A. Seyler, E. Gerasopoulos

- ‘Evaluation of the LOTOS-EUROS NO₂ simulations using ground-based measurements and S5P/TROPOMI observations over Greece’
 15th International Conference on Meteorology, Climatology and Atmospheric Physics (26-29 September 2021, Ioannina, Greece)
 I. Skoulidou, M.E. Koukouli, A. Manders, A. Segers, D. Karagkiozidis, M. Gratsea, D. Balis, A. Bais, E. Gerasopoulos, A. Richter, T. Stavrakou, J. van Geffen, H. Eskes

- ‘Return period analysis to assess the long-term impact of climate change on olive sector in Andalusia, Spain - results from the Med-Gold project’
 European Geosciences Union General Assembly 2021 (19-30 April 2021, online)
 M. Gratsea, K.V. Varotsos, J. Lopez-Nevedo, S. Lopez-Feria, C. Giannakopoulos

- ‘Using NDACC MAX-DOAS Central Processing System data for TROPOMI NO₂ and HCHO column validation: first results’
 9th DOAS Workshop (13-15 July 2020, Utrecht, Netherlands)
 M.M. Friedrich, F. Hendrick, G. Pinardi, C. Fayt, M. Van Roozendaal, A. Bais, S. Beirle, T. Bösch, S. Casadio, P. Castracane, A. Dehn, S. Donner, U. Friess, M. Gratsea, D. Karagkiozidis, K. Kreher, K. Lnge,

M. Navarrop-Comas, A. Piters, R. Querel, J. Remmers, A. Richter, J.L. Tirpitz, T. Wagner, M. Yela

- ‘Mediterranean agro-climate projections and the case of olives in Andalusia: results from the MED-GOLD project’

European Meteorological Society Annual Meeting (9-13 September 2019, Copenhagen, Denmark)

K. Varotsos, C. Giannakopoulos, M. Gratsea, V. Tenentes

- ‘Climatological analysis of extreme precipitation in five European countries: Results from the TRIBUTE project measurements’

16th Plinius Conference on Mediterranean Risks (9-11 October 2018, Montpellier, France)

K. Varotsos, C. Giannakopoulos, M. Gratsea, V. Tenentes, I. Keramitsoglou, C. Kiranoudis

- ‘Evaluation of various bias correction methods for Mediterranean agro-climate projections: first results from the Med-Gold project’

MedCLIVAR 2018 Conference (17-21 September, Belgrade, Serbia)

C. Giannakopoulos, K. Varotsos, A. Karali, M. Gratsea

- ‘LIFE UrbanProof: current and future climate trends in Mediterranean cities’

14th International Conference on Meteorology, Climatology and Atmospheric Physics (15-17 October 2018, Alexandroupolis, Greece)

C. Giannakopoulos, K. Varotsos, A. Karali, G. Lemesios, M. Gratsea, V. Tenentes

- ‘Retrieval of aerosol vertical profiles over Athens using MAX-DOAS measurements’

11th International Conference on Air Quality – Science and Application (12-16 March 2018, Barcelona, Spain)

M. Gratsea, T. Bösch, P. Kokkalis, A. Richter, M. Vrekoussis, S. Kazadzis, A. Papayannis, V. Amiridis, N. Mihalopoulos, E. Gerasopoulos

- ‘Validation and Verification of S5P NO₂, using ground-based, airborne and satellite data’

Atmospheric Composition Validation and Evolution workshop, ESA (18-20 October 2016, Rome, Italy)

A. Richter, F. Wittrock, E. Peters, A. Schönhardt, A. Meier, M. Ostendorf, H. Bovensmann, J.P. Burrows, M. Vrekoussis, S. Schreier, M. Gratsea, E. Gerasopoulos

- ‘An overview of biomass burning impacts on Athens air quality and analysis of its increasing significance’

13th International Conference on Meteorology, Climatology and Atmospheric Physics (19-21 September 2016, Thessaloniki, Greece)

E. Gerasopoulos, M. Gratsea, E. Liakakou, M. Lianou, B. Psiloglou, N. Kappos, H. Kambezidis, N. Mihalopoulos

- ‘Impact of biomass combustion on the urban air quality of Athens’

10th International Conference on Air Quality – Science and Application (14-18 March 2016, Milan, Italy)

M. Gratsea, E. Gerasopoulos, E. Liakakou, N. Mihalopoulos

- ‘MAX-DOAS observation of CHOCHO, HCHO and NO₂ over Nairobi and Athens’

DPG Spring meeting (March 2015, Heidelberg, Germany)

L. Alvarado, A. Richter, E. Peters, F. Wittrock, J.P. Burrows, M. Vrekoussis, M. Gratsea, E. Gerasopoulos

- ‘Spatial and temporal variability of NO₂ in Athens observed by MAX-DOAS’
NORS/NDACC/GAW workshop (5-7 November 2014, Brussels, Belgium)
A. Richter, M. Gratsea, F. Wittrock, J.P. Burrows, M. Vrekoussis, E. Gerasopoulos

- ‘NO₂ measurements over Athens using the MAX-DOAS technique’
12th International Conference on Meteorology, Climatology and Atmospheric Physics (28-31 May 2014, Heraklion, Greece)
M. Gratsea, M. Vrekoussis, F. Wittrock, A. Schonhardt, A. Richter, E. Gerasopoulos

- ‘A method for calculating O₁D and NO₂ photolysis frequencies using satellite based UV solar radiation retrievals’
12th International Conference on Meteorology, Climatology and Atmospheric Physics (28-31 May 2014, Heraklion, Greece)
I.P. Raptis, S. Kazadzis, B. Bohn, N. Mihalopoulos, M. Gratsea, H. Berresheim, F. Rohrer, M. Ada

- ‘Spatial and temporal variability of NO₂ in Athens observed by MAX-DOAS’
European Geosciences Union General Assembly 2014 (27 April-2 May 2014, Vienna, Austria)
A. Richter, M. Gratsea, F. Wittrock, J.P. Burrows, M. Vrekoussis, E. Gerasopoulos

- MAX-DOAS observation of HCHO and CHOCHO over Athens and Nairobi’
European Geosciences Union General Assembly 2014 (27 April-2 May 2014, Vienna, Austria)
L. Alvarado, A. Richter, E. Peters, F. Wittrock, J.P. Burrows, M. Vrekoussis, M. Gratsea, E. Gerasopoulos

- ‘1.5 Year AOD Observations at Navarino Environmental Observatory (NEO), in Messinia – Southern Greece (Eastern Mediterranean)’
European Geosciences Union General Assembly 2013 (7-12 April 2013, Vienna, Austria)
E. Gerasopoulos, M. Gratsea, V. Amiridis, C. Zerefos, M.O. Andreae

- ‘Aerosol observations and predictions in the southeastern Europe during the extreme summer 2007’
2-7 September 2012 European Aerosol Conference, EAC (2-7 September 2012, Granada, Spain)
E. Athanasopoulou, E. Gerasopoulos, H. Vogel, M. Gratsea, B. Vogel, S. Kazatzis and E. Liakakou

- ‘Optical properties of aerosols over Athens, Greece, and their relation to chemical composition’
11th International Conference on Meteorology, Climatology and Atmospheric Physics (29 May-1 June 2012, Athens, Greece)
D. Paraskevopoulou, E. Gerasopoulos, E. Liakakou, M. Gratsea, P. Zampas, C. Theodosi, N. Mihalopoulos

- ‘ACEMED experimental campaign over Greece for the evaluation of CALIPSO’s aerosol classification scheme’
11th International Conference on Meteorology, Climatology and Atmospheric Physics (29 May-1 June 2012, Athens, Greece)
V. Amiridis, E. Marinou, S. Kazadzis, E. Gerasopoulos, P. Kokkalis, R.E. Mamouri, A. Papayannis, N. Kouremeti, E. Giannakaki, E. Liakakou, D. Paraskevopoulou, M. Gratsea, K. Allahverdi, G. Kouvarakis, D. Balis, A. Bais, N. Mihalopoulos, I. Daglis, & C. Zerefos

- 'Dust impact on urban air quality'
6th International Workshop on Sand/Duststorms and Associated Dustfall (7-9 September 2011, Athens, Greece)
E. Gerasopoulos, M. Gratsea, S. Kazadzis, V. Amiridis, M. Vrekoussis, E. Liakakou
-

REVIEWING ACTIVITIES

2018-present, Reviewer in 2 International Scientific Journals (Atmospheric Environment, Euro-Mediterranean Journal for Environmental Integration)

Abstract

The adverse health effects of urban air pollution on a large proportion of the world population living in urban environments, along with its impact on the climate, results to continuous, low-cost air monitoring and measurement validations being a necessity. This study is focused on the investigation of the temporal and spatial variation of certain atmospheric pollutants in the greater area of Athens, mainly using ground-based remote sensing techniques and in particular, the differential optical absorption spectroscopy (DOAS) technique. The visible and near-UV molecular absorption bands were used in this study for the DOAS measurements. The atmospheric pollutants that were measured with a Multi-Axis (MAX) DOAS instrument, are: nitrogen dioxide (NO_2), formaldehyde (HCHO) and glyoxal (CHOCHO) and a detailed temporal and spatial distribution of these trace gases is provided; a consistent picture of the daily, weekly and seasonal variations is given. Oxygen dimer (O_4) measurements were also used as input information in a retrieval algorithm for the calculation of the vertical distribution of the aerosol extinction. Lidar and sun-photometer measurements were used for the evaluation of the retrieved profiles. The MAX-DOAS technique proved to be a reliable method for measuring aerosol levels and their vertical distribution in the urban environment of Athens, thus, new perspectives have opened up for assessing urban aerosol pollution on a long term-basis in Athens from continuous and uninterrupted MAX-DOAS measurements. During the present study, the need to investigate the effect of the economic crisis to the air quality of the city has also risen: the increased price of heating oil resulted in an increase of biomass combustion for heating purposes, which in turn has led to severe smog episodes. Therefore, the combined effect of the reduced fossil fuel consumption and the increasing biomass combustion, as inferred from long-term carbon monoxide (CO) measurements and in conjunction with black carbon measurements, was examined. The importance of this study lies on the fact that it quantifies the diachronic changes in air pollution in Athens and associates it with several socioeconomic factors (e.g. measures, economic crisis, behavioural changes), while it can also be considered as a reference in the future for assessing and evaluating expected mitigation measures.

Keywords: ground-based MAX-DOAS, aerosol profiles, urban gaseous pollutants

Contents

1	Introduction	13
1.1	Atmospheric pollution and spatial distribution	13
1.2	Atmospheric pollutants and studies for the Attica basin	14
1.2.1	Topography	14
1.2.2	Measurement studies.....	15
1.2.3	Atmospheric composition studies.....	17
1.3	Purpose and originality of research.....	21
2	Instrumentation and theoretical background	23
2.1	Differential optical absorption spectroscopy (MAX-DOAS).....	23
2.1.1	MAX-DOAS technique	23
2.1.2	Operation principles and fundamental set-up of a MAX-DOAS system.....	26
2.2	Basic concepts of remote sensing	29
2.2.1	AMF - Air Mass Factor	29
2.2.2	Scattering and absorption of electromagnetic radiation	30
2.3	Inverse model and retrieval algorithm	32
2.4	Ancillary measurements	33
2.4.1	Lidar (LIght Detection And Ranging).....	33
2.4.2	Cimel photometer	34
2.4.3	BC - CO measurements.....	35
3	Slant column MAX-DOAS measurements of nitrogen dioxide, formaldehyde, glyoxal and oxygen dimer in the urban environment of Athens	37
3.1	Introduction	40
3.2	Data and methodology	42
3.2.1	Site description.....	42
3.2.2	Instrumentation and data retrieval.....	42
3.3	Results and discussion	45
3.3.1	Data presentation and basic statistical analysis.....	45
3.3.2	Seasonal variability.....	48
3.3.3	Cloud screening	51
3.3.4	Diurnal variation and weekend effect	52
3.3.5	Estimation of urban sources contribution.....	56

3.3.6 Impact of local circulation patterns	58
3.4 Summary and conclusions	59
4 Retrieval and evaluation of tropospheric aerosol extinction profiles using MAX-DOAS measurements over Athens, Greece.....	61
4.1 Introduction.....	64
4.2 Methodology.....	66
4.2.1 Location	66
4.2.2 Instrumentation and data retrieval.....	66
4.2.3 BOREAS profile retrieval algorithm	70
4.3 Results and discussion.....	71
4.3.1 Selected case studies.....	71
4.3.2 Aerosol extinction vertical profile retrievals	72
4.3.3 MAX-DOAS aerosol extinction profiles evaluation.....	74
4.3.4 AOD evaluation.....	80
4.4 Summary and conclusions.....	84
5 The combined effect of reduced fossil fuel consumption and increasing biomass combustion on Athens' air quality, as inferred from long term CO measurements.....	86
5.1 Introduction	89
5.2 Methodology	91
5.2.1 Sampling	91
5.2.2 Data analysis.....	92
5.3 Results and discussion	93
5.3.1 Biomass burning episodes identification	93
5.3.2 Contribution of biomass burning to evening CO concentrations.....	97
5.3.3 Comparison of CO measurements: site representativeness.....	99
5.3.4 Analysis of interannual variability	100
5.4 Summary and conclusions	103
6 Conclusions.....	105

Introduction

This study is focused on the investigation of the temporal and spatial distribution of certain atmospheric pollutants in the greater area of Athens, mainly using ground-based remote sensing techniques and more specifically the differential optical absorption spectroscopy (DOAS) technique. This chapter provides a brief overview of the quality and composition of the atmosphere, both globally and on a continental scale, as well as locally, with a focus on urban pollution. The specific characteristics of the Attica basin and the main pollutants on which the specific work is focused are also presented. Finally, the objectives and the originality of the work are mentioned.

1.1 Atmospheric pollution and spatial variability

The quality of the atmosphere on a local scale, close to the surface, is determined by the concentration of air pollutants, which depends on the emission rate, the dispersion and the height of the atmospheric boundary layer. On a larger scale, atmospheric composition represents the state of the global atmosphere, including phenomena such as dust from arid areas, ash from volcanic eruptions and the transport of pollutants over long distances.

Air pollution is a global issue with a strong presence in Europe and the Northern Hemisphere and its impact on the climate and the environment is a new field of atmospheric science research. Seven million deaths are recorded each year worldwide as a result of air pollution (WHO, World Health Organization). Transboundary and intercontinental transport of air pollutants, as well as ozone pollution in the northern hemisphere endanger agriculture, natural ecosystems and have a strong impact on the climate. Examples of intercontinental air pollution transport are dust transport episodes from desert areas of Asia to northwestern America, strongly affecting the energy balance and air quality (Husar et al., 2001), as well as the contribution of Southeast Asia to the arctic haze and to the presence of black carbon (BC) in the Arctic (Koch et al., 2007). Dust from desert areas of northwest Africa has been found even in areas of the Amazon forest (Yu et al., 2015a). In the 1990s, nitrogen dioxide (NO₂) emissions in Asia exceeded those in Europe and America and continue to be higher to this day (Akimoto, 2003). Transport of ozone and its precursors from North America affects the surface ozone in Europe (Guerova et al., 2006) and, accordingly, European pollution increases surface ozone concentrations in North Africa, the Mediterranean and the Near East (Duncan and Bey, 2004). The Mediterranean is considered a crossroad for the transport of air masses from Europe, the Balkans and Africa, where anthropogenic emissions are met with natural ones (dust from the Sahara, biomass combustion) (Kanakidou et al., 2007). Enhanced levels of air pollution have already been recorded in the eastern Mediterranean (Zyrichidou et al., 2009; Kanakidou et al., 2011) and pollutants from America have been found in the free troposphere above the Mediterranean (Lelieveld et al., 2002).

At the urban pollution scale, the first major smog incident, with 4,000 deaths, was recorded in London in 1952. Concentrations of airborne pollutants in urban areas are associated with major cardiorespiratory health problems (e.g. Dimitriou et al., 2013; Beeson et al.; 1998, Dockery et al. 1993). Since 54% of the world population lives in urban environments (WUP, 2014), adverse health effects are an important parameter in the need to study gaseous pollutants. Except from the effects on health, air pollution also contributes to the erosion of buildings and monuments in urban areas, whilst it has a major impact on the climate, enriching the troposphere with greenhouse gases and particulate matter, which thereby affects the energy balance of the atmosphere (e.g. Chubarova et al., 2011). In all megacities (> 10⁷ inhabitants) worldwide, atmospheric measurements record exceedances of the levels set by the World Health Organization (WHO) for gaseous pollutants. More specifically, in terms of NO₂, 5 megacities show exceedances (Los Angeles, Mexico City, Moscow, New York, Sao Paulo) with values up to 2 times higher than those set by the WHO. In terms of particulate matter, exceedances are observed in the majority of the world's megacities, with Beijing having an average annual particulate matter concentration of 400 µg / m³ (Gurjar et al., 2008; Mage et al, 1996). Exposure of urban populations to air pollutants is a priority issue for both European and international conventions (e.g. United Nations Economic Commission for Europe Convention on Long-range Transboundary Air Pollution - CLRTAP, www.unece.org/env/lrtap/), under which specific concentration limits are set. Therefore, the degradation of air quality in urban areas is one of the most important issues to be addressed in megacities and thus, the systematic recording of air pollutants can provide important information about natural and anthropogenic emissions.

1.2 Atmospheric pollutants and studies for the Attica basin

1.2.1 Topography

The levels of gaseous and particulate pollutants in Athens are greatly influenced by the special topography of the city. The Attica basin is surrounded by four mountains: Parnitha (1400 m) to the northwest, Penteli (1100 m) to the northeast, Ymittos (1050 m) to the east and Egaleo (450 m) to the west. The main opening of the basin is to the south, in the Saronic Gulf (Figure 1.1). Under specific meteorological conditions, the special topography of the city favours the accumulation of air pollutants. During pollution episodes, the height of the atmospheric boundary layer (BL) is lower than the average climatic values and the prevailing winds are usually weak, entrapping the pollutants in the basin (Kassomenos et al., 1995). The nocturnal temperature inversion under cloudless conditions during winter, also contributes to the entrapment of pollutants. The main sources of air pollutants in Athens are transportation and industrial emissions, as well as central heating emissions during winter (Lalas et al., 1982). Specifically, 50% of nitrogen oxide emissions and 65% of volatile organic compounds in Athens have been attributed to road traffic (Markakis et al., 2010; Moussiopoulos et al., 1995). The industrial zone to the southwest (Elefsina) and the port of Piraeus to the south of the city centre are also important sources of nitrogen oxides (Kassomenos et al., 1995). Moreover, dust transport episodes from North Africa also contribute to the aerosol load of the city (e.g. Gerasopoulos et al., 2009; Kosmopoulos et al., 2017) and the area of Athens can be considered as an example of

various aerosol types such as dust, local pollution, marine, biomass combustion and their mixtures (Soupiona et al., 2019).

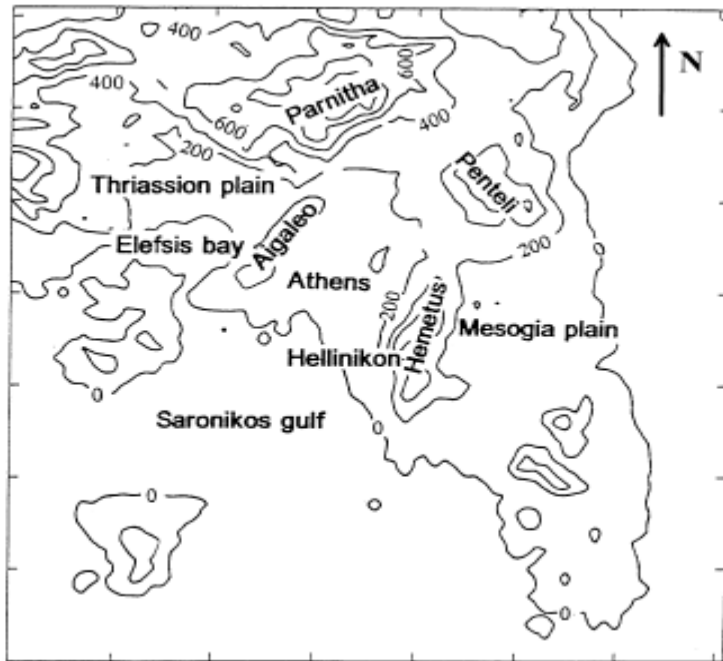


Figure 1.1. Map of Attica (72 x 72 km). Contour lines are by 200 m

1.2.2 Measurement studies

Athens ranks third worst among 25 large European cities in pollution due to increased levels of particulate matter and first in ozone exceedances (Pascal et al., 2013). Long-term particulate matter measurements in Athens have recorded a significant number of exceedances of the limits set by the European Union (Directive 2008/50 / EC) for PM_{10} (e.g. Chaloulakou et al., 2003) (Fig.1.2). Specifically, in-situ measurements have recorded an annual average concentration of $53.6 \mu\text{g}/\text{m}^3$ at a central monitoring station in Athens (Theodosi et al., 2011), exceeding the limit of $50 \mu\text{g}/\text{m}^3$. The corresponding annual mean value for the optical thickness of the suspended particles has been calculated to be 0.23 ± 0.17 (Gerasopoulos et al., 2011). Long-term ozone measurements at suburban stations have recorded the high average value of $120 \mu\text{g}/\text{cm}^3$ during summer months (Kalabokas and Repapis 2004). Anthropogenic emissions related to intensive urbanization, lead to frequent smog events in the city of Athens. From 1980 to this day, several studies have been carried out in Athens focusing on the city's air pollution in order to understand the physical and chemical mechanisms of gaseous pollutants and smog formation. Most of them have been carried out on the basis of in-situ measurements (e.g. Lalas et al., 1983; Barde and Button, 1990; Viras and Siskos, 1992; Ziomas et al., 1998; Kalabokas et al., 1999; Kalabokas and Repapis 2004). More recent studies have used ground-based remote sensing techniques, such as lidar, MFR and active long path DOAS (e.g. Avdikos et al., 2006; Kalabokas et al., 2008; Gerasopoulos et al., 2011; Papayiannis et al., 2012, Psiloglou et al., 2013) or satellite observations (e.g. Retalis et al., 1999; Vrekoussis et al., 2013). There has been a gradual decrease in annual NO_2 concentrations since 1987 (Fig. 1.3) and specifically from 1998 to 2006 the

levels have decreased by 11% (Mavroidis and Chaloulakou, 2011). Changes in the composition of the urban atmosphere of Athens have been observed since 2008, when the economic crisis began. Satellite observations showed a reduction of columnar NO₂ in the troposphere by 30-40% (Vrekoussis et al., 2013), as a result of reduced consumption of fossil fuels for transportation and heating. At the same time, the biomass combustion for heating purposes increased, the incomplete combustion of which enriches the atmosphere with carbon monoxide (CO) and contributes to the creation and accumulation of suspended particles. Prior to the onset of the economic crisis, vehicle emissions were estimated to be the only source of CO, with heating emissions accounting for only 0.01% of total emissions (Viras and Siskos, 1992). The upward trend in the 1980s in terms of CO levels - the average annual concentration had reached 8.5 µg/m³ - was reversed from the early 1990s onwards, due to the replacement of conventional vehicles with catalytic converters, leading to a reduction of 0.5 µg/m³ per year (Viras et al., 1996). The decrease of these levels continued at a slower pace from 2000 to 2008, when the rate of the decrease in the average annual price increased again due to the economic crisis (Vrekoussis et al., 2013).

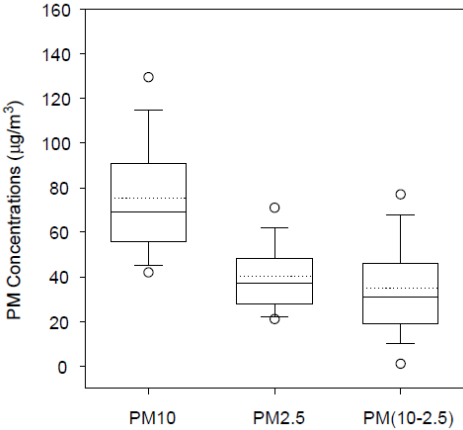


Figure 1.2. PM10, PM2.5 and PM10–2.5 concentration whisker plots (Chaloulakou et al., 2003)

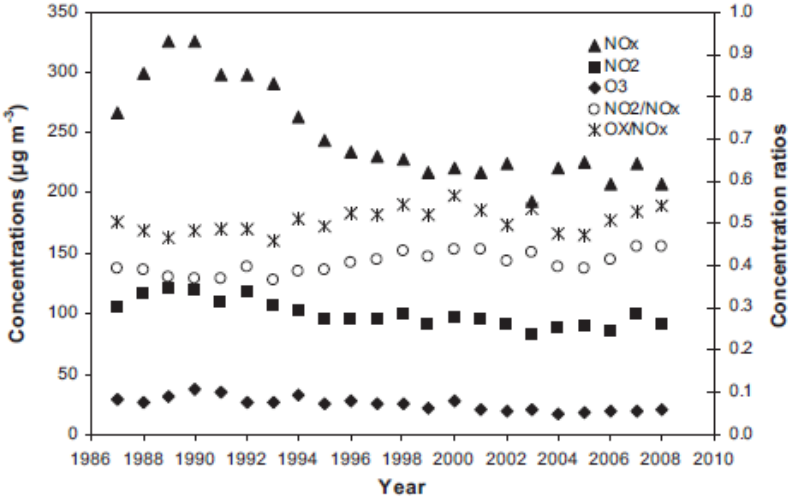


Figure 1.3. Annual mean concentrations for NO_x, NO₂, O₃ at a traffic station in the city centre (Mavroidis and Chaloulakou, 2011)

1.2.3 Atmospheric composition studies

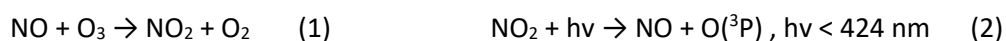
Photochemical and smog formed under strong stationary emissions during evening are the most common pollution phenomena in Attica. Photochemical smog is formed under conditions of intense solar radiation, high temperatures and it is associated with high concentrations of nitrogen oxides (mainly NO₂), ozone, hydrocarbons and their by-products. Despite the fact that there is a contribution from stationary sources, the photochemical smog is mainly associated with road traffic emissions. As the key role of VOCs in photochemical smog formation has been recognized (Finlayson-Pitts and Pitts, 2000), the development of strategies to control and reduce O₃, NO_x and particulate matter levels in urban environments requires measuring molecules that are indicators of the oxidation rate of VOCs. Such molecules are formaldehyde (HCHO) and glyoxal (CHOCHO) (Finlayson-Pitts and Pitts, 2000). As for O₃ and NO_x, since their chemistry is strongly related (reactions 1 and 2) and since O₃ is a secondary pollutant, NO_x could be a good indicator of photochemical smog formation.

The smog due to stationary sources has a strong presence in the area in the recent years and it is formed under conditions of high emissions (mainly from stationary sources of fossil fuel or biomass emissions) of pollutants, such as carbon monoxide (CO), sulfur dioxide, particulate matter and black carbon, combined with increased relative humidity levels. Good indicators for the study of smog are CO and black carbon (Fourtziou et al., 2016).

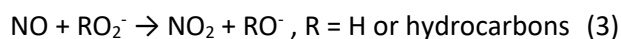
The compounds used as smog indicators in the present study and their role are briefly described as follows:

i) Nitrogen dioxide (NO₂)

NO₂ plays an important role in tropospheric and stratospheric chemistry (Crutzen, 1979). In the lower stratosphere and upper troposphere, it partially determines the distribution of ozone through its catalytic destruction (Seinfeld and Pandis, 2006). In the lower troposphere, NO₂ chemistry partially controls the oxidative capacity of the atmosphere (having the ability to remove electrons from molecules), the presence of tropospheric ozone (through its formation during photochemical smog), as well as the lifetime of greenhouse gases, such as methane (CH₄). It also contributes to the formation of nitrate particles and acidic aerosols. The distribution of NO₂ and O₃ in the atmospheric boundary layer directly affects air quality, as well as human health (e.g. Seinfeld and Pandis, 1998). NO₂ absorbs mainly in the visible spectrum and accurate estimates of absorption from NO₂ in the atmosphere are necessary in the case of calculating the atmospheric radiation balance. The basic formation (1) and cleavage (2) reactions of NO₂ are (Sander et al., 2006):



Any other reaction that converts NO to NO₂ (3) is a photochemical source of ozone production.

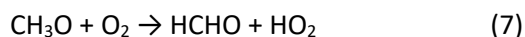
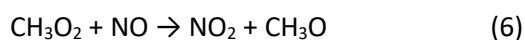
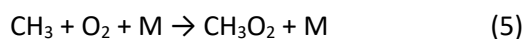
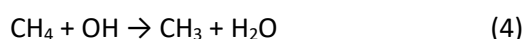


In fact, the photochemistry of ozone and NO₂ is characterized by complex processes. At regional scale, the ozone concentration is significantly determined by a series of reactions that include mainly volatile organic compounds and CO, while at local scale the dynamics of NO-NO₂-O₃ prevails and is characterized by the very rapid reactions (1) and (2) mentioned above (Pleijl et al., 2009). In the case

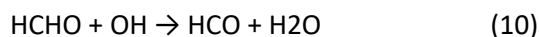
of low concentrations of nitrogen oxides, these reactions form ozone as the predominant product, while on the other hand, in the case of high concentrations of nitrogen oxides, NO₂ predominates. The spatial and temporal distribution of NO₂ in the troposphere is strongly variable and is influenced by both anthropogenic (e.g. fossil fuel and biomass burning, crop intensification with extensive use of fertilizers) and natural sources (lightning, soil oxidation). High NO₂ concentrations are also observed in industrial areas (Kassomenos et al., 1995). Its lifetime has been estimated to be about 27 hours within the atmospheric boundary layer and 4-5 days in the upper tropospheric layers (Leue et al., 2001). Under certain conditions, tropospheric NO₂ can be transported over long distances, thus contributing to the transboundary transport of pollution (Leue et al., 2001; Velders et al., 2001; Wenig et al., 2003).

ii) Formaldehyde (HCHO)

Formaldehyde is a significant atmospheric pollutant and its levels, in the troposphere, range from a few ppt in clean environments (Lowe and Schmidt, 1983) to a few tens of ppb in polluted environments, such as large urban centers. It is an important factor in atmospheric photochemistry as an intermediate product of the photochemical oxidation of volatile organic compounds (VOCs) and several hydrocarbons, including methane (CH₄) (Levy 1971, Finlayson and Pitts, 1976). The formation of formaldehyde from methane, in the presence of NO in urban environments is described by the following series of reactions:



Under specific meteorological conditions, in the presence of high concentrations of NO_x and VOCs and under the influence of UVB radiation, formaldehyde contributes to the formation of ozone and photochemical smog (Seinfeld and Pandis, 2006). Also, its presence affects the photochemistry of hydroxyl radicals (OH) and hydroperoxy radicals (OH_x) (Sumner et al. 2002, Liu et al. 2007), contributing to the energy balance of the atmosphere. Its photolysis (8 & 9) and its reaction with hydroxyl radicals (10 & 11) are the main routes of its removal from the atmosphere, as well as the main source of chemical formation of CO (Atkinson et al., 2000).



It is released into the atmosphere either as a primary pollutant from vehicle emissions and industries, or as a secondary pollutant through the previously analysed processes. Enhanced formaldehyde levels have been found in environments characterized by high levels of VOCs and pollution (Lee et al, 1998; Palmer et al., 2003; Heckel et al., 2005). Due to its short lifetime in the atmosphere, of the order of a few hours (Arlander et al., 1995), formaldehyde is a very good indicator of hydrocarbon emissions. For the same reason, its spatial distribution worldwide is characterized by great heterogeneity in relation

to other pollutants, as its concentration decreases rapidly as we move away from its emission sources. Unlike other hydrocarbons, formaldehyde can be measured using remote sensing.

iii) Glyoxal (CHOCHO)

The presence of glyoxal in urban environments, is mainly attributed to the oxidation of volatile organic compounds (Calvert et al., 2000), as its primary emissions (biogenic processes and biomass combustion) are considered extremely low compared to secondary (Volakmer et al., 2005). Extremely small amounts have been reported in exhaust emissions (Grosjean et al., 2001). Its very short life in the atmosphere, of the order of 1-2 hours in conditions of intense solar radiation (Volkamer et al., 2005), determined by its photolysis and reaction with OH radicals, makes it a very good indicator of oxidation processes of the volatile organic compounds. High glyoxal concentrations have been reported in congested urban environments (Volkamer et al., 2005), as well as in areas with high biogenic emissions (Wittrock et al., 2006; Vrekoussis et al., 2009, 2010).

iv) Particulate Matter (PM)

Suspended particles (solid or liquid particles with a diameter of $0.0002 \mu\text{m} < d < 500 \mu\text{m}$, dispersed into the atmosphere) play an important role in climate through their direct (transfer of solar radiation) and indirect effect (cloud formation) on the energy balance of the atmosphere (e.g. IPCC, 2007). They vary in size and composition and their precise characterization using remote sensing techniques is still a challenge for the scientific community. The processes of formation, transport and transformation of suspended particles are not yet fully understood. Their large temporal and spatial distribution in the troposphere makes it difficult to identify them in terms of their species and their source of origin. Although a large proportion of particulate matter is of natural origin, in high concentrations it can be harmful to human health. The amounts of mineral dust deposited in human lungs during dust episodes are comparable to those received during exposure in heavily polluted urban areas (Mitsakou et al., 2008). They are divided into coarse particles with a diameter of $2.5\text{-}10 \mu\text{m}$ and fine particles with a diameter of less than $2.5 \mu\text{m}$ (Fig. 1.4). Coarse particles are found mainly in dust transported from desert areas and in marine aerosols, while fine particles are characteristic of urban areas (Seinfeld and Pandis, 1998). Specifically for the Mediterranean region, aerosols from African dust transport can rise to high altitudes during transport and then mix with urban particles, contributing to pollution levels in those areas (e.g. Gerasopoulos et al., 2006, Mitsakou et al., 2008). Suspended particles are also divided into primary, which are emitted directly into the atmosphere, and secondary, which are formed through chemical reactions and phase change processes from gaseous to particulate. Organic secondary particles, which are an important component of the urban atmosphere, are formed when volatile organic compounds, such as isoprene, terpenes and aromatic hydrocarbons, are oxidized to form semi-volatile or low-solubility organic compounds (Carlton et al., 2009). These compounds will then either condense on the surface of pre-existing particles or form new particles (nucleation). In the present study, we will be mainly concerned with the optical properties of the suspended particles, i.e. the absorption and scattering of electromagnetic radiation, as discussed in more detail in Chapter 2.

Names	Fine particles			Coarse particles		
	Transient nuclei range	Accumulation range		Mechanical aerosol range		
Size, μm	.001	.01	.1	1	10	100
	①	②	③	④	⑤	
Sources	- Combustion - Heterogeneous nucleation	- Coagulation from transient nuclei - Condensation - Combustion		- Windblown dust - Large particle emissions - Sea spray		
Lifetime	Less than 1 hour	Days		Hours Days	Minutes Hours	

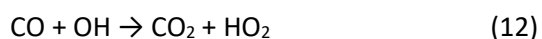
Figure 1.4. Nomenclature; sources, lifespan and size of the suspended particles are the three categories observed in the atmosphere. (Willeke and Whitby 1975)

v) Black carbon (BC)

Black carbon (BC) consists of elemental carbon and is formed during the incomplete combustion of fossil fuels, biofuels and biomass, as well as by specific industries, such as the printing industry and printing inks. It absorbs strongly in the visible part of the spectrum of solar radiation and therefore its presence in the atmosphere has a positive sign in the energy balance. Although the exact effect on the radiation balance depends on how it mixes with the other components of the suspended particles (Jacobson, 2001), BC emissions contribute significantly to global warming, ranking second after carbon dioxide (Bond et al. 2013). Its lifespan in the atmosphere ranges from a few days to weeks, so it can be transported over long distances and mixed with other suspended particles. In this way intercontinental atmospheric brown clouds can be formed, with a vertical growth of 3-5 km (Ramanathan and Carmichael, 2008).

vi) Carbon monoxide (CO)

The main source of carbon monoxide is the partial oxidation of hydrocarbons and its key role in tropospheric chemistry makes this element one of the most important air pollutants (Crutzen and Zimmermann, 1991). It reacts strongly with hydroxyl radicals. In urban environments it has been found that these reactions contribute 10% to the total consumption of hydroxyl radicals (Ren et al., 2003).



Globally, the main sources of CO emissions are the fossil fuel combustion (15%) and the oxidation of atmospheric CH₄ (25%). CO production in the northern hemisphere is about 100% higher than in the southern hemisphere (Logan et al., 1981). It has been estimated that about 2/3 of the CO in the atmosphere originates from anthropogenic activities (Seinfeld and Pandis, 2006). Its residence time in the atmosphere is 30-90 days. Its concentration in background conditions is 40-220 ppb and in urban areas it can reach 10 ppm.

1.3 Purpose and originality of research

The present study is mainly based on the Differential Optical Absorption Spectroscopy (DOAS) of diffuse radiation, which is used for the first time in Athens and fills the gap between in-situ measurements, which have local character and satellite measurements, which have a small spatial resolution and do not capture the spatial distribution of pollutants within the basin. This technique is based on the absorption of molecular structures in the visible and near ultraviolet parts of the electromagnetic spectrum. Measurements with the Multi Axis DOAS (MAX-DOAS) have the advantage of continuous recording of spectra at low cost, resulting in the acquisition of long time series of data. The multiple viewing directions also provide the possibility to study the spatial distribution of the selected pollutants, as well as their vertical distribution. An additional originality is the fact that the MAX-DOAS system, operating at the premises of the National Observatory of Athens to the north of the city (Penteli mountain) at an altitude of 500 meters above sea level, allows monitoring of the entire Attica basin formed by the four mountains surrounding the city. The exact location of the instrument and its viewing directions can be seen in Figure 3.1 (Chapter 3). Therefore, a long-term study can be carried out regarding the spatial and temporal distribution of specific pollutants in the whole area of Athens. The MAX-DOAS instrument used in this study is part of the BREDOM network (Bremian DOAS network for atmospheric measurements, http://www.iup.uni-bremen.de/doas/groundbased_data.htm).

The gaseous pollutants studied by DOAS spectroscopy in Athens are nitrogen dioxide (NO₂), formaldehyde (HCHO) and glyoxal (CHOCHO). Especially regarding glyoxal, it is the first time that measurements are carried out in Athens. Regarding formaldehyde, only sporadic measurements have been performed, with the exception of the work of Bakeas et al. (2003), where measurements were performed for a period of six (6) months. Therefore, this is the first time that the seasonal cycle of these gaseous pollutants is recorded in the region of Attica. It is also the first time that an attempt is made to calculate the vertical distribution of suspended particles in Athens using MAX-DOAS measurements. Although in terms of particulate matter, systematic measurements are performed in Athens with lidar systems giving reliable results (e.g. Papayiannis et al., 2008), MAX-DOAS excels in providing continuous measurements with low cost, which may prove to be extremely useful in the future, as according to the IPCC emission forecast scenarios (Intergovernmental Panel on Climate Change, 2008) the reduction of organic particulate emissions is expected to be particularly small compared to other emissions, such as SO₂ and BC which are expected to decrease by 80% and 50% respectively by the end of the 21st century.

During this study, the phenomenon of biomass combustion, which has a strong presence in recent years and greatly burdens the quality of the atmosphere in Athens was also investigated. Specifically, in 2011, the economic crisis in Greece affected the price of heating oil, resulting in a gradual decrease in its use by the inhabitants of the city and an increase in biomass combustion. This has led to frequent smog episodes during night hours (Fourtziou et al., 2017), when the shallow nocturnal boundary layer combined with certain meteorological conditions (temperature inversion, weak winds) traps the pollutants in the lower atmospheric layers. Due to the fact that this phenomenon has a strong presence at night and can not be covered by the measurements of MAX-DOAS, which performs measurements only during the daylight, the need to use in-situ measurements during intense winter experimental

campaigns has been risen. The effect of the reduced use of fossil fuels and the parallel increase of the use of biomass on long-term carbon monoxide (CO) trends in Athens was investigated for the first time.

Specifically, the objectives of the present study can be summarized as follows:

- ❖ Use of the MAX-DOAS passive remote sensing system for:
 - ❖ Description of the seasonal variation of nitrogen dioxide (NO₂), formaldehyde (HCHO) and glyoxal (CHOCHO) and investigation of their spatial distribution in the whole area of Athens.
 - ❖ Investigation of the daily variation of the above mentioned gaseous pollutants, taking into account their spatial and temporal distribution.
 - ❖ Estimation of the contribution of urban pollution sources to the levels of the studied air pollutants in the urban area of Athens.
 - ❖ Investigation of the effect of meteorology with emphasis on the prevailing local wind systems on the long-term measurements of the studied gaseous pollutants.
 - ❖ Description, based on the previous results, of the dominant role of anthropogenic sources or photochemical processes in the levels of the above mentioned pollutants in Athens.
- ❖ Retrieval of the vertical distribution of the aerosol extinction coefficient and calculation of the optical thickness of the aerosols, using the BOREAS algorithm, the SCIATRAN radiative transfer model and the MAX-DOAS measurements.
- ❖ Assessment of the reliability of the above results by comparing them with the corresponding results obtained from the active remote sensing system lidar and the Cimel sun photometer.
- ❖ Investigation of the role of biomass combustion in the quality of the atmosphere of the urban environment of Athens. This investigation is based on carbon monoxide (CO) and black carbon (BC) in situ measurements.

During the first stage of the study, continuous measurements for an 18-month period were performed, in order to retrieve data for NO₂, HCHO, CHOCHO and oxygen dimer (O₄) with the MAX-DOAS remote sensing system, which is part of the BREDOM network (Bremian DOAS network for atmospheric measurements) of the University of Bremen and operates at the premises of the National Observatory of Athens (NOA) in Penteli. During the second stage, the results were processed, in order to provide answers to the questions / objectives of this work. In the context of this stage and for the evaluation of the algorithm used to calculate the aerosols' vertical distribution, it was necessary to use additional measurement data from a CIMEL sun photometer, part of NASA's AERONET network and operating at NOA's monitoring station in the city centre, as well as from a lidar system, part of EARLINET network, which carries out measurements at the National Technical University of Athens. Along with the remote sensing measurements, intensive winter in-situ campaigns were carried out at NOA's monitoring station in the city centre for addressing the need to observe and investigate the phenomenon of the increased biomass combustion during winter.

The results of this study are presented in Sections 3, 4 and 5.

Instrumentation and theoretical background

The scope of this chapter is to describe the instruments and methodologies used to carry out the experimental part of the present study, as well as to explain concepts that are necessary for the understanding of these procedures. It focuses on the description of the technique of the differential absorption differential optical spectroscopy - as it is the main method that was used - both at theoretical level and at level of structure and operation of the MAX-DOAS system. The theoretical background of the BOREAS retrieval algorithm used to calculate the vertical distribution of aerosols is also described. Then, a brief reference is made to the basic concepts of radiation propagation used by remote sensing applications, and finally, the instruments used to perform the necessary auxiliary measurements are also described.

2.1 Differential optical absorption spectroscopy (MAX-DOAS)

Multiple AXis Differential Optical Absorption Spectroscopy (MAX-DOAS) is a relatively new atmospheric measurement technique (Hönninger et al., 2004) that has become widely used in recent years (e.g. Heckel et al., 2005; Pinardi et al., 2013; Seyler et al., 2017) and which uses scattered solar radiation from multiple viewing directions. The concentration of the studied trace gases is calculated through numerical analysis of the atmospheric absorption spectra. Ground measurements with MAX-DOAS have increased sensitivity in the lower atmospheric layers and in combination with Radiative Transfer Models (RTM) and inversion techniques, can provide information on the vertical distribution of trace gases and aerosols in the atmosphere.

2.1.1 MAX-DOAS technique

The general idea of the MAX-DOAS technique is to record spectra of scattered solar radiation at different elevation angles α , i.e., the angle formed between the viewing direction of the telescope and the horizontal direction. For an individual measurement at an elevation angle α , the measured optical density refers to Slant Column Density (SCD), which is the concentration $c(s)$ of the trace gas integrated along the light path s :

$$SCD_{\alpha} = \int C(s)ds = \frac{1}{\sigma} \log \frac{I_0}{I_{\alpha}} \quad (2.1)$$

where σ denotes the absorption cross section, I_0 the reference spectrum and I_{α} the measured spectrum (Fig. 2.1).

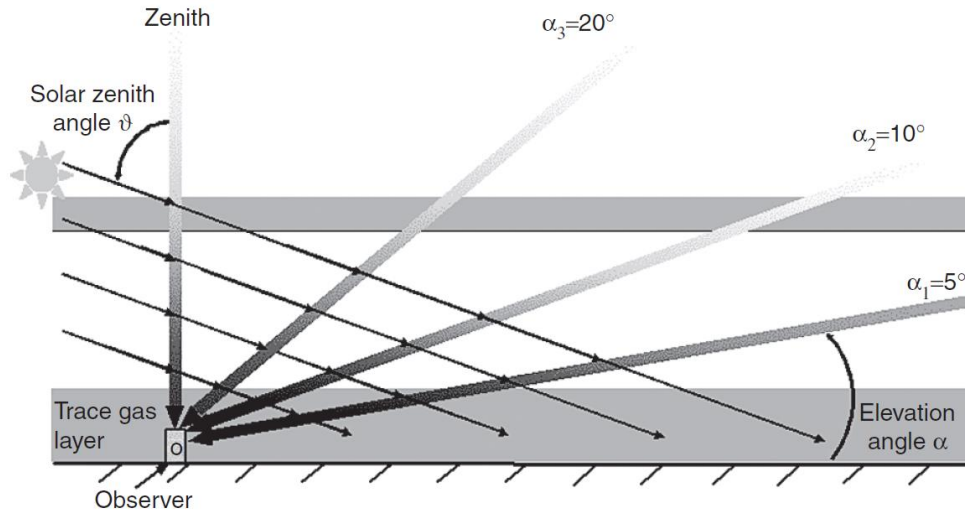


Figure 2.1. Geometry of MAX-DOAS and the associated radiation transport in the atmosphere (Platt and Stutz, 2008)

The DOAS methodology is based on the Beer-Lambert's law, according to which the attenuation of electromagnetic radiation of wavelength λ and intensity $I(\lambda)$ when passing through matter of thickness ds is given by the equation:

$$dI(\lambda) = I(\lambda) \cdot p(s) \cdot \sigma(\lambda, T) ds \quad (2.2)$$

where $\sigma(\lambda, T)$ denotes the absorption cross section of the absorbing matter and $p(s)$ the matter's density across a light path s (Fig.2.2). The integration of equation 2.2 for a finite optical path defines the relationship between the initially emitted radiation $I_0(\lambda)$ and the radiation intensity $I(\lambda)$ after passing through the matter (Equation 2.3). The logarithm of the ration $I_0(\lambda) / I(\lambda)$, is the optical thickness $\tau(\lambda)$ of the matter (Equation 2.4).

$$I(\lambda, \sigma) = I_0(\lambda) e^{-\sigma(\lambda, T) \int p(s) ds} \quad (2.3)$$

$$\tau = -\ln\left(\frac{I(\lambda, \sigma)}{I_0(\lambda)}\right) = \sigma(\lambda, T) \int p(s) ds = \sigma(\lambda, T) \cdot SCD \quad (2.4)$$

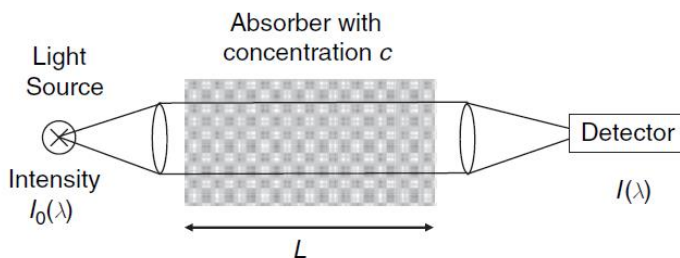


Figure 2.2. The basic principle of absorption spectroscopic trace gas detection. A beam of light passes through a volume containing the absorber with concentration c (Platt and Stutz, 2008)

However, the Beer-Lambert's law cannot be applied to atmospheric measurements due to the following reasons:

- i) In addition to absorption by trace gases, attenuation of radiation is also caused by scattering by molecules or aerosols. Especially for aerosols, the attenuation cannot be accurately calculated.
- ii) Absorption by various components of the atmosphere is added to the total absorption, thus influencing the measurement of the studied trace gas.
- iii) In the case of satellite measurements, the detected radiation depends greatly on the surface albedo.

These restrictions are eliminated by the application of the differential optical absorption spectroscopy (DOAS) technique. The DOAS technique is based on absorption measurements using spectrum rather than monochromatic light source. In this way, it is possible to distinguish the absorption structures of different elements, as well as the attenuation due to scattering. It was first described by Perner and Platt (1979) and a detailed description has been given by Platt (1994).

The basic principle of the DOAS method is the separation of absorption into broadband and narrowband spectral features. Therefore, the absorption cross-section $\sigma(\lambda)$ of a given element can be expressed as the sum of the absorption cross-sections of the broad $\sigma_c(\lambda)$ and the narrow structure $\sigma'(\lambda)$ (Equation 2.5) and equation 2.3 can be converted to equation 2.6.

$$\sigma(\lambda) = \sigma_c(\lambda) + \sigma'(\lambda) \quad (2.5)$$

$$I(\lambda, \sigma) = I_o(\lambda) e^{-\sigma_c(\lambda) \cdot SCD} \cdot e^{-\sigma'(\lambda) \cdot SCD} \quad (2.6)$$

$\sigma'(\lambda)$ denotes the differential absorption cross section. The distinction between the narrow and the broad absorption cross-section depends on the amplitude of the spectrum, as well as the amplitude of the absorption peaks that need to be examined. In order to remove the broad atmospheric absorption structures, as well as the effects of Rayleigh and Mie scattering, the measured spectrum is divided by a fitting polynomial. Also, the spectral characteristics of Fraunhofer lines are removed by subtracting a Fraunhofer reference spectrum from the measured spectrum.

The differential optical thickness is defined in accordance with the differential absorption cross section, by equation 2.7. Finally, the slant column density for a specific trace gas can be calculated using equation 2.8.

$$\tau'(\lambda, \sigma, \sigma') = \tau(\lambda, \sigma) - \tau(\lambda, \sigma - \sigma') \quad (2.7)$$

$$SCD = \tau'(\lambda, \sigma, \sigma') / \sigma' \quad (2.8)$$

An example of DOAS fitting curve applied to CHOCHO spectrum is shown in Figure 2.3

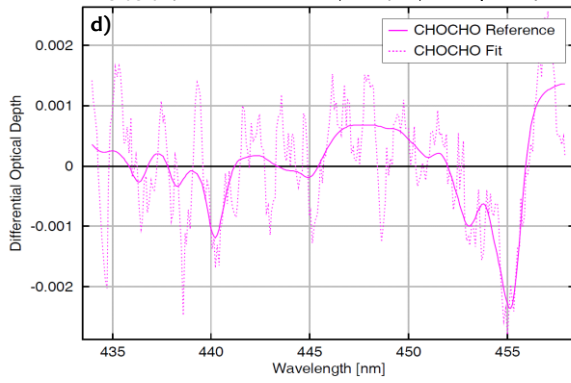


Figure 2.3. The dashed and solid curves represent the DOAS fit and the reference cross section scaled to the slant column values, respectively.

In order to calculate the SCD of tropospheric trace gases, the differential SCD (DSCD) is used i.e. the difference between the SCD at $\alpha \neq 90^\circ$ and at $\alpha=90^\circ$:

$$\text{DSCD}(\alpha, \theta) = \text{SCD}(\alpha, \theta) - \text{SCD}(90^\circ, \theta) = \frac{1}{\sigma} \log \frac{I_{90^\circ}}{I_\alpha} \quad (2.9)$$

As the measured SCD is highly dependent on the geometry of the instrument and the meteorological conditions, it is usually converted to vertical column density (VCD). The conversion from SCD to VCD is achieved through the air mass factor (AMF) which is defined as the enhancement of the average path followed by the photons in the atmosphere compared to the vertical path (Platt and Stutz, 2008) (section 2.2.1)

2.1.2 Operation principles and fundamental set-up of a MAX-DOAS system

The basic principle of a MAX-DOAS system, briefly, is the collection of scattered solar radiation from different directions through a rotating telescope and the transmission of the received signal, through quartz optical fibers, to the spectrometer. Fiber optics effectively depolarize the incoming radiation and provide flexibility in adjusting instrument settings. The spectrum is recorded by a Charge Coupled Device (CCD) detector and is saved in a computer, which controls the operation of the instrument (Wittrock et al., 2004) (Figure 2.4).

In the case of the instrument used for the present study, ultraviolet and visible radiation of the solar spectrum enters the telescope through a quartz window. A lens focuses the incoming radiation on an optical fiber bundle, which ends at a grating spectrometer, where the individual fibers are distributed along the entrance slit. A cylindrical tube is attached to the quartz window of the telescope, in order to block the direct solar radiation from entering. A shutter has been placed inside the telescope unit, in order to cut off the optical path from the quartz window to the lens during calibration measurements. A mercury-cadmium lamp (Hg-Cd) is used for the wavelength calibration; each pixel of the CCD detector is matched with the right wavelength. In this way, errors due to spectrum displacement are avoided, as well as error propagation in the measurement results. A camera has been

placed just below the telescope entrance window, in order to provide input on have an idea of the weather conditions at the time of the measurements and to be able to carry out post quality control and corrections of the measurements (QA / QC). The accuracy of the elevation angle is checked by an inclinometer. Silica gel is also used to remove the humidity from the telescope unit and to avoid possible condensation of water vapors on the optical elements or possible problems in the electrical circuits.

The grating spectrometer used in this study is a L.O.T. 260S (600 l/mm ruled grating) with spectral resolution of about 0.8 nm at Full Width at Half Maximum (FWHM) and spectral range 330-500 nm. Therefore, it is capable of up to 350 spectral lines. The measured spectrum is recorded by a CCD detector (Andor DV-440BU) of 2048x512 pixels. The CCD detector is an integrated circuit etched onto a silicon surface forming light sensitive elements called pixels. The incident radiation is absorbed and the exposed surface emits electrons (photoelectric effect). The electrons bind to the potential well and remain near the semiconductor-insulator (silicon) interface. They are gradually transmitted through electrical signals and are recorded as output digital signals. The spectrometer unit is constantly cooled to -37°C, in order to avoid changes in the optical properties of the instrument and to minimize dark current.

For ground-based observations with MAX-DOAS, the telescope collects radiation from different viewing directions (observation geometry) allowing conclusions to be drawn about the spatial distribution of certain trace gases. At the vertical viewing direction (zenith direction), the photons have travelled a relatively long distance in the stratosphere, compared to the short light path travelled in the troposphere, before finally reaching the telescope. In contrast, off-axis geometries focus on the lower atmospheric layers, increasing the instrument's sensitivity to absorbers within the atmospheric boundary layer. Since the MAX-DOAS analysis is a differential method and no absolute calibration is needed, the method is sensitive, even at low concentrations of the measured trace gas. The installation of MAX-DOAS at the National Observatory of Athens in Penteli is shown in Figure 2.5.

The altitude at which the photon is last scattered before reaching the telescope is called the last scattering altitude (LSA). The LSA effectively determines the length of the last section of the path taken by the photons through the lowest atmospheric layer and is an important parameter in understanding the sensitivity of MAX-DOAS measurements in relation to different vertical distributions of trace gases and suspended particles. As expected, the LSA becomes smaller for the lower elevation angles, increasing the sensitivity to trace gases within the atmospheric boundary layer. LSA is also small when large load of suspended particles is present in the atmosphere (Hönninger et al., 2004).

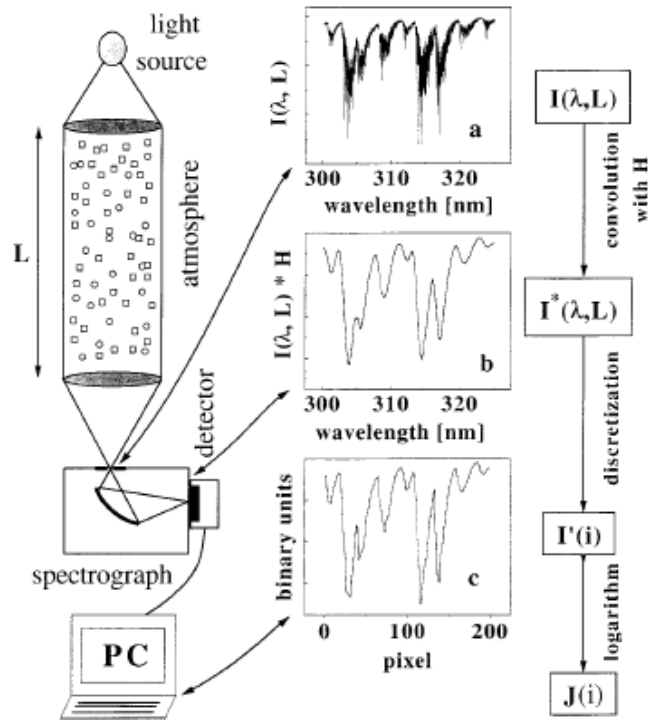


Figure 2.4. Schematic view of a DOAS instrument used to measure tropospheric trace-gas concentrations. Collimated light undergoes absorption processes on its way through the atmosphere. Panel (a) shows an example of this light entering the spectrograph. This absorption spectrum shows the rotational structure of the absorption bands. In panel (b) the same spectrum convoluted by the spectrograph's instrumental function reaches the detector. In the detector the wavelength is mapped to discrete pixels (panel c) and the final spectrum is stored in the computer for numerical analysis (Stutz and Platt 1996).

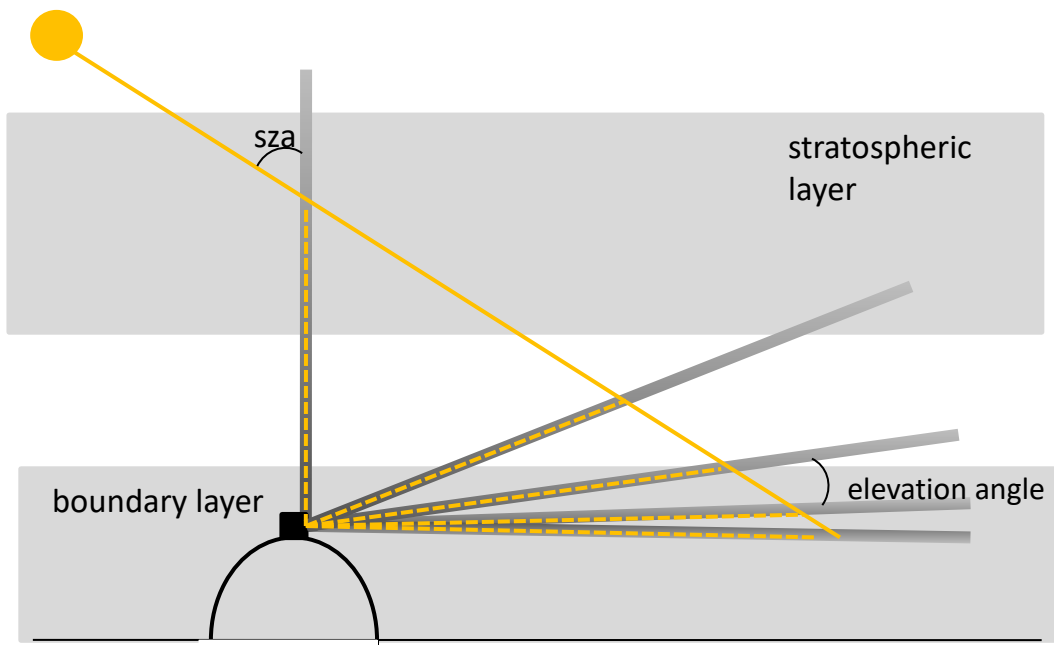


Figure 2.5. Schematic overview of the observation geometries of MAX-DOAS at the premises of the National Observatory of Athens in Penteli at an altitude of 527 m a.s.l.. The yellow lines represent the optical path of photons reaching the telescope for 5 elevation angles. The enhancement of the optical path within the atmospheric boundary layer at small elevation angles is obvious.

MAX-DOAS observations can also be used for aerosol analysis through oxygen dimer (O_4) measurements. Since the vertical distribution of O_4 is highly dependent on altitude, O_4 measurements are particularly sensitive to changes in the optical path and thus, can provide information on the vertical distribution of atmospheric aerosols. In terms of accuracy due to calibration, this method excels when compared to other techniques (such as sunphotometers or lidar) since it is based on differential absorption and does not require absolute calibration or the utilisation of the Langley technique. Apart from the atmospheric aerosols, the optical path of the photons is also affected by the presence of clouds, altering the levels of the SCD_{O_4} compared to those obtained under clear sky conditions. Optically thick clouds usually lead to an increase of the optical path due to the multiple scattering that occurs inside the clouds. The same increasing effects have the optically thin cirrus clouds at high altitudes during measurements at small elevation angles. In contrast, sparse clouds at low altitudes tend to reduce the measured SCD_{O_4} levels at all elevation angles (Wagner et al., 2011).

2.2 Basic concepts of remote sensing

In order to understand the concepts used to extract and explain results derived from remote sensing applications - and in particular from MAX-DOAS measurements - it is advisable to briefly describe some of their key points and basic principles.

2.2.1 AMF - Air Mass Factor

For DOAS measurements that use scattered solar radiation, the optical path depends on the position of the Sun and therefore the slant column density (SCD) depends, inter alia, on the solar zenith angle (sza) and the observational geometry of the telescope. Therefore, for more reliable results the use of the Air Mass Factor (AMF), which relates the calculated SCD to the VCD, as already mentioned in section 2.1.1, is required

The AMF is calculated using appropriate radiative transfer models (RTM). At first, models that considered only single scattering in the atmosphere (e.g. Noxon et al., 1979; Solomon et al., 1987) - i.e. photons scattered only once before being detected - were used. The models based on this assumption gave satisfactory results. Nevertheless, models were later developed that took into account the presence of multiple scattering in the atmosphere (e.g. Dahlback et al., 1991; Rozanov et al., 1997; Marquard and Platt, 1997). Although multiple scattering models give a more realistic description of the atmosphere, the results were less accurate (Marquard et al., 2000).

The standard computational procedure for calculating the AMF of a particular absorber using RTM can be described in three steps:

1. The RTM runs two simulations of the atmosphere: one with the studied trace gas being present (using an approximate vertical distribution of the specific trace gas) and one with the trace gas being completely absent. The corresponding radiations $I(\lambda, \sigma)$ and $I(\lambda, 0)$ are calculated.
2. The VCD of the absorber is calculated through integration of the considered vertical distribution of its concentration.
3. The AMF is calculated:

$$AMF = \frac{\ln [I(\lambda,0)/I(\lambda,\sigma)]}{\sigma \cdot VCD} \quad (2.10)$$

The actual VCD is then calculated using the AMF according to the equation:

$$VCD = \frac{SCD}{AMF} \quad (2.11)$$

The above imply two limitations in the calculation and use of the AMF: (i) It is calculated as a function of the a priori VCD and therefore depends on it. (ii) While the SCD is calculated using a range of wavelengths, the AMF used to calculate the VCD is calculated for an individual wavelength value.

2.2.2 Scattering and absorption of electromagnetic radiation

The scattering of electromagnetic radiation arises from the interaction of photons and the electron cloud. If a photon of a certain wavelength is absorbed by a molecule in the atmosphere, the molecule goes from the ground state to an excited energy state. Depending on the frequency of the incident radiation, the molecular excitation can happen in three ways: i) the electrons of the molecule go to higher energy levels, ii) the rotational energy level of the molecule increases, iii) the vibrational energy level of the molecule increases (Serway et al., 1989). The molecule must return to its ground energy state in a very short time and this is achieved mainly by emitting in a random direction a photon of energy equal to the absorbed photon (radiative decay). This mechanism describes the scattering of solar radiation by molecules in the atmosphere. Scattering is a quantum phenomenon, but it can also be interpreted in terms of classical physics. According to the classical approach, the incident radiation polarizes the molecules by inducing oscillating electric dipoles, which in turn (as moving charges) emit radiation of the same wavelength as the incident one. When the scattering molecule is much smaller than the wavelength of the incident radiation, then the electromagnetic radiation is re-emitted in all directions and spherical scattering is observed (Rayleigh scattering). When the scattering molecule is larger than the wavelength of the incident radiation, then the laws of optical scattering prevail and most of the radiation is scattered forward (Mie scattering). If the scattering happens because of the coupling of the motion of the electrons and the nuclei (vibrational energy), then the scattered radiation has a different wavelength than the incident one and the phenomenon is called Raman scattering.

However, in the case of relatively high atmospheric pressure (~ 1 atm), which is the case of the lower atmospheric layers, there is a possibility that the energy emitted after the excitation of the molecule, is converted into kinetic energy and heat, increasing the temperature locally. This phenomenon is

called thermalization and then we say that the photon is absorbed. Absorption is also observed when the interaction of solar radiation with the molecules of the atmosphere, leads to photoionization (removal of electrons) or photolysis of the molecules (initiation of photochemical reactions).

Below, some physical parameters related to the scattering and absorption of electromagnetic radiation are described.

Single Scattering Albedo (ω) is the ratio of the radiation attenuation due to scattering relative to the total attenuation (absorption and scattering):

$$\omega = \sigma_{scat} / (\sigma_{scat} + \sigma_{abs}) \quad (2.12)$$

σ_{scat} denotes the scattering cross section and σ_{abs} the absorption cross section. Therefore, it is a dimensionless quantity ranging between 0 (only absorption) and 1 (only scattering).

The **asymmetry factor (g)** determines the radiation pressure exerted on a particle, is a measure of scattering direction and is also important in the approximate theory of multiple scattering by large particles (aerosols or cloud droplets). The asymmetry factor for scattering of unpolarised radiation is defined as the weighted mean over the sphere of the cosine of the scattering angle, with the particle phase function as weighting function. For forward scattering, g is near one, for backscattering is near minus one and for isotropic and Rayleigh scattering is zero. In the presence of suspended particles in the atmosphere, the asymmetry factor has been found to be 0.74 and 0.67 at 440nm and 670nm, respectively (AOD > 0.4) (Eck et al., 2001). In another study (Chubarova et al., 2011), it was found to be 0.65 for fine and 0.89 for coarse particles at 440 nm. The corresponding values for the 670nm are 0.53 and 0.85. In the presence of water clouds the asymmetry factor is around 0.86 in the visible spectrum (Chou et al., 1998).

The **Angström exponent (α)** describes the spectral dependence of the aerosol optical depth (τ), which largely depends on the aerosols' size. The equation for the Angström exponent calculation relates the optical depth to two different wavelengths (λ και λ_0):

$$\tau(\lambda) = \tau(\lambda_0) \left[\frac{\lambda}{\lambda_0} \right]^{-\alpha} \quad (2.13)$$

Actually, coefficient (α) represents the slope (first derivative) of the optical thickness with respect to wavelength in logarithmic scale. The high values of the Angström exponent ($\alpha \geq 2$) are associated with fine particles, which in turn are associated with the presence of urban pollution, and the small values ($\alpha < 1$) are associated with coarse particles, such as dust aerosols (Eck et al., 1999; Westphal and Toon, 1991).

The **scattering phase function** describes the angular distribution of the scattered radiation. It is defined as a function of the angle θ between the direction of incident and scattered radiation:

$$P(\theta) = \frac{F(\theta)}{\int_0^\pi F(\theta) \sin\theta d\theta} \quad (2.14)$$

F denotes the intensity of the incident radiation. $P(\theta)$ could be defined as the probability that a photon will scatter out of the beam path through an angle θ (Seinfeld and Pandis, 2006).

2.3 Inverse model and retrieval algorithm

The inversion of the radiative transfer equation is a necessary process, in order to calculate the vertical distribution of trace gases and of the attenuation coefficient of solar radiation from aerosols using MAX-DOAS measurement data. As the equation depends largely on the suspended particles and after a series of studies (Frieb et al., 2006; Sinreich et al., 2005; Wagner et al., 2002; Wagner et al., 2004), in order to retrieve the aerosol extinction profile, the fitting of forward-modelled absorption signals of the oxygen dimer (O_4) - which is characterized by a stable and well-known vertical distribution - in the measurement data has been suggested. The BOREAS (Bremen Optimal estimation REtrieval for Aerosol and trace gasS) retrieval algorithm of the Institute of Environmental Physics of the University of Bremen (Bösch et al., 2017) was used for this purpose. This is an inverse modeling technique based on optimal estimation, as explained in the following paragraph.

A vector \mathbf{y} that results from observations and corresponds to a spectrum of diffuse solar radiation for example, can be related to the actual distribution of atmospheric gas \mathbf{x} through a forward model \mathbf{F} (Eq. 2.13). The forward model \mathbf{F} calculates the radiation transfer in the atmosphere. The parameter vector \mathbf{b} of the model includes all the variables that affect the measurements (except for the variable under study, i.e. the trace gas in this case) and the vector \mathbf{b}_o is the optimal estimation of these parameters. Examples of variables included in \mathbf{b} are the observation geometry (solar zenith angle, observation angle), surface properties (e.g. albedo), the presence of other trace gases and particulate matters, the "ring effect" phenomenon, characteristics of the instrument, such as the slit of the spectrophotometer. The right side of the equation contains three sources of errors: ε is the measurement error, $\Delta\mathbf{F}$ is the - usually systematic - error of the model and the derivative $\partial\mathbf{F}/\partial\mathbf{b} * (\mathbf{b}-\mathbf{b}_o)$ describes the errors resulting from the uncertainties of the model parameters \mathbf{b} .

$$\mathbf{y} = \mathbf{F}(\mathbf{x}, \mathbf{b}_o) + \Delta\mathbf{F} + \frac{\partial\mathbf{F}}{\partial\mathbf{b}}(\mathbf{b} - \mathbf{b}_o) + \varepsilon \quad (2.13)$$

The inversion of equation 2.13 can result to the calculation of \mathbf{x} given \mathbf{y} . Given the presence of errors, a statistical estimation can be made and the results must be weighed according to the a priori knowledge of the trace gas distribution vector \mathbf{x}_a . The optimal solution of \mathbf{x} that includes all of the above constraints, is called retrieval or optimal estimation.

Equation 2.13 can be developed around the a priori distribution \mathbf{x}_a as follows:

$$\mathbf{y} = \mathbf{F}(\mathbf{x}_a, \mathbf{b}_o) + \mathbf{K}_x(\mathbf{x} - \mathbf{x}_a) + \text{error terms} \quad (2.14)$$

The term $\mathbf{K}_x = \partial\mathbf{F}/\partial\mathbf{x}$ is the weighted function at $\mathbf{x}=\mathbf{x}_a$. An inverse method \mathbf{R} calculates the vector of the \mathbf{x}_o distribution of the trace gas corresponding to the measurement \mathbf{y} :

$$\mathbf{x}_o = \mathbf{R}(\mathbf{y}, \mathbf{x}_a, \mathbf{b}_o) \quad (2.15)$$

Actually, the inverse model is an approach to estimating the variables that determine the evolution of a system using system parameters that can be measured and our knowledge on how observations relate to system variables.

2.4 Ancillary measurements

In order to address the questions of this research and to evaluate the results of the retrieval algorithm, it was deemed necessary to use ancillary measurements. The instruments used and their basic operational principles are briefly described below.

2.4.1 Lidar System (Light Detection And Ranging)

It is an active remote sensing technique that uses laser to emit short light pulses into the atmosphere and detects/processes the return signal by a receiver typically consisting of a telescope, photodetectors and data acquisition electronics. Due to the interaction of the emitted laser beam with components of the atmosphere, a small fraction of it is backscattered; the processing of the return signal gives information about the distance of the target from the instrument and its vertical distribution in the atmosphere. The basic principle of lidar operation is illustrated in Figure 2.6. The lidar instrument consists of a laser source, which generates the light pulses that probe the atmosphere, a telescope and optics to collect the back-scattered radiation and a receiver which amplifies and converts the light echo into an electrical signal.

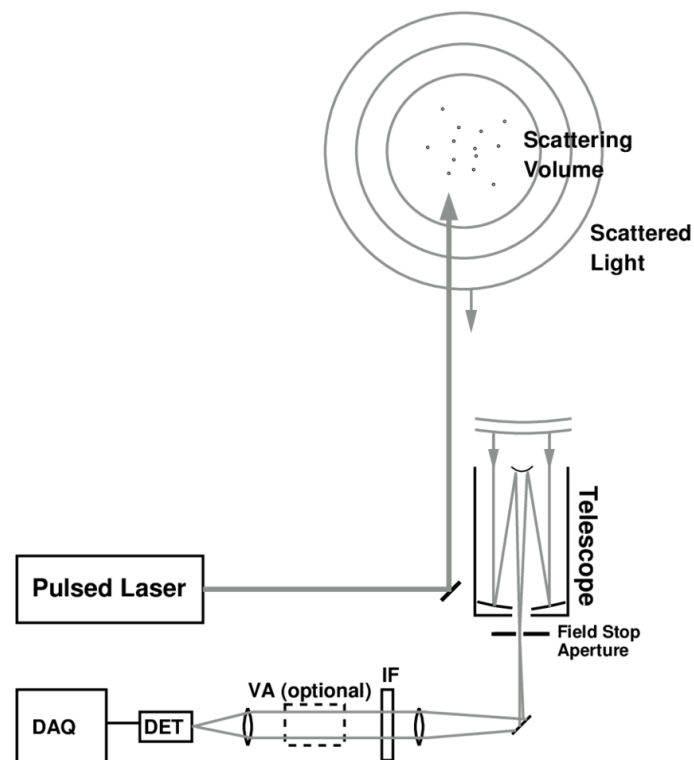


Figure 2.6. Basic principle of lidar operation; IF: interference filter, VA: variable attenuator, DET: detector, DAQ: data acquisition system.

The lidar system used for the present study, has been operating since February 2000 at the National and Technical University of Athens (Papayannis et al., 2005) and is part of the EARLINET network. It is a Raman lidar system operating at six wavelengths. The transmitter features a pulsed Nd: YAG laser, emitting high energy pulses at 355, 532 and 1064 nm, with a repetition frequency of 10 Hz. It has a beam expander to reduce the beam divergence and increase its diameter. The receiver is a Cassegrainian telescope with a focal length of 600 mm and aperture diameter of 300 mm. It is connected to the spectral analyzer via fiber optics and detects signals at 355, 387, 407, 532, 607 and 1064 nm. The system can also operate as a depolarisation lidar, which additionally to the elastic scattering at the initial three wavelengths, can also utilize the depolarization (a measure of particle sphericity) at 532 nm to draw conclusions about the optical properties of the suspended particles.

2.4.2 Cimel photometer

The Cimel Sun Photometer is a passive remote sensing system and consists of an optical head, a box containing the system's electronics and a robotic pointing system for moving the optical head along both the zenith and azimuthal axes. A microprocessor calculates the sun's position and guides the optical head. The optical head has two detectors for direct sun and diffuse radiation measurements, which are used for the calculation of the aerosols' optical properties. The full angle field of view is about 1.2°. The sun detector is protected by a quartz (SiO₂) filter, which allows spectral measurements of solar radiation in the spectral range from 380 nm to 1020 nm. The diffuse radiation detector has lenses with larger aperture to allow better dynamic range for the sky radiances, and the spectral range is the same (380-1020 nm).

Direct sunlight measurements are used to calculate the aerosol optical depth at the wavelengths that the instrument operates. Each measurement records the voltage of the sensor at the different wavelengths. Given that the voltage at the top of the atmosphere (V_0) is known, the measured voltage (V) provides information about the transfer of the radiation in the atmosphere and by applying the Beer-Lambert's law, the optical thickness at a certain wavelength is calculated (τ_λ):

$$V_\lambda = \frac{V_{0\lambda}}{R^2} e^{(-\tau_\lambda \cdot \frac{1}{\cos\theta})} \quad (2.16)$$

The angle θ denotes the solar zenith angle and the term R the Sun-Earth distance in astronomical units. The V_0 calibration constant is determined by the Langley method, which is based on the spectral attenuation of solar radiation and Beer-Lambert's law.

The Cimel Sun Photometer (Holben et al., 1998) data used in the present study, was provided by the NASA AERONET network; direct radiation measurements were being performed at eight wavelengths (340, 380, 440, 500, 675, 870, 940, 1020 nm) and diffuse measurements in four (440, 675, 870, 1020 nm). Further analysis of the measurements provides information on the aerosol optical properties in the atmospheric column (Dubovik et al. 2006). The uncertainty of measurements for high optical depth values ($AOD_{440} > 0.4$) is estimated to be around 0.03, while for AOD_{440} values less than 0.2 the accuracy is even lower (0.05-0.07) (Dubovik et al., 2000). The Cimel Sun – Photometer has been operating in Athens since 2010 (Raptis et al., 2020).

2.4.3 BC - CO Measurements

Thermo Fisher Multi Angle Absorption Photometer MAAP 5012 and Magee Scientific Aethalometer AE-42 were used for the black carbon measurements.

The Multi-Angle Absorption Photometer (MAAP) determines the online light absorption of a PM deposit on a filter, by simultaneously measuring the transmissivity and reflectivity of the filter at multiple angles. More specifically, a multi-angle absorption photometer is used to analyze the modification of the radiation fields due to the deposition of particles in the anterior and posterior hemispheres of a glass-fiber tape. The data inversion algorithm is based on a radiation transfer method and takes into account multiple scattering processes within the collected particles and between the particle layers and the filter core, using an explicit arithmetic method. The air sample that enters the instrument, is deposited on the glass-fiber film and is led to the detection chamber, where a visible light source of 670 nm is directed at the sample (Fig. 2.7). The light propagating in the anterior hemisphere and reflected in the posterior, is measured by a series of photodetectors. The light beam attenuates relatively to the initial beam, which is the reference measurement of the clean filter. The reduction of light transmission, multiple reflection intensities and air sample volume are continuously integrated over the sample run period to provide real time concentration measurements of black carbon.

The MAAP has been extensively tested and evaluated and the uncertainty of the absorption coefficient has been estimated to be 12% (Petzold and Schönlinner, 2004).

The AE-42 aethalometer measures the light absorption by suspended particles at seven wavelengths (370 470, 520, 590, 660, 880 and 950 nm). The basic operational principle is to measure the rate of change of the attenuation of light from suspended particles that are continuously collected on a quartz tape using an air pump. Measurement at 880 nm is related the black carbon concentration. The method explicitly does not require any knowledge or assumption about the existence, origin or magnitude of any optical nonlinearity arising from the properties of the aerosol particles collected on the tape.

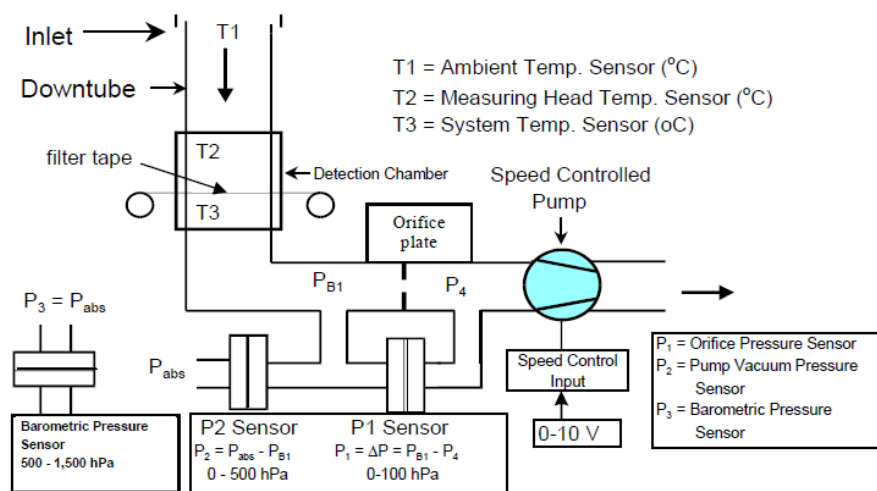
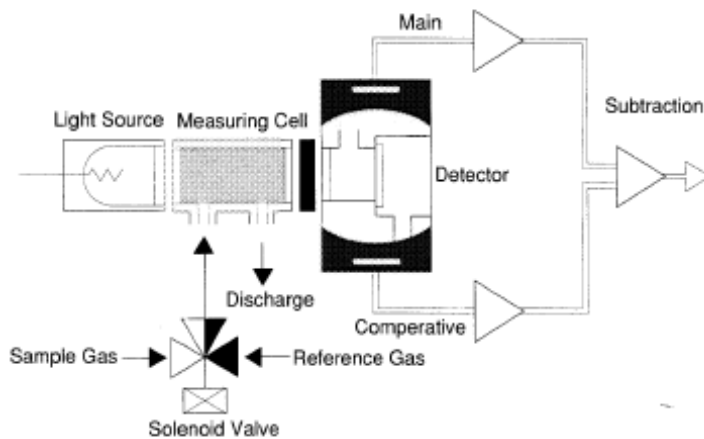


Figure 2.7. Basic principle of MAAP 5012 operation.

For the in-situ CO measurements, the Horiba APMA-360 analyzer was used, which, in brief, calculates the CO concentration based on the strong CO absorption peaks at specific wavelengths. It consists of a light source, a cell, a detector, an optical filter and a flow regulator (Fig. 2.8). During operation, oxidation catalysts remove the CO in the sample gas, so it can be used as a reference gas with zero CO concentration. Even if there are interfering components present in the sample gas, capable of affecting the measurements, their influence can be ignored as they are present in equal amounts in both air samples (measurement gas and reference gas). The samples enter alternately into the cell and their difference determines the signal produced. The measurements are characterized by high accuracy and stability for long time periods.



Σχήμα 2.8. Basic operationan principle of Horiba APMA-360.

Slant column MAX-DOAS measurements of nitrogen dioxide, formaldehyde, glyoxal and oxygen dimer in the urban environment of Athens

Slant column (SD) densities of nitrogen dioxide (NO_2), formaldehyde (HCHO), glyoxal (CHOCHO) and oxygen dimer (O₄) were successfully retrieved for the first time in Athens using spectral measurements from the ground-based MAX-DOAS instrument. The data cover the period from October 2012 to March 2014. The measurements were carried out at the premises of the National Observatory of Athens (NOA) in Penteli (38.0°N, 23.9°E, 527 m a.s.l.) under eight azimuthal directions and eight elevation angles.

Measurements at low elevation angles provide important information for investigating the spatial heterogeneity of pollution in the horizontal plane; the values of SC_{NO_2} , SC_{HCHO} and SC_{CHOCHO} for the +1° elevation angle and viewing direction towards the urban area range from 0.6 to $24 \cdot 10^{16}$, 0.8 - $9.6 \cdot 10^{16}$ και 0.3 - $5.2 \cdot 10^{15}$ molec·cm⁻² (average daily values for the whole period), respectively. The data were filtered with respect to the clouds, subtracting the days with heavy cloud cover, and only a small effect was found on the data. This result allowed the use of the retrieved SCDs for the temporal investigation (seasonal and daily) of the studied pollutants.

Seasonal variation characterized by summer maximum and winter minimum was observed for HCHO and CHOCHO due to photochemistry, while for NO_2 the maximum values were recorded during winter; in the polluted urban area, the winter levels are about 145% higher than during summer.

The the daily variation of the three trace gases on seasonal and weakly basis, shows a strong connection with primary anthropogenic sources regarding NO_2 and a weaker connection with anthropogenic sources - compared to photochemistry - regarding HCHO and CHOCHO . More specifically, NO_2 has a morning maximum at 10:00 LT which is attributed to traffic emissions during the morning rush hour. The daily variation of formaldehyde is characterized by a wide afternoon peak in winter and a strong maximum at 12:00 LT in summer. A similar variation was found for glyoxal in summer, while in winter it is different with a gradual increase from morning until noon. In addition, the effect of the etesian winds on the dispersion of pollutants is obvious and emphasizes the dominant role of the photochemical production of HCHO.

Reduced anthropogenic emissions over the weekend were found to affect the measured SC_{NO_2} values, reducing them by 30% -50%. This effect is less pronounced for HCHO and CHOCHO levels, which range from 3% to 17% and 3% -33%, respectively. This finding is expected for VOCs with strong biogenic emissions.

The contribution of the local urban sources to the total measured concentrations of the studied pollutants was investigated and the impact of the local circulation patterns was also assessed. It was found that the contribution of urban NO_2 sources is 45% during winter and 60% during summer and

the corresponding contribution of HCHO and CHOCHO sources ranges from 5% to 15% and 15-30% during daytime. Regarding the regional circulation patterns, it was found that high SC_{NO_2} values are related to westerly winds that transport air masses from the industrial area of the city. Respectively, the north and northeast winds contribute to the dispersion of pollutants and are associated with low NO_2 levels.

Overall, the analyses of the automated MAX-DOAS measurements over the Attica basin provided a detailed temporal and spatial distribution of NO_2 , HCHO and CHOCHO for more than one year. They gave a consistent picture of the daily, weekly and seasonal variations of the studied pollutants and their horizontal distribution. The resulting temporal and spatial patterns demonstrate: (i) the predominant contribution of anthropogenic sources to NO_x levels, (ii) the fact that VOCs are secondary products with additional primary sources other than anthropogenic, and (iii) the significant role of photochemistry in the pollution of Athens.

The text of this study, published in the international peer-reviewed journal Atmospheric Environment, is attached.



Contents lists available at ScienceDirect

Atmospheric Environment

journal homepage: www.elsevier.com/locate/atmosenv

Slant column MAX-DOAS measurements of nitrogen dioxide, formaldehyde, glyoxal and oxygen dimer in the urban environment of Athens



Myrto Gratsea^{a, b, *}, Mihalis Vrekoussis^{c, d, e}, Andreas Richter^c, Folkard Wittrock^c, Anja Schönhardt^c, John Burrows^c, Stelios Kazadzis^f, Nikos Mihalopoulos^{a, b}, Evangelos Gerasopoulos^a

^a Institute for Environmental Research and Sustainable Development, National Observatory of Athens, Greece

^b Environmental Chemical Processes Laboratory, Department of Chemistry, University of Crete, Greece

^c Institute of Environmental Physics and Remote Sensing, University of Bremen, Germany

^d Center of Marine Environmental Sciences – MARUM, Bremen, Germany

^e Energy, Environment and Water Research Center (EEWRC), The Cyprus Institute, Cyprus

^f Physikalisch-Meteorologisches Observatorium Davos, World Radiation Center, Switzerland

HIGHLIGHTS

- Slant column densities retrieved for the first time in Athens using a MAX-DOAS system.
- Diurnal and seasonal variability of NO₂ suggest link to anthropogenic emissions.
- Temporal variability of HCHO and CHOCHO suggests stronger link to photochemistry.
- Elevated NO₂ levels when W winds are prevailing, low levels under N-NE winds.
- The cloud influence is weak at the +1° elevation angle.

ARTICLE INFO

Article history:

Received 7 December 2015

Received in revised form

23 March 2016

Accepted 25 March 2016

Available online 1 April 2016

Keywords:

Ground-based MAX-DOAS

Tropospheric NO₂

Formaldehyde

Glyoxal

Oxygen dimer

Urban air pollution

ABSTRACT

Slant column (SC) densities of nitrogen dioxide (NO₂), formaldehyde (HCHO), glyoxal (CHOCHO) and oxygen dimer (O₄) were successfully retrieved for the first time in Athens, by using spectral measurements from a ground-based multi-azimuth Multi-AXis Differential Optical Absorption Spectroscopy (MAX-DOAS) system. The data span the period from October 2012 to March 2014 and measurements were conducted at NOAA's (National Observatory of Athens) station in Penteli (38.0°N, 23.9°E, 527 m a.s.l.) at eight azimuth angles and eight off-axis elevation angles. The SC_{NO2}, SC_{HCHO} and SC_{CHOCHO} measurements at +1° elevation angle, pointing towards the urban area, range from 0.6 to 24·10¹⁵, 0.8–9.6·10¹⁵ and 0.3–5.2·10¹⁵ molec·cm⁻² (mean daily values throughout the whole period), respectively. Seasonal modulation characterised by summertime maximum and wintertime minimum was observed for HCHO and CHOCHO, while for NO₂ the maximum values were recorded during winter. Changes in the diurnal variability of all trace gases with season and day of the week are investigated suggesting a strong link to primary anthropogenic sources for NO₂ and a weaker one, compared to photochemistry, for HCHO and CHOCHO. In addition, the impact of the reduced anthropogenic emissions during weekends on the measured SC values was quantified and 30%–50% lower SC_{NO2} values were found during weekends. The contribution of local urban emissions to the overall recorded amounts of the selected species was assessed. Using meteorological data from NOAA's station in Penteli, the impact of the local circulation patterns on the SC levels was estimated, and a strong relation between western wind direction, which is related to the industrial area, and enhanced SC measurements was found.

© 2016 Elsevier Ltd. All rights reserved.

* Corresponding author. Institute for Environmental Research and Sustainable Development, National Observatory of Athens, Greece.

E-mail addresses: mgratsea@noa.gr, gmyrto@hotmail.com (M. Gratsea).

Abstract. Slant column (SC) densities of nitrogen dioxide (NO_2), formaldehyde (HCHO), glyoxal (CHOCHO) and oxygen dimer (O_4) were successfully retrieved for the first time in Athens, by using spectral measurements from a ground-based multi-azimuth Multi-AXis Differential Optical Absorption Spectroscopy (MAX-DOAS) system. The data span the period from October 2012 to March 2014 and measurements were conducted at NOA's (National Observatory of Athens) station in Penteli (38.0°N, 23.9°E, 527 m a.s.l.) at eight azimuth angles and eight off-axis elevation angles. The SC_{NO_2} , SC_{HCHO} and $\text{SC}_{\text{CHOCHO}}$ measurements at +1° elevation angle, pointing towards the urban area, range from 0.6 to $24 \cdot 10^{16}$, 0.8 - $9.6 \cdot 10^{16}$ and 0.3 - $5.2 \cdot 10^{15}$ molec·cm⁻² (mean daily values throughout the whole period), respectively. Seasonal modulation characterised by summertime maximum and wintertime minimum was observed for HCHO and CHOCHO, while for NO_2 the maximum values were recorded during winter. Changes in the diurnal variability of all trace gases with season and day of the week are investigated suggesting a strong link to primary anthropogenic sources for NO_2 and a weaker one, compared to photochemistry, for HCHO and CHOCHO. In addition, the impact of the reduced anthropogenic emissions during weekends on the measured SC values was quantified and 30% - 50% lower SC_{NO_2} values were found during weekends. The contribution of local urban emissions to the overall recorded amounts of the selected species was assessed. Using meteorological data from NOA's station in Penteli, the impact of the local circulation patterns on the SC levels was estimated, and a strong relation between western wind direction, which is related to the industrial area, and enhanced SC measurements was found.

3.1 Introduction

Urban smog, a term coined from smoke and fog, is a frequent phenomenon in Athens since the 1980s, resulting from pollution emitted by anthropogenic activities related to intense urbanization and road traffic as well as partial industrialisation. During the last few decades, several studies have been carried out in Athens focusing on air pollution. These studies used in-situ measurements (e.g. Lalas et al., 1983, Barde and Button., 1990, Viras and Siskos, 1992, Ziomas et al., 1998, Kalabokas et al., 1999, Kalabokas and Repapis 2004), ground-based remote-sensing techniques, such as active DOAS and LIDAR (e.g. Avdikos et al., 2006, Kalabokas et al., 2012, Papayiannis et al., 2012, Psiloglou et al., 2013) and space-based observations (e.g. Vrekoussis et al., 2013). Here, we report on measurements performed in Athens with a novel passive Multi-Axis Differential Optical Absorption Spectroscopy (MAX-DOAS) instrument. In contrast to previous ground-based remote observations monitoring air composition at a fixed viewing direction, the deployed MAX-DOAS has the advantage of sequentially pointing at multiple azimuth angles. The instrument installed at the premises of National Observatory of Athens in Penteli (527m a.s.l., Fig. 1), scans the whole urban area of Athens providing information on both the vertical and the horizontal distribution of important trace gases in the troposphere above the Athens basin. In this work, MAX-DOAS slant column retrievals of nitrogen dioxide (NO_2), the oxygen dimmer (O_4), formaldehyde (HCHO) and glyoxal (CHOCHO) are presented for the time period from October 2012 until March 2014. The importance of these species is summarized below.

Nitrogen dioxide (NO_2) is an important tropospheric pollutant, participating among others, in catalytic cycles leading to ozone formation; it is destroyed by oxidation to nitric acid (Seinfeld and Pandis, 2006). It affects human health increasing the risk of respiratory symptoms (Chaloulakou et al., 2008, Schwartz

et al., 1991). In urban environments, its main source is fossil fuel combustion (e.g. Noxon, 1978). Although combustion processes emit NO_2 only in small quantities, they also emit nitrogen monoxide (NO) which rapidly forms NO_2 when reacting with ozone molecules. Over 50% of NO_x (NO plus NO_2) emissions in the urban environment of Athens are attributed to road transport (Markakis et al., 2010). Additional important NO_x sources in Athens are the industrial area (Elefsina) to the West-Southwest of the city center and the Piraeus port to the South-Southwest (Kassomenos et al., 1995). A large (31%) reduction in tropospheric NO_2 levels has been observed since 2008, as a result of the economic crisis (Vrekoussis et al., 2013). Due to its strong absorption lines in the visible region of the spectrum, NO_2 is readily observed using optical absorption spectroscopy (e.g. Brewer et al., 1973, Solomon et al., 1987).

Formaldehyde (HCHO) is an intermediate short-lived (Arlander et al, 1995) product of the oxidation of volatile organic compounds (VOCs) and of many hydrocarbons, including methane (CH_4) (Levy 1971, Finlayson and Pitts, 1976). Consequently, it can be used as an indicator for the presence of hydrocarbons and volatile organic compounds (VOCs) (Finlayson-Pitts and Pitts, 2000). Under particular meteorological conditions, an abundance of NO_x and VOCs with sufficient UVB radiation may lead to the development of photochemical smog (Seinfeld and Pandis, 2006). HCHO also contributes to the radical budget of the atmosphere mainly as a primary source for the hydroperoxy radical (HO_2) (Platt et al., 1979). Prior to this study there have been only sporadic measurements reported concerning formaldehyde amounts in Athens (Amanatidis et al., 1997, Klemm et al., 1998), with the exception of a study by Bakeas et al., (2002) where measurements for a six month time period are reported.

Glyoxal's (CHOCHO) presence in the atmosphere is attributed to the oxidation of VOCs (Calvert et al., 2000), since its primary emissions are believed to be small compared to its secondary sources (Volkamer et al., 2005). High concentrations of glyoxal have been reported in polluted urban environments (Volkamer et al., 2005) as well as over areas with high biogenic emissions (Wittrock et al., 2006; Vrekoussis et al., 2009; 2010). Moreover, glyoxal is a short-lived species, so it can be used as an indicator of VOC oxidation processes (Volkamer et al., 2005). Thus far, to our knowledge there are no reported CHOCHO measurements conducted in Athens.

The oxygen dimer (O_4) is the collision complex of two oxygen molecules (O_2)₂. It has several absorption bands in the near ultraviolet (UV), visible (VIS) and near infrared (IR) and it absorbs weakly under clear sky conditions (Perner and Platt, 1980). Given that the O_4 has a well known and almost constant vertical concentration profile, the absorption enhancement by O_4 can be used to calculate the mean optical path of the transmitted light (Pfeilsticker et al., 1997). MAX-DOAS measurements of O_4 at different elevation angles can provide information about the atmospheric aerosol profile, since aerosols change the optical path in a way which depends on their vertical distribution (Wittrock et al., 2004; Heckel et al., 2005; Wagner et al., 2004).

This paper is structured as follows: in Section 2 a presentation of the topography of the Athens basin is given followed by the description of the MAX-DOAS instrument and the DOAS technique used. Time series of the measurements, seasonal and diurnal cycles and the impact of wind fields on pollutants levels are presented in Section 3. The cloud influence on the measured SC densities is also investigated. Finally, in Section 4, the main conclusions of this study are presented.

3.2 Data and methodology

3.2.1 Site description

The particulate and gaseous pollutants levels in Athens are strongly influenced by the special topography of the city (Fig. 1). The city of Athens, along with Piraeus to the south, and their suburbs, is surrounded in a semicircular way by four mountains: Aegaleo (450 m) to the West, Parnitha (1400 m) to the North, Penteli (1100 m) to the Northeast and Hymettus (1050 m) to the East. The basin is open to the South and Southwest. Under specific meteorological conditions, Athens' topography favors the accumulation of atmospheric pollutants (Kassomenos et al., 1995).

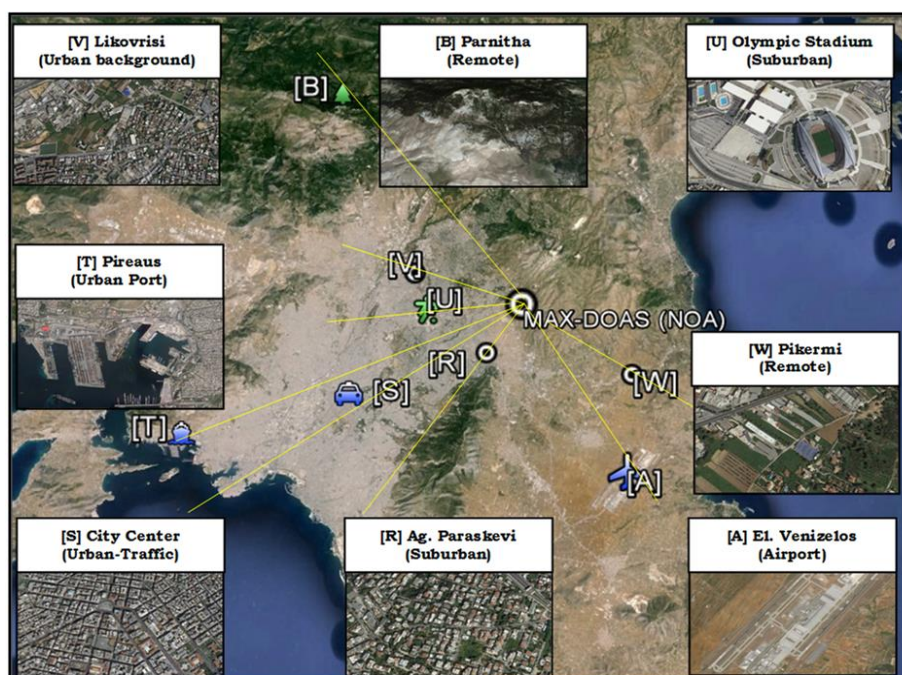


Figure 3.1. MAX-DOAS location at NOA's premises in Penteli mountain, and viewing directions over Athens.

3.2.2 Instrumentation and data retrieval

The MAX-DOAS instrument used in this study is part of the BREDOM network (Bremian DOAS network for atmospheric measurements, http://www.iup.uni-bremen.de/doas/groundbased_data.htm). It is installed in Penteli (38.05°N, 23.86°E, 527m a.s.l) at the premises of the National Observatory of Athens (Fig. 2, left panel).

Briefly, the instrument comprises a telescope unit, connected via an optical fiber bundle to a grating spectrometer (LOT 260S, 600l/mm ruled grating) equipped with a cooled (-40°C) CCD detector (Andor 2048 x 512 pixels). The spectral coverage of the spectrometer is 330 – 500 nm with a spectral resolution

of approximately 0.7 nm. The telescope unit is mounted on a pan-tilt-head (Fig. 2, right panel) in order to be able to point towards any direction in the sky. The field of view of the telescope is about 1°.



Figure 3.2. Telescope of the MAX-DOAS instrument installed at the premises of the National Observatory of Athens (left panel). Panoramic view of the azimuth scan (right panel).

During routine operation, measurements are performed at various azimuth and elevation angles as well as to the zenith. Eight elevation angles relative to the horizon were selected: -1° , 0° , $+1^\circ$, $+2^\circ$, $+4^\circ$, $+8^\circ$, $+15^\circ$ and $+30^\circ$. Since the greater part of the optical path is in the lower troposphere, measurements at low elevation angles have higher sensitivity to the concentration of absorbing trace species close to the surface (Hönninger et al., 2004, Wittrock et al., 2004). Concerning the azimuthal direction, eight viewing azimuth angles with respect to south were selected: -60° , -30° , 40° , 52.5° , 65° , 77.5° , 100° and 140° . For simplicity we refer to these directions as W, A, R, S, T, U, V and B respectively (Fig. 2). Although there is unobstructed view towards all directions, direction 'B' pointing towards the Parnitha mountain cannot be considered as completely unobstructed since Parnitha's altitude is 1400 m and its distance from Penteli's station is about 15 km. Direction 'V' is characterised as urban background, 'U' and 'R' as suburban, 'T' and 'S' are typical urban directions, 'A' is pointing to the airport and 'W' is a remote unobstructed direction. The duration of one full scanning cycle through all directions is about 15 minutes. The instrument has been operating continuously since October 2012.

The acquired spectra are analysed using the DOAS technique (Differential Optical Absorption Spectroscopy, Platt and Stutz 2008), which applies the Beer-Lambert's law. The optical thickness, i.e. the logarithm of the ratio of the observed to a reference spectrum, is separated into two components: a high and a low frequency one. The absorption by trace gas molecules and the signature of rotational Raman scattering (Ring effect) are represented by the high frequency part, while the attenuation by scattering processes in the atmosphere and the low-frequency part of the absorption are represented by the low frequency part. The determination of the differential slant column density (SC), which is the product of the retrievals, is then achieved by fitting to the optical depth (a) the laboratory cross-sections of the retrieved species (Table 1) and (b) a polynomial accounting for the low-frequency component. The polynomial used is of degree 4 for NO_2 , HCHO and O_4 and of degree 3 for CHOCHO. Slant column densities for NO_2 , HCHO, CHOCHO and O_4 have been retrieved employing specific fitting windows for each trace gas (Table 1). Figure 3 depicts four characteristic fits for NO_2 , HCHO, CHOCHO and O_4 . Typical detection limit values for near noon conditions at $+1^\circ$ elevation angle are 2.7×10^{-14} molec/cm² for NO_2 , 3.5×10^{-15} molec/cm² for HCHO and 2.1×10^{-14} molec/cm² for CHOCHO.

Table 3.1. Spectral fitting windows and absorption cross sections used in the data analysis.

Molecule	Fitting windows (nm)	Absorption cross sections
NO ₂	425 - 490	Vandaele et al. [1997]
HCHO	336 - 359	Meller and Moortgat [2000]
CHOCHO	434 - 458	Volkamer et al. [2005]
O ₄	338 - 380	Hermans et al. [2003]

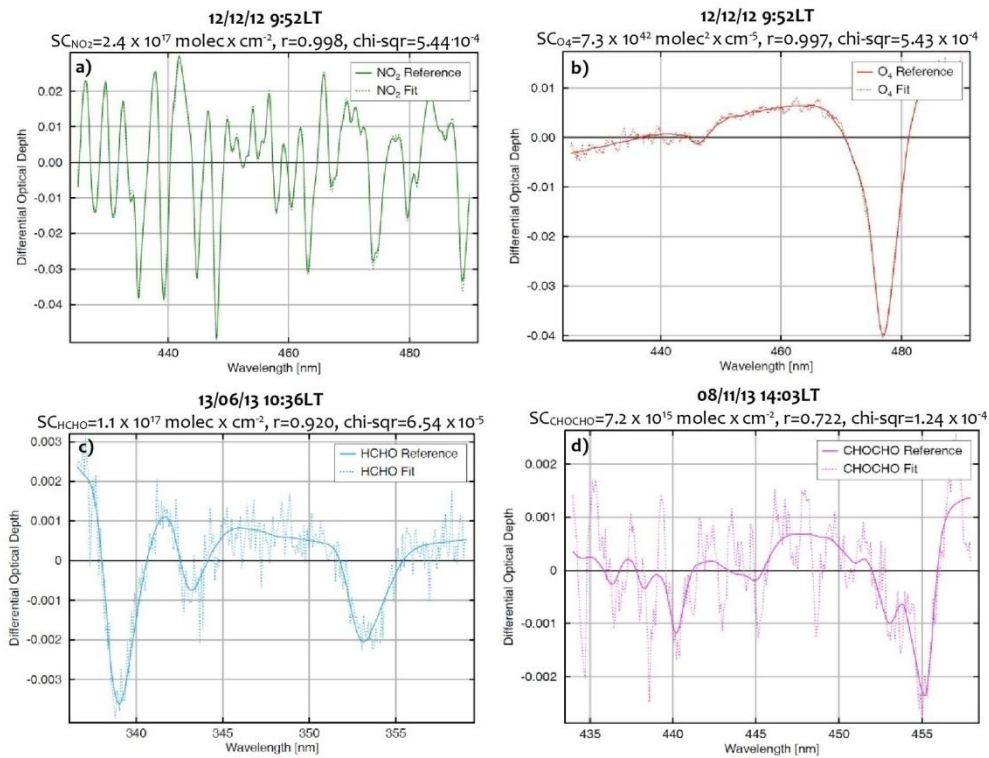


Figure 3.3. Example of NO₂ (fig. 3a), O₄ (fig.3b), HCHO (fig. 3c) and CHOCHO (fig. 3d) DOAS fits. The solid line depicts the reference cross section scaled to the slant column values, and the dashed line depicts the fit (sum of scaled cross-section and residual).

The spectrum used as reference is the concurrent zenith observation obtained within the same measurement cycle for each measurement in the off-axis viewing angles. Hence, the retrieved SC corresponds to the difference in slant columns between the spectrum observed at lower elevation and the concurrent zenith sky measurement. The concentration as a function of altitude could be estimated by using a profiling algorithm (e.g. Roscoe et al., 2014). In this work, we focus on the spatial and temporal variability of the trace gases, which can already be discussed using the differential slant columns. Similarly, differential slant column densities have also been used in other studies for characterising atmospheric conditions (e.g. Leigh et al., 2007, Heckel et al., 2005, Wagner et al., 2004, Hönninger et al., 2002).

During the period from October 2012 to March 2014, 480 days of MAX-DOAS data were recorded, leading to an overall data capture of 89%. In order to limit the possible impact of stratospheric absorption interferences on the measurements and to simplify the interpretation of results, values corresponding to solar zenith angles (SZA) larger than 75° degrees were not considered.

For the interpretation of the results, detailed meteorological data (wind-speed, wind-direction and temperature) retrieved from the ground-based station of the National Observatory of Athens in Penteli (<http://penteli.meteo.gr/stations/penteli/>), is also used.

3.3 Results and discussion

3.3.1 Data presentation and basic statistical analysis

In order to investigate the spatial homogeneity of the measurements, the correlation coefficients between NO₂ measurements at the +1° (representative of the layer close to the surface) and +30° (representative of the integrated tropospheric column including higher layers) elevation angles in all azimuthal directions were calculated (Table 2). As expected, high correlations are revealed between neighboring azimuthal directions. In line with this finding, direction ‘S’ pointing at the city center, has been chosen as typical to characterise urban air quality in Athens. Respectively, direction ‘W’, which is a sparsely populated area, has been chosen as characteristic of remote environment conditions. These two directions are henceforth used for the presentation of the results. Measurements at +30° elevation show higher correlation coefficients (not shown here), since at higher elevations the measurements are less sensitive to lower troposphere and boundary layer pollution (Wittrock et al., 2004, Hönninger et al., 2004, Platt and Stutz 2008) and thus less affected by changes in surface pollution levels. In addition, the spatial separation between the measurement volumes in the lower troposphere is considerably smaller at +30° than at +1° elevation for geometrical reasons, reducing gradients and increasing correlation.

Table 3.2. Correlation matrix of SC_{NO2} for all viewing directions at +1° elevation angle. The values in the gray box show the high correlation between all the directions pointing to the city centre.

Directions	W	A	R	S	T	U	V	B
W		0.963	0.743	0.732	0.726	0.735	0.751	0.821
A	0.963		0.836	0.810	0.790	0.785	0.773	0.804
R	0.743	0.836		0.985	0.949	0.911	0.826	0.728
S	0.732	0.810	0.985		0.984	0.954	0.877	0.772
T	0.723	0.790	0.949	0.984		0.987	0.931	0.825

U	0.735	0.785	0.911	0.954	0.987	0.966	0.866
V	0.751	0.773	0.826	0.877	0.931	0.966	0.938
B	0.821	0.804	0.728	0.772	0.825	0.866	0.938

The time series of daily-averaged SC densities for the remote (W) and urban (S) area are presented in Figure 4. Basic statistical quantities for NO₂, HCHO, CHOCHO and O₄ are presented in Figure 5. The analysis is based on the daily values and refers to the entire measurement period.

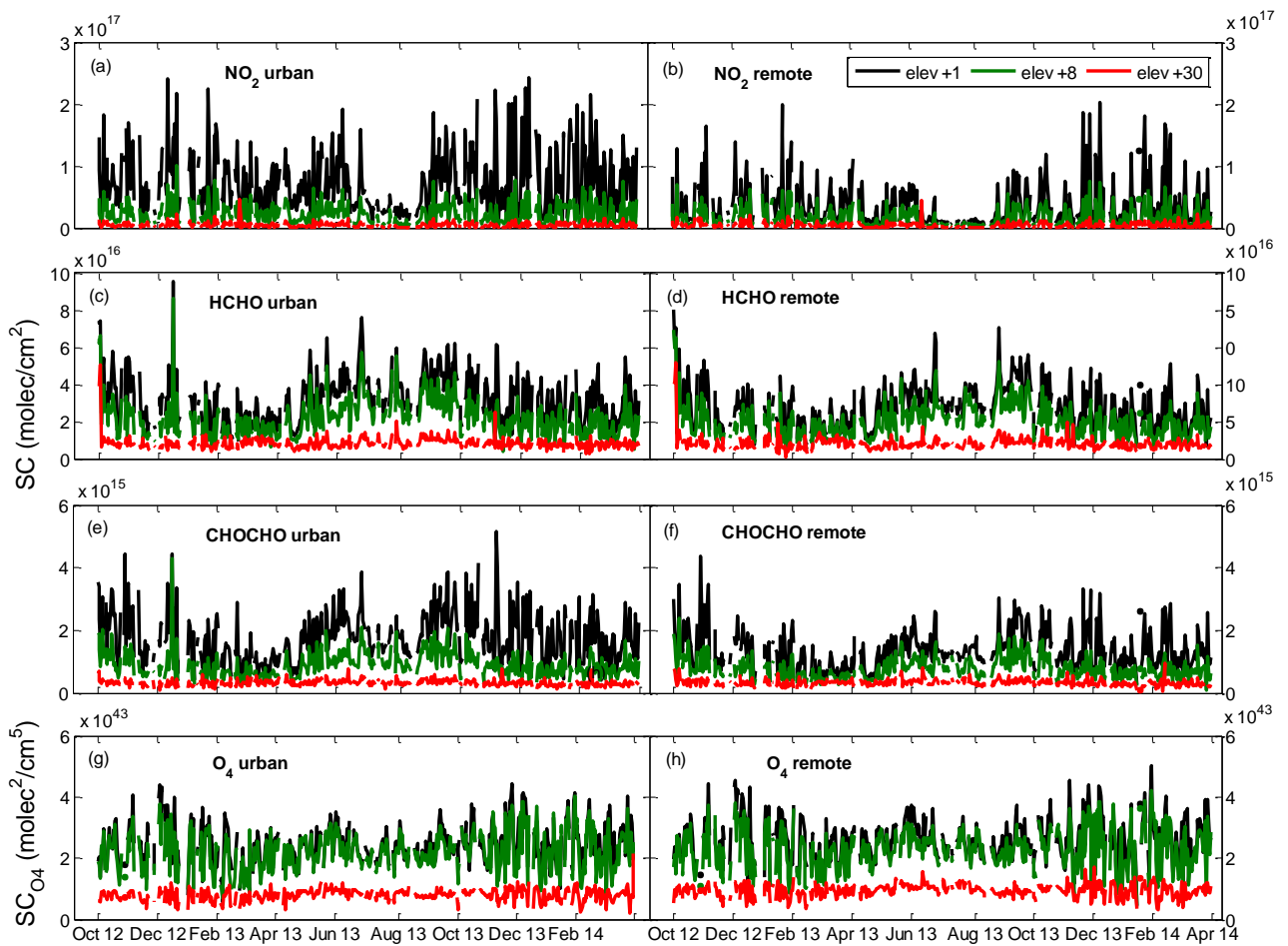


Figure 4. Time series of daily-mean SC density values for three elevation angles (black, green and red lines represent +1°, +8° and +30° elevation angles, respectively) for urban (left panels) and remote (right panels) area for NO₂, HCHO, CHOCHO and O₄.

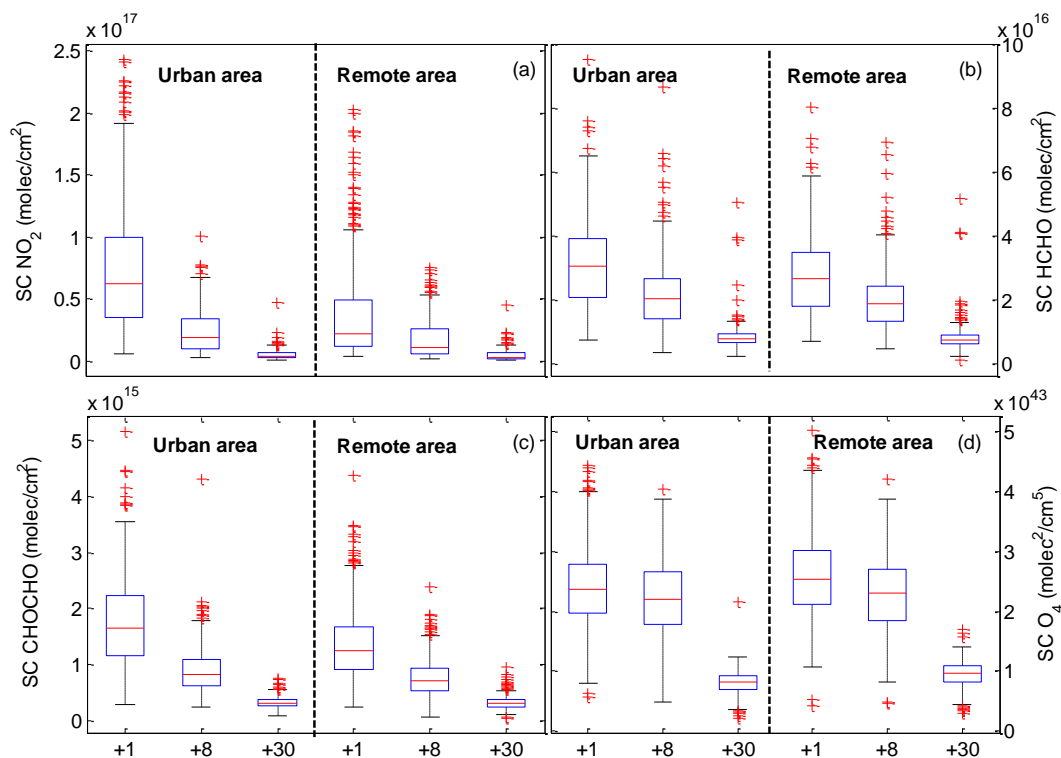


Figure 5. Whisker plots for three elevation angles ($+1^\circ$, $+8^\circ$ and $+30^\circ$) for urban (left triplet on each subplot) and remote (right triplet on each subplot) area for NO_2 , HCHO , CHOCHO and O_4 resulting from daily values. On each box the central red line is the median, the edges of the box are the 25th and 75th percentiles. The whiskers extend to the most extreme data points, not considering outliers which are represented by the red crosses. The value considered as outlier is any value that lies more than one and a half times the length of the box from either end of the box.

At first, an obvious observation is that the difference in SC_{NO_2} densities as a function of elevation angle is greater over the polluted area (Figure 4a and 4b), in agreement with earlier findings (Hönninger et al., 2004, Leigh et al., 2007). The enhanced values of SC_{NO_2} at lower elevation angles are explained by: a) longer optical light path within the boundary layer (Wittrock et al., 2004, Hönninger et al., 2004, Platt and Stutz, 2008) and b) higher NO_2 levels at lower levels as result of surface emission sources. This is why the difference between the remote and urban direction become more apparent at low elevation angles. In particular, at $+1^\circ$ elevation, the SC_{NO_2} densities in the urban direction are on average twice as high as in the remote direction, while for $+8^\circ$ and $+30^\circ$ elevations the excess is 38% and 5%, respectively. Based on daily SC_{NO_2} values at $+1^\circ$ elevation angle, the daily SC_{NO_2} levels for the urban area vary from $0.6 \cdot 10^{16} \text{ molec}\cdot\text{cm}^{-2}$ to $24 \cdot 10^{16} \text{ molec}\cdot\text{cm}^{-2}$, with an average value of $(7.3 \pm 4.7) \cdot 10^{16} \text{ molec}\cdot\text{cm}^{-2}$. The corresponding values for the remote area range from $0.3 \cdot 10^{16} \text{ molec}\cdot\text{cm}^{-2}$ to $20 \cdot 10^{16} \text{ molec}\cdot\text{cm}^{-2}$ with an average value of $(3.7 \pm 3.5) \cdot 10^{16} \text{ molec}\cdot\text{cm}^{-2}$. The seasonal variation of the SC_{NO_2} in the urban and remote area is discussed in detail in section 3.2.

SC_{HCHO} time series are shown in Figures 4c and 4d. Once more, the difference between the remote and urban area is most evident at $+1^\circ$ elevation angle: the SC_{HCHO} densities over the urban area are higher by an average of 13%. Similar difference (9%) is found at $+8^\circ$ elevation while almost no difference is noted at the $+30^\circ$ elevation. Overall, over the urban area the daily SC_{HCHO} values at $+1^\circ$ elevation angle

vary from a minimum of $0.8 \cdot 10^{16}$ molec \cdot cm $^{-2}$ to a maximum of $9.6 \cdot 10^{16}$ molec \cdot cm $^{-2}$, with an average value of $(3.1 \pm 1.3) \cdot 10^{16}$ molec \cdot cm $^{-2}$. The corresponding values for the remote area range from $0.7 \cdot 10^{16}$ molec \cdot cm $^{-2}$ to $8.1 \cdot 10^{16}$ molec \cdot cm $^{-2}$ with an average of $(2.8 \pm 1.2) \cdot 10^{16}$ molec \cdot cm $^{-2}$ (Fig. 5).

Figures 4e and 4f present daily SC_{CHOCHO} values. CHOCHO measurements at +1° elevation angle are on average 30% higher in the urban direction compared to the remote direction, while the corresponding excess for +8° elevation angle is 16%. Similarly to NO₂ and HCHO measurements, almost no difference is observed for the +30° elevation. The average SC_{CHOCHO} value for the urban area is $(1.8 \pm 0.8) \cdot 10^{15}$ molec \cdot cm $^{-2}$ and the corresponding value for the remote is $(1.4 \pm 0.6) \cdot 10^{15}$ molec \cdot cm $^{-2}$ (Fig. 5).

From Figure 4 it is clearly deduced that the difference in SC values between low and higher elevation angles is larger for NO₂ compared to HCHO and CHOCHO, indicating that the NO₂ vertical profile is more strongly weighted to the lower troposphere than that of the secondary VOCs which are produced in the atmosphere itself.

Finally, the daily SC_{O₄} values are presented in Figures 4g and 4h for the urban and remote directions, respectively. The SC_{O₄} of the lower viewing directions are well separated from the +30° elevation, except for specific days when the retrieved SC_{O₄} at the different elevation angles converge. This convergence is indicative of increased aerosol load during these days; aerosols decrease the length path of the photons, so the observed O₄ absorption is also reduced. Thus, the slant columns at different elevation angles result in similar levels due to similar light paths (Wittrock et al., 2004, Wagner et al., 2004, Heckel et al., 2005). This pattern appears more frequent during springtime and it is associated to dust transport from North Africa (Gerasopoulos et al., 2006), but also during wintertime due to increased aerosol emissions (domestic heating sources) (Gerasopoulos et al., 2014; Paraskevopoulou et al., 2015). Clouds also play an important role, especially for observations close to the horizon, by changing the average light path and thus the expected actual slant column. The small difference of SC_{O₄} levels during the whole period between the +1° and the +8° elevation angle has also been reported, even during clear days, in other studies (e.g. Wagner et al., 2004). The O₄ levels do not seem to vary significantly between the remote and the urban area indicating: a) relatively small gradients in aerosol load and b) that the differences observed in the trace gas SCs for different azimuth angles are not the result of differences in light path length.

3.3.2 Seasonal variability

The monthly average SC densities for the retrieved species are presented for the typical remote and urban area, for all elevation angles (Fig. 6). A clear seasonal cycle is observed for SC_{NO₂}, with winter maxima and summertime minima (Fig. 6a). Winter versus summer shows 80% and 180% higher values for the urban and for the remote area (+1° elevation angle), respectively. Reduced NO₂ levels during summer can be attributed to: (a) lower anthropogenic NO_x emissions during summer vacations (Kalabokas et al., 1999) mainly as result of reduced traffic, and enhanced anthropogenic emissions during winter due to fossil fuel burning for heating purposes, (b) the prevailing Etesian Northern winds encountered mainly during July and August (e.g. Pezzoli, 2005) characterising 54 out of the 62 days and leading to efficient removal of pollution from the Athens' basin, (c) lower dispersion efficiency in winter due to near surface thermal inversion resulting in shallower boundary layer with high NO₂

concentrations and (d) longer NO_2 lifetime in winter due to decreased NO_2 photolysis rate, along with reduced hydroxyl radical levels, which leads to reduced conversion of NO_2 to HNO_3 .

A clear seasonal variation is also observed for HCHO (Fig. 6b). The increased summer levels of SC_{HCHO} are attributed to the photochemical production of HCHO. It has been previously estimated that the photochemical production of HCHO in Athens represents 83% of the measured formaldehyde during summer, while the corresponding ratio for winter is 33% (Bakeas et al., 2003). The average SC_{HCHO} at $+1^\circ$ elevation angle are 37% higher during summer months (June to August) compared to winter months (December to February), both for the urban and the remote direction. During summer, lower SC_{HCHO} values are encountered in July and August. Although the solar irradiation is still high during these two months, the efficient ventilation by the strong Etesian Northern winds, which favors the effective dispersion of pollutants, along with lower primary HCHO emissions, can result in reduced HCHO levels. Similar seasonal variation of HCHO has been reported for urban areas in several studies (e.g. Tanner and Mong 1984, Ho et al., 2002, Possanzini et al., 1996). However, only sporadic measurements of HCHO have been reported for Athens in the past (Klemm et al., 1998, Amanatidis et al., 1997) and just two works which report on the seasonal variation (Kalabokas et al., 1997, Bakeas et al., 2003). In particular, Kalabokas et al. (1997) found no clear seasonal variation of HCHO in Athens, in agreement with the later observations of Bakeas et al. (2003). At first, the relatively small difference in SC_{HCHO} values between remote and polluted areas in this study (Fig. 6b), suggests that the impact of direct anthropogenic sources on HCHO levels is small. However, after taking into account the different photochemical production of HCHO in winter and summer (33% and 83% respectively), as calculated by Bakeas et al. (2003) for distinguishing photochemical from anthropogenic HCHO production, a potential link between HCHO levels and anthropogenic sources can be deduced. More specifically, for the urban area the calculated average SC_{HCHO} value attributed to non photochemical sources is $1.89 \cdot 10^{16} \text{ molec}\cdot\text{cm}^{-2}$ in winter and $0.65 \cdot 10^{16} \text{ molec}\cdot\text{cm}^{-2}$ in summer. This indeed suggests the potential impact of anthropogenic sources on SC_{HCHO} levels, reflecting the intensification of human activities during winter.

A similar to HCHO seasonal pattern is also observed for CHOCHO (Fig 6c). CHOCHO is only produced by VOCs having at least 2C atoms, whereas HCHO is produced by the oxidation of methane as well by VOC having 2 or more carbons. They are both removed from the boundary layer and the lower troposphere by photolysis and reaction with OH. However, CHOCHO reacts with OH and is photolysed more rapidly than HCHO, thus it has shorter chemical lifetime. Provided that the source of VOCs is at the surface and that the production of HCHO is dominated by VOCs, then both HCHO and CHOCHO have practically the same source, and their seasonal variability is likely to be similar close to source regions. However their horizontal and vertical distributions are expected to be different in a transported and chemically transformed pollution plume. The average $\text{SC}_{\text{CHOCHO}}$ densities are about 23% and 15% higher during summer compared to winter, for the urban and the remote area ($+1^\circ$ elevation angle), respectively. CHOCHO presents a more distinct difference between the remote and the polluted direction compared to HCHO, which indicates a potentially stronger relation to direct anthropogenic sources. The link to direct anthropogenic sources is also supported by the smaller difference found between summer and winter months.

The O_4 seasonal variation is not so pronounced (Fig 6d). From February to April the difference between low and high elevation measurements is smaller indicating stronger extinction, which could be attributed to high aerosol load in the atmosphere. Stronger extinction is also reflected by the slightly

(approximately 10%) lower levels of SC_{O_4} during these months. No considerable difference regarding the levels between remote and urban area is noted and this could be attributed to the fact that O_4 absorption depends on many factors (clouds, dust, visibility) apart from anthropogenic aerosols, which are characteristic of the urban area. Clouds and Saharan dust affect the remote and urban measurements almost in the same way, since most of the time their horizontal distribution is uniform. Additionally, the small difference could also be attributed to efficient aerosol transport from the city to the background areas throughout the day.

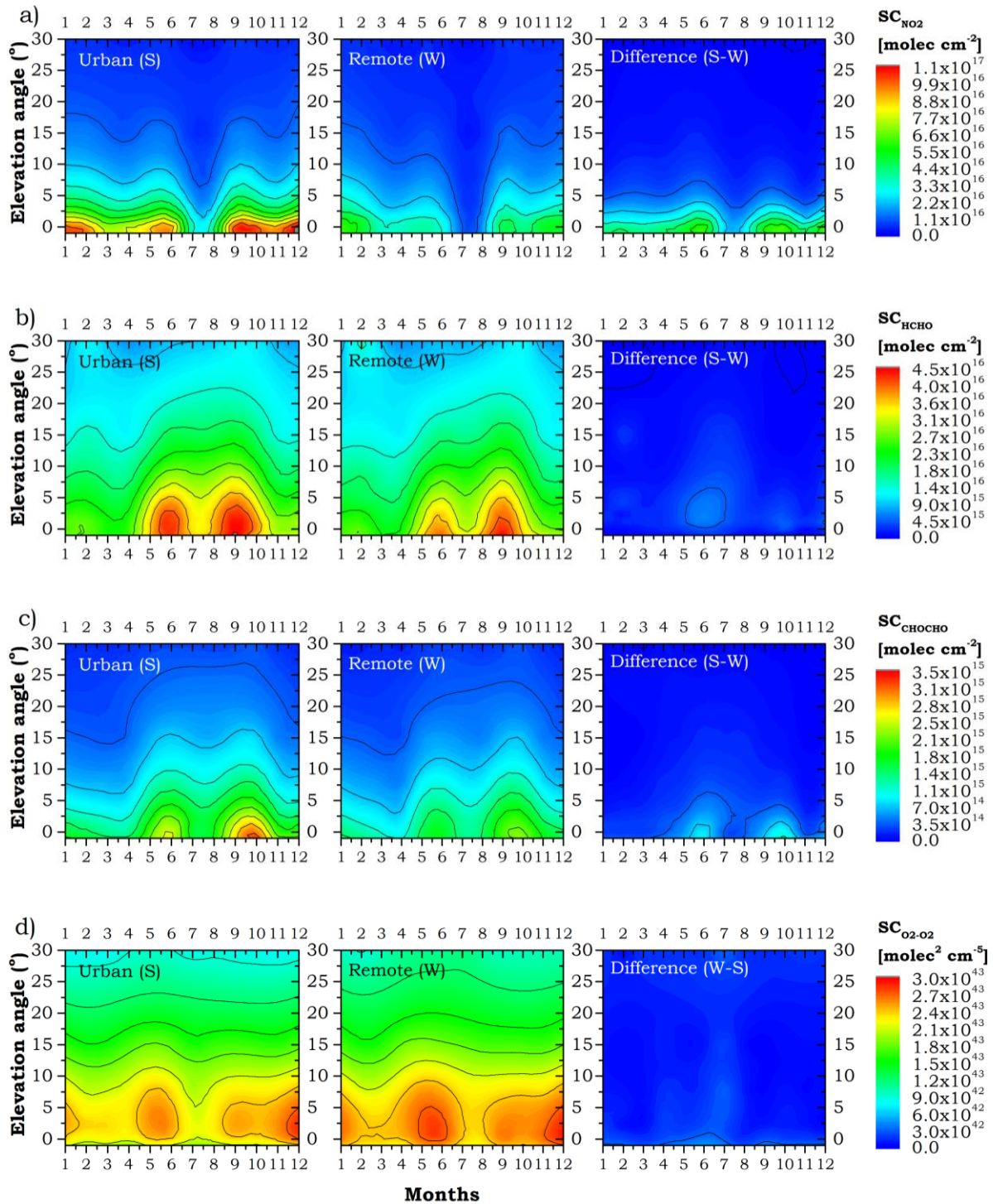


Figure 6. Monthly average SC densities for NO₂ (a), HCHO (b), CHOCHO (c) and O₄ (d) for all elevation angles for polluted (left column) and remote (central column) areas. The right column depicts the difference between the remote and the urban area.

3.3.3 Cloud screening

During the 1.5 year of MAX-DOAS observations, days with high cloud and aerosol load have occurred, possibly «contaminating» the obtained SC densities by influencing the atmospheric radiative transfer and thus affecting the analysis of the observations. To address this restriction for further analyses, meteorological observations from the National Observatory of Athens for cloud coverage were used to screen out cases with large cloudy cover. Overall, 30% of the measurements were removed by the cloud screening. Figure 7 shows the monthly means of SC densities for all four retrieved trace gases with and without cloud screening at the +1° elevation.

In general, no significant differences are observed, suggesting that uncertainties in the following analyses for the +1° elevation due to cloud influences are small and do not affect the findings. This can be understood by the fact that most clouds are above the main light path of the 1° viewing direction which is nearly horizontally. Greater influence was found, as expected, during winter months. In general, for NO₂ the mean difference for the urban area is 5%, for HCHO, CHOCHO and O₄ the difference is 6%, 8% and 3%, respectively. No difference exceeding 20% was found, even during months with frequent heavy cloud conditions (November-December). Concluding, the effect of clouds on SC retrieved for the +1° elevation does not considerably alter the interpretation of the results. Therefore, the following analyses focus on +1° elevation measurements.

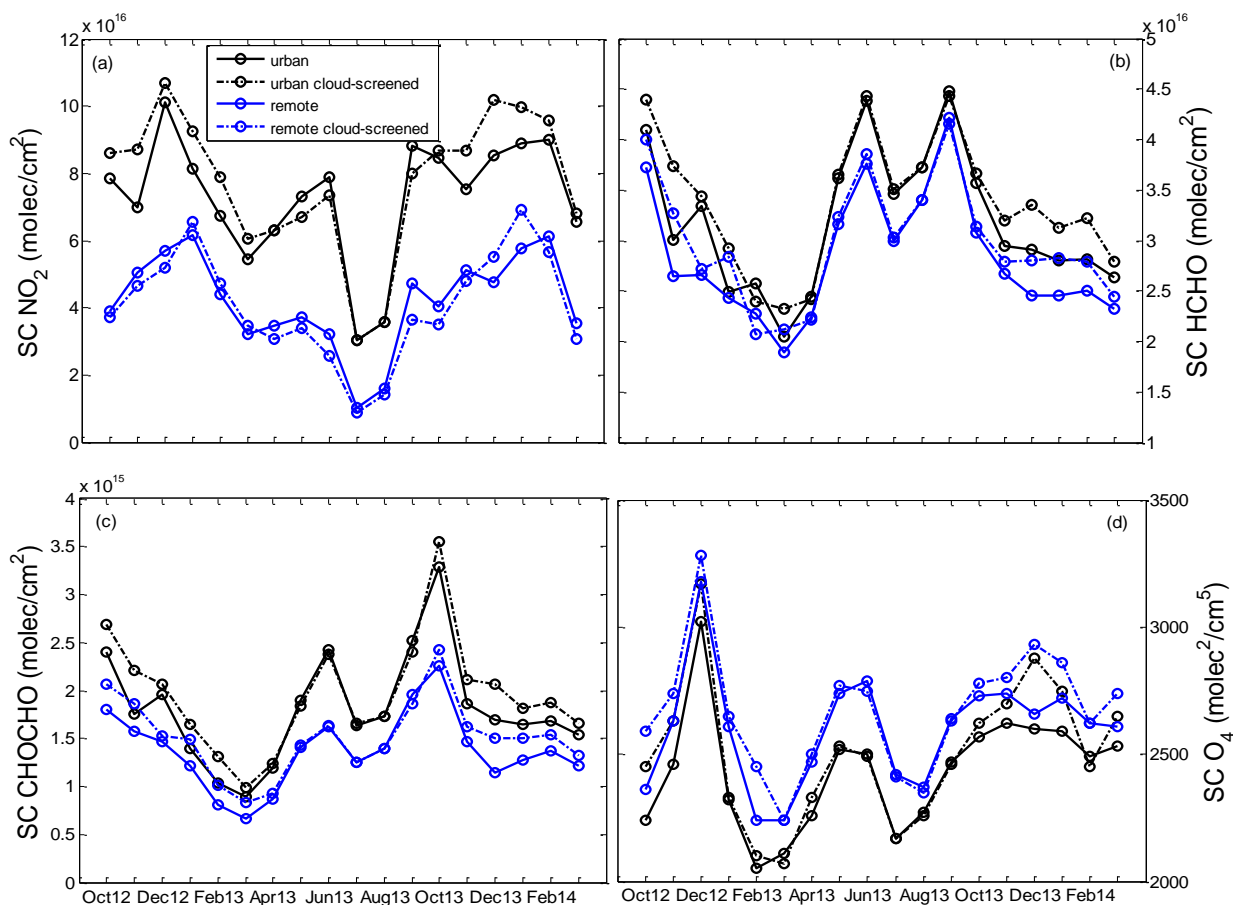


Figure 7. Monthly average SC densities for NO_2 (a), HCHO (b), CHOCHO (c) and O_4 (d) for the $+1^\circ$ elevation angle for urban (black lines) and remote (blue lines) areas with (dashed lines) and without (solid lines) cloud screening.

3.3.4 Diurnal variation and weekend effect

The mean diurnal course of the retrieved species SC densities at $+1^\circ$ elevation angle was calculated separately for the cold (November-March) and the warm period (April-October). The mean daily temperature value of the cold and the warm period was 9.8°C and 20.6°C , respectively. The diurnal profiles were obtained by averaging data of 215 days for the warm period and of 265 days for the cold period. Additionally, taking into account that air pollution in Athens is influenced by wind conditions, we examine the effect of air masses originating from polluted (S-SW) and rural (N) areas to the MAX-DOAS observations towards the urban and the remote area respectively. For that purpose, diurnal profiles were calculated separately considering data just for days when wind direction was between 180° and 270° (S-SW) for the urban area and between 315° and 45° (N) for the remote area. This separation gives us more detailed information about the influence of the origin of the air masses on the MAX-DOAS observations. Local time (LT) is used for drawing conclusions about the effect of human activities on the results (cold period $\text{LT}=\text{UTC}+2$, warm period $\text{LT}=\text{UTC}+3$).

The diurnal cycle of SC_{NO_2} (Fig. 8) seems to be rather different between the cold and the warm period, with the main discrepancy found in the afternoon. In all cases, a morning maximum at around 10:00 LT is observed due to increased traffic related NO_x emissions (rush hours in Athens are estimated to

be from 08:00 LT until 11:00 LT, Katsoulis 1995, Kourtidis et al., 1999). The steady build up of NO_2 starts with the beginning of the morning rush hour until noon. The diurnal maximum of NO_2 , emerging 2 hours after the beginning of the traffic rush hour, is explained by NO_x chemistry; vehicles emit NO which then reacts with ozone or peroxy radicals and produces NO_2 . Later in the day, the NO_2 dissociation due to photochemical processes (Boersma et al., 2008), along with the growth of the boundary layer, lead to NO_2 decline. In the evening, a second maximum appears around 15:00 LT during winter, while in summer NO_2 keeps reducing until late evening. This could be attributed to the different winter and summer boundary layer evolution, along with more intense photochemistry occurring during summer. In winter the photochemical processes start to decelerate soon after noon, while NO_x is still being emitted, producing the second maximum of the day, both in the remote and in the urban area. It is worth noting that the warm and cold period diurnal cycles of SC_{NO_2} exhibit the typical urban daily pattern (e.g. Bigi and Harrison 2010) and are in agreement with other in-situ measurements for Athens (e.g. Kalabokas and Bartzis 1998, Moussiopoulos et al., 1998, Rappenglück et al., 1998, Katsoulis 1995). Peaks are more distinct during weekdays compared to weekends, in both remote and urban area, and this is related to higher anthropogenic activity, mainly traffic.

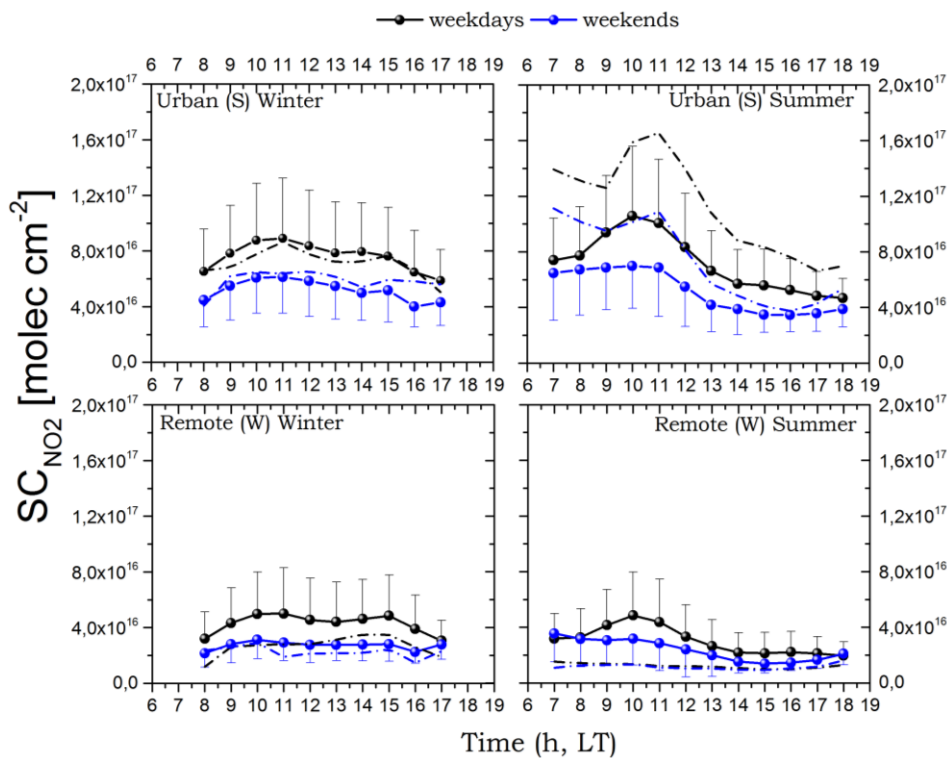


Figure 8. Average diurnal variation of SC_{NO_2} densities, at $+1^\circ$ elevation angle, for each period (warm and cold) for the observations towards the remote and the urban areas. The black and blue lines represent the weekdays and the weekends respectively. The solid lines represent the diurnal variation as obtained by averaging all data for the warm and the cold period separately. The dashed lines depict the result in diurnal variation considering data just for days when wind direction is between 180° and 270° for the urban area and between 315° and 45° for the remote area. The vertical lines represent the standard deviation of the variable for each point. To avoid busy graphs, only one part of the bar is presented, implying similar size in both sides.

Many factors such as hydrocarbons and VOCs emissions by motor vehicles, photo-oxidation of hydrocarbons as well as photolysis of HCHO could impact the observed HCHO diurnal course. The observations point out that during the cold and warm periods the diurnal patterns differ (Fig. 9). In the cold period, there is a small morning peak, indicative of the presence of anthropogenic sources (vehicular exhaust and central heating), and a broader afternoon peak in the urban area. Although the statistical significance of the morning peak cannot be supported due to the large error bars, it should be noted that its presence is repeated in both areas. The increase of HCHO begins much earlier in the cold (peak at 09:00 LT) than in the warm (peak at 11:00 LT) period in the urban area. This is possibly due to high ambient humidity during winter, which triggers the formation of HONO (heterogeneous hydrolysis of NO₂ on aerosol surfaces) initiating urban photochemistry (Atkinson et al., 2000). During the warm period there is a maximum around noon and a steady decrease afterwards, especially in the remote area, suggesting that photochemistry plays a dominant role in HCHO production during summer. Regarding to the weekend effect on HCHO, there is almost no difference between weekdays and weekends, which is an indication of weak link to direct anthropogenic sources. The only exception to this is the winter morning maximum during weekdays, which is repeated in both site types.

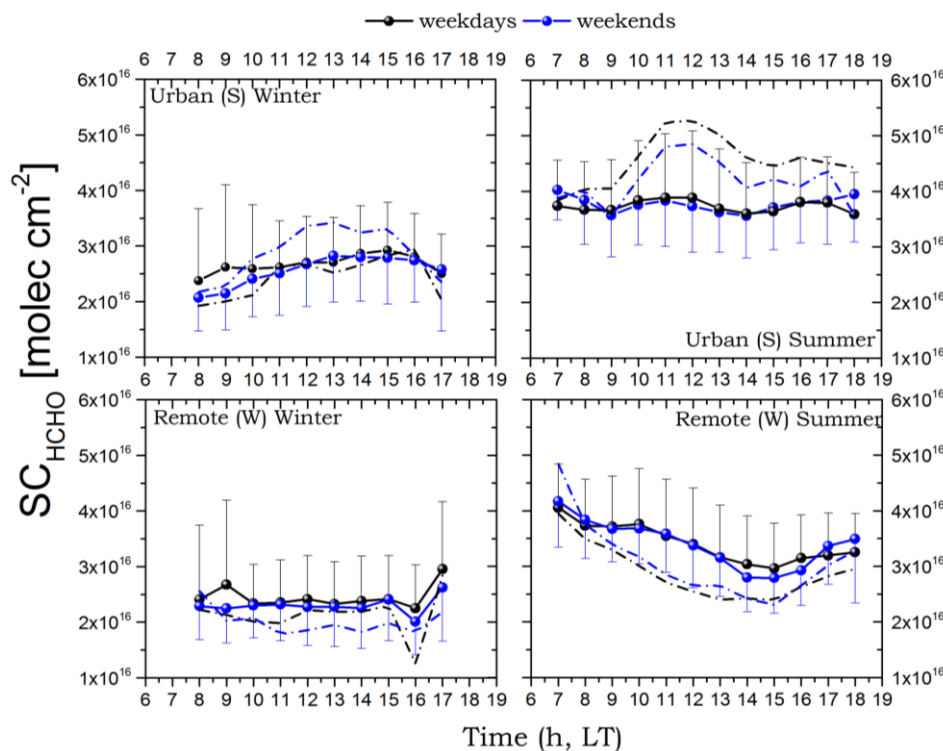


Figure 9. Average diurnal variation of SC_{HCHO} densities, at $+1^\circ$ elevation angle, for each period (warm and cold) for the observations towards remote and urban areas. The black and blue lines represent the weekdays and the weekends respectively. The solid lines represent the diurnal variation as obtained by averaging all data for the warm and the cold period separately. The dashed lines depict the result in diurnal variation considering data just for days when wind direction is between 180° and 270° for the urban area and between 315° and 45° for the remote area. The vertical lines represent the standard deviation for each point as described in Fig.7.

SC_{CHOCHO} increases rapidly shortly after sunrise both in the warm and in the cold period (Fig.10). This increase highlights intense VOC oxidation processes during morning hours. The persisting high

CHOCHO levels during the cold period, even after solar noon, reflect either a higher glyoxal production rate compared to the photochemical loss or a reversible partitioning into the aerosol phase (e.g. Knote et al., 2014). In contrast, during the warm period there is a clear maximum at 12:00 LT followed by a sharp decrease. This pattern reflects that CHOCHO photochemical loss begins to be dominant during the warm period at small SZAs and continues to be important for the rest of the day after solar noon (Volkamer 2005). No distinct difference is observed in the patterns between weekdays and weekends, with SC_{CHOCHO} levels being slightly lower during winter weekends, while in summer the peak is more intense during weekdays. More detailed discussion about the weekend effect on the retrieved species is provided in the next two paragraphs.

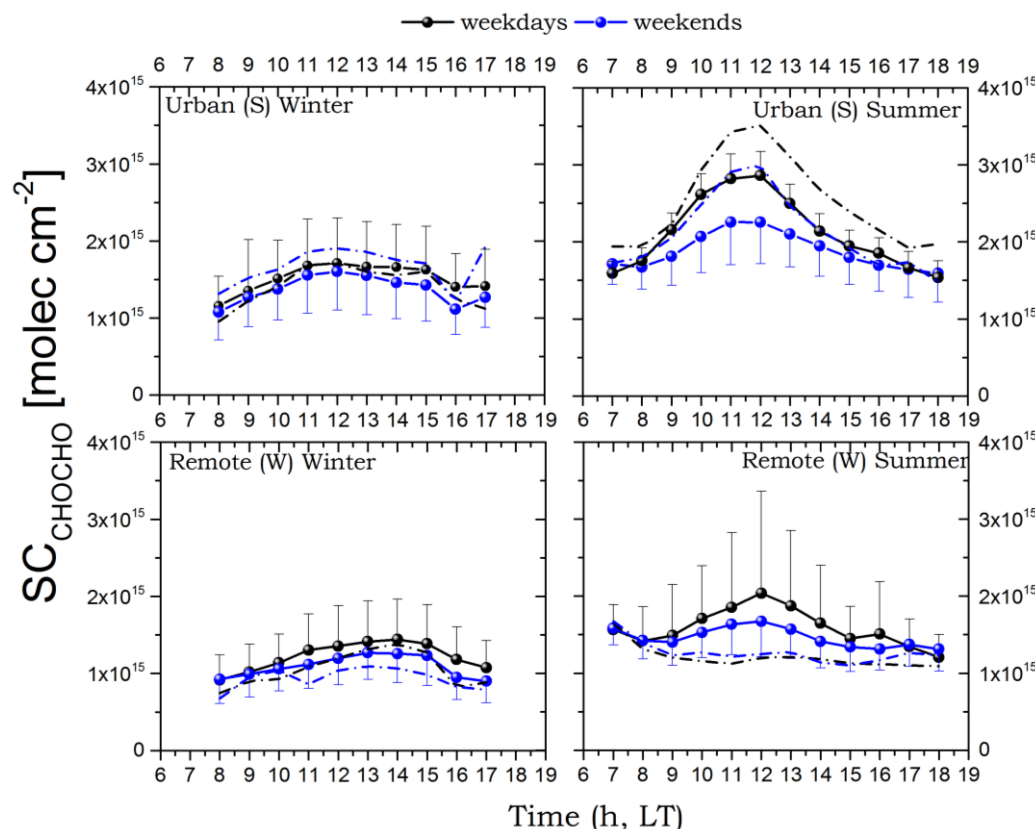


Figure 10. Average diurnal variation of SC_{CHOCHO} densities, at $+1^\circ$ elevation angle, for each period (warm and cold) for the observations towards remote and urban areas. The black and blue lines represent the weekdays and the weekends respectively. The solid lines represent the diurnal variation as obtained by averaging all data for the warm and the cold period separately. The dashed lines depict the result in diurnal variation considering data just for days when wind direction is between 180° and 270° for the urban area and between 315° and 45° for the remote area. The vertical lines represent the standard deviation for each point as described in Fig. 7.

The influence of the frequent strong northern winds (Etesian winds) blowing during July and August, dispersing the pollutants, is clearly seen in all cases. In the urban area, when these winds were excluded from the analysis and only the S-SW conditions were considered, the SC densities almost double for all trace gases, while the patterns remain the same. Similarly, in the remote direction, when the northern winds were the only ones to be considered in the analysis, the levels of the trace gases are significantly reduced. The case of HCHO during summer in the urban area where the diurnal

variation changes with wind direction is interesting, highlighting the dominant role of photochemistry in HCHO production (Fig.9 right top panel). The wind effect does not seem to be significant during winter.

Monthly averaged SC_{NO_2} density values were also calculated separately for weekdays and weekends (not shown here). Higher values are observed during weekdays due to higher traffic emissions and this is in agreement with results reported in other studies for Athens (e.g. Kanakidou et al., 2011, Psiloglou et al., 2013). The average SC_{NO_2} density values for the remote area for weekdays and weekends are $3.7 \cdot 10^{16}$ and $2.5 \cdot 10^{16}$ molec/cm² respectively (32% difference). The corresponding values for the urban area are $7.7 \cdot 10^{16}$ and $5.2 \cdot 10^{16}$ molec/cm² (32% difference). The observed weekend effect is more pronounced during winter when weekdays exceed weekend's levels by 30-50%. Smaller difference is encountered during April–July and is more evident in the remote area.

For HCHO and CHOCHO the weekend effect is not so pronounced. In particular, for HCHO the difference ranges between 3% and 17% for both site types while the corresponding values for CHOCHO are between 3% and 33%. However, there are some cases, in April and May, when the weekend values are much higher than during weekdays. For HCHO this difference is 20% for April and 25% for May, both in the remote and the urban area. The corresponding values for CHOCHO for the remote area are 25% and 17% and for the urban area 8% and 10%. The results demonstrate similarities regarding the weekend effect on HCHO and CHOCHO. Assuming that the degree of difference between weekends and weekdays is an indicator of the impact of anthropogenic sources on the levels of certain pollutants (the greater the difference, the greater the impact), it can be deduced that HCHO and CHOCHO levels are linked in almost the same way to anthropogenic sources.

3.3.5 Estimation of urban sources contribution

To estimate the contribution of local NO_x sources to the urban area's NO_2 levels, the SC_{NO_2} density measurements at the +1° elevation over the remote area were subtracted from those of the urban area. The days were first divided into three characteristic time periods: i) morning (07:00-11:00 LT), ii) noon (11:00-14:00 LT) and iii) evening (14:00-18:00 LT). Before presenting the results, the limitations of this analysis are unfolded: (a) the remote area is also affected by urban pollution through short range transport patterns and (b) the light path for a given elevation angle is different for the urban and for the remote azimuthal viewing direction. In order to address the first limitation, we excluded from the analysis the days when western winds (225°-315°) with velocity greater than 3 m/s (light breeze wind threshold) were prevailing, conditions which favour the transport of polluted air masses from the urban to the remote area. As already shown in section 3.1, the O_4 levels do not seem to vary significantly between the remote and the urban area, indicating similar light paths for these two azimuthal viewing directions and giving us the opportunity to keep on with the analysis despite the second limitation.

The contribution of the urban NO_2 sources is calculated to be around 45% and 60% during winter (November-March) and summer months (April-October) respectively and it does not seem to change significantly throughout the day (Table 3). Similar results are reported by Markakis et al., (2010), showing that in the urban environment of Athens 50% of the NO_x emissions are due to road transport.

Their outcomes are based on an emission inventory developed using activity and statistical data from national sources. The urban NO₂ sources seem to contribute more during summer and that could be attributed to frequent pollution episodes during the warm period due to high temperatures and intense photochemistry which lead to high ozone production which in turn converts more produced NO into NO₂ in the urban area where high NO emissions are present.

For HCHO the urban sources contribution is not so intense as in the NO₂ case and seems to exhibit a diurnal variation with lower values in the morning and higher levels during noon and evening (Table 3). More specifically, at the +1° elevation angle, the morning contribution is around 5% and 15% for the rest of the day for both seasons.

The urban CHOCHO sources contribution has been calculated to be around 25% in the morning and 15% at noon and evening at the +1° elevation during the cold period. During the warm period, the contribution is 30% in the morning and noon and slightly lower (~20%) in the evening. The latter could be attributed to the CHOCHO photolytic loss which gains importance against CHOCHO production towards lower SZAs (Volkamer et al., 2005). It should be noted that the primary contribution of CHOCHO from local sources to the VOC levels at urban environments is not expected to be high in view of other possible sources (Volkamer et al., 2005).

Table 3. Urban sources contribution for NO₂, HCHO and CHOCHO.

Urban sources contribution		NO ₂	HCHO	CHOCHO
Winter	7:00-11:00LT (UTC+2)	0.46	0.05	0.24
	12:00-14:00LT (UTC+2)	0.45	0.16	0.17
	14:00-18:00LT (UTC+2)	0.41	0.17	0.16
Summer	7:00-11:00LT (UTC+3)	0.57	0.02	0.30
	12:00-14:00LT (UTC+3)	0.61	0.15	0.27
	14:00-18:00LT (UTC+3)	0.60	0.17	0.22

3.3.6 Impact of local circulation patterns

The influence of local and regional circulation patterns on the measured NO_2 , HCHO and CHOCHO levels over Athens basin is being investigated in this study by using wind speed and direction records from NOA's meteorological station, collocated at MAX-DOAS installation location. The average daily wind vectors were computed from measurements obtained during daytime, and in particular during the same time span as MAX-DOAS' measurements .

The influence of the wind direction on the daily SC_{NO_2} density values at $+1^\circ$ elevation angle is presented separately for the urban and remote area (Fig. 11a-b). It is evident that N-NE winds are related to low NO_2 slant column density values, mainly due to lack of pollution sources close to the Athens basin from this sector. The results are in agreement with past studies (e.g. Bakeas and Siskos 2002, Kassomenos et al., 1995), where the influence of Northern winds on the ventilation of the Athens area is mentioned. The maximum values of SC_{NO_2} occur when the prevailing wind direction is from west. Westerly winds bring the urban emitted NO_2 towards the MAX-DOAS installation in Penteli and at the same time they favor the accumulation of pollutants in the Athens basin due to the special topography of the area. Westerly winds also favor the transport of polluted air-masses from the industrial area (Elefsina) towards the Athens basin, through the existing passage between Parnitha and Aegaleo mountains. The impact of westerlies on pollution episodes has been highlighted in several studies (e.g. Bakeas and Siskos 2002, Rappenglück et al., 1998, Kallos et al., 1993). The SC_{NO_2} density values in the urban area are less influenced by wind direction. This can be attributed to the continuous and intense emissions in the city centre due to traffic, resulting in more uniform NO_2 spatial distribution compared to the remote areas.

The retrieved SC_{HCHO} amounts for the urban area show only weak dependence on the prevailing wind direction (Fig. 11c-d). In contrast, the same analysis for the remote area revealed enhanced SC_{HCHO} amounts during westerlies, due to primary and secondary anthropogenic emissions from the city center. Lastly, the $\text{SC}_{\text{CHOCHO}}$ present a homogenous distribution of values for all directions except for westerlies suggesting formation pathways from anthropogenic precursors (e.g. acetylene, aromatics) (Fig. 11 e-f).

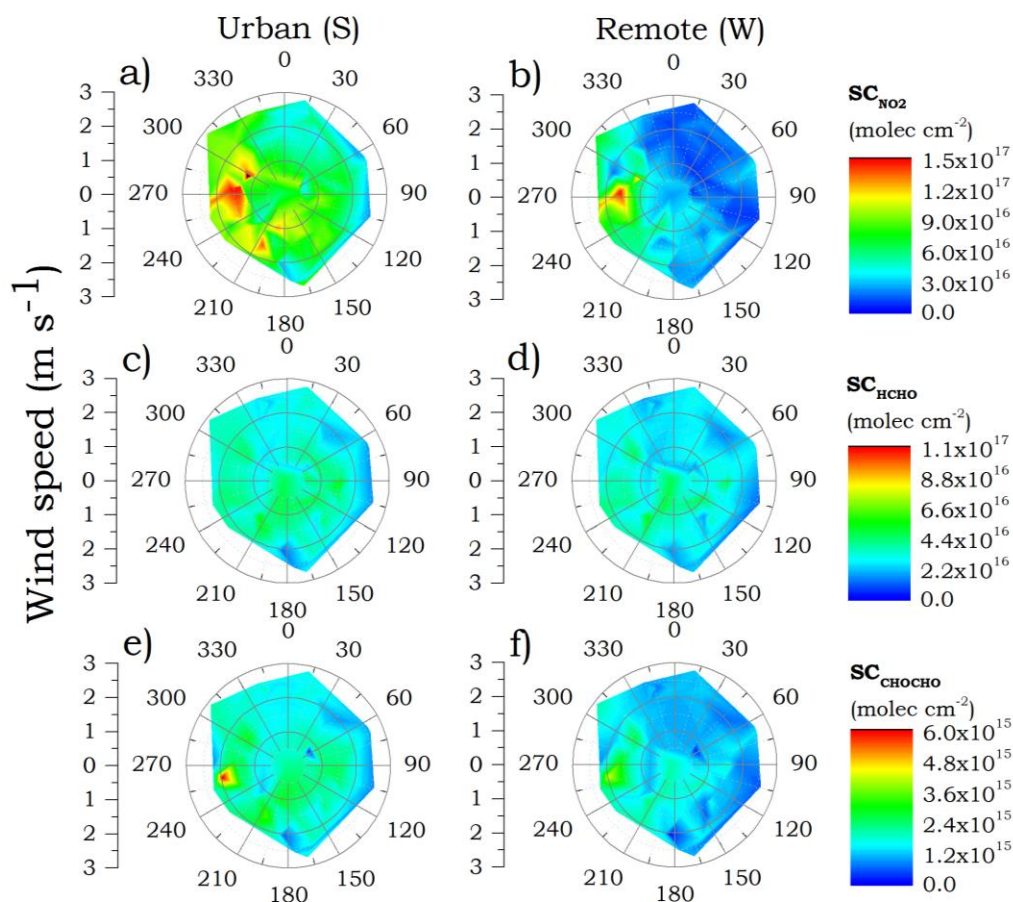


Figure 11. Daily SC density values for NO_2 (a, b), HCHO (c, d) and CHOCHO (e, f) as a function of wind direction, for remote (right column) and urban (left column) directions.

3.4 Summary and conclusions

First results from MAX-DOAS measurements in Athens were presented covering a period of 18 months (Oct 2012-Mar 2014). Slant column (SC) densities of NO_2 , HCHO , CHOCHO and O_4 , have been retrieved, covering eight different azimuthal viewing directions, spread over the extended Athens agglomeration, and eight elevation angles. The slant column observations at low elevation angles provide important information for examining the horizontal spatial inhomogeneity of pollution levels in Athens basin. Although the light path is different for each azimuthal direction, the directions representing the remote and the urban area ('W' and 'S' respectively) are both pointing southwards, thus the difference is not significant. The calculation of airmass factors (AMF) and the further derivation of vertical column (VC) densities are beyond the scope of this study. VC densities as well as trace gases' profile information will be part of future work.

The data was cloud screened, excluding heavy cloudy days, and only a small impact of clouds on the 1° elevation data was found. Thus the retrieved SC densities were used to investigate the temporal

variability (seasonal and diurnal) of the selected species. A clear NO_2 seasonal variation is observed with winter maximum and summer minimum. For the polluted urban area, the average winter levels are about 145% higher than summer levels. Seasonal variation is also observed for HCHO and CHOCHO but with summer maximum due to photochemical production.

The observed daily variability of the NO_2 (morning maximum at 10:00 LT and a winter secondary evening peak at 15:00 LT) was attributed to anthropogenic emissions and photochemical sinks. Formaldehyde's diurnal pattern is dominated by a broad afternoon peak during winter in the urban area, while during summer there is a morning maximum (12:00 LT) and a steady decrease then after. During winter the glyoxal's diurnal pattern is characterised by a steady increase after sunshine reaching a maximum value at 14:00LT. In summer a strong maximum appears at noon followed by a sharp decrease. The results for HCHO and CHOCHO suggest a strong link to photochemistry and a weaker link to primary anthropogenic emissions. The influence of Etesians winds, dispersing the pollutants, is evident in all cases and highlights the dominant role of HCHO photochemical production.

For NO_2 , a clear weekly pattern was found; 30% to 50% lower SC_{NO_2} values recorded during weekends. This highlights the significant contribution of local anthropogenic emissions (mainly traffic) to the observed NO_2 columns. The weekend effect is not so intense for HCHO and CHOCHO levels which are 3%-17% and 3%-33%, respectively, lower during weekends. This is to be expected for VOCs which have significant biogenic sources.

By subtracting the NO_2 amounts of the remote area from the ones of the urban area, the NO_2 contribution from local urban emission sources was assessed. The contribution was found to be as large as 45% and 60% (during winter and summer respectively) at the $+1^\circ$ elevation angle with no distinct diurnal variability. The corresponding contribution of the urban HCHO sources is 5% in the morning and 15% during the rest of the day, for both seasons. The CHOCHO urban source contribution is 25-30% in the morning and 15-20% in the evening.

The wind direction does not influence significantly the levels of SC_{HCHO} and $\text{SC}_{\text{CHOCHO}}$, especially in the urban area. The SC_{NO_2} densities present lower values under N-NE winds, while westerlies result in elevated SC_{NO_2} levels. This finding is explained by the local topography of Athens and the location of the main emission sources relative to the instrument.

Concluding, our analysis of the automated multi-azimuth MAX-DOAS measurements over the Athens basin provided detailed temporal and spatial distributions of NO_2 , HCHO and CHOCHO for more than a year. They yield a consistent picture of the diurnal, weekly and seasonal variations of these species and their vertical and horizontal distribution around the measurement location. The temporal and spatial patterns point towards: (a) the dominance of anthropogenic sources on NO_x levels, (b) the fact that the VOCs are largely secondary products having additional sources and (c) the significantly active role of photochemistry in Athens. Some of the findings though, need further analysis: formaldehyde's and glyoxal's significantly higher levels during weekends in April and May need to be investigated and checked for sampling effects. Future work will concentrate on applying profile inversions on the data set to investigate the vertical distribution of the trace gases in more detail. Furthermore, the SC_{O_4} measurements will be used to obtain quantitative information on the aerosol load and aerosol extinction profiles during cloud free time periods.

Retrieval and evaluation of tropospheric aerosol extinction profiles using MAX-DOAS measurements over Athens, Greece

The vertical distribution of the suspended particles was retrieved for Athens for specific case studies using ground-based MAX-DOAS measurements. This is the first time that MAX-DOAS measurements are used for this purpose in the urban environment of Athens. The profiles were retrieved at 477 nm using O₄ measurements (DSCDs) and applying the BOREAS algorithm, which is based on the SCIATRAN radiative transfer model and the iterative Tikhonov regularisation technique (Chapter 2.3). In order to evaluate the results, four case studies were selected and the MAX-DOAS profiles were compared to the corresponding profiles from lidar and the AOD from a solar photometer (CIMEL). Although the comparison is very important for the evaluation of the results, certain limitations should be taken into account due to the different operation principles, characteristics and measurement principles of each instrument. More specifically, (i) the measurements with the MAX-DOAS technique are representative of a wide area, which, while including the measurement areas of the other two instruments, is not limited to them. (ii) the MAX-DOAS retrievals are representative for 500-4000 m a.s.l., while the lidar profiles are valid for altitudes higher than 1000 m above the station and finally (iii) the AOD AERONET measurements describe the columnar aerosol properties representative of an area ranging from few up to 10 km radius above the Athens area, depending on solar elevation. Furthermore, (iv) the aerosol extinction profile from backscatter lidar measurements is of higher vertical resolution and is subjected to uncertainties, thus the comparison with MAX-DOAS is performed on a qualitative basis. Also, the (v) sun-photometer AOD observations probe the extinction in the full atmospheric column while MAX-DOAS retrievals are sensitive only to the lowest kilometers, leading to differences in the presence of aerosol layers at altitudes above 4 km.

Despite the limitations mentioned above, the retrieved profiles from the MAX-DOAS measurements are in very good agreement with the lidar profiles in terms of vertical distribution, with correlation coefficient (r) >0.90 in all cases. The FGE (fractional gross error) is satisfactory ($0.20 < \text{FGE} < 0.80$) in all cases, demonstrating a good performance of the BOREAS algorithm. The underestimation by MAX-DOAS at small relative azimuth angles can be attributed to the geometry of Mie scattering relatively to the location and viewing direction of MAX-DOAS, leading to MAX-DOAS failure to see part of the urban particulate pollution. Overall, the agreement between the two techniques is encouraging, suggesting that MAX-DOAS can accurately capture the vertical distribution of suspended particles.

The MAX-DOAS AOD is in satisfactory agreement with the corresponding CIMEL measurements. The correlation coefficient ranges between 0.47 and 0.67 in three out of the four cases. MAX-DOAS appears to underestimate AOD in the presence of coarse particles and when measurements are performed at small relative azimuth angles between the sun and the instrument's viewing direction. Better

agreement is found when the measurements are performed in the morning hours when the relative azimuth angles are large. Overall, the average AOD difference between the two instruments is 0.03.

Overall, the MAX-DOAS technique can be considered as a reliable method for measuring aerosol levels and their vertical distribution in the urban environment of Athens; new perspectives are opened up for assessing urban aerosol pollution on a long term-basis in Athens from continuous and uninterrupted MAX-DOAS measurements.

The text of this study, published in the international peer-reviewed journal Atmospheric Measurement Techniques, is attached.



Retrieval and evaluation of tropospheric-aerosol extinction profiles using multi-axis differential optical absorption spectroscopy (MAX-DOAS) measurements over Athens, Greece

Myrto Gratsia^{1,2}, Tim Bösch³, Panagiotis Kokkalis^{8,4}, Andreas Richter³, Mihalis Vrekoussis^{5,6}, Stelios Kazadzis^{7,1}, Alexandra Tsekeri⁴, Alexandros Papayannis⁹, Maria Mylonaki⁹, Vassilis Amiridis⁴, Nikos Mihalopoulos^{1,2,6}, and Evangelos Gerasopoulos¹

¹Institute for Environmental Research and Sustainable Development, National Observatory of Athens, Athens, Greece

²Environmental Chemical Processes Laboratory, Department of Chemistry, University of Crete, Heraklion, Greece

³Institute of Environmental Physics and Remote Sensing, University of Bremen, Bremen, Germany

⁴Institute for Astronomy, Astrophysics, Space Applications and Remote Sensing, National Observatory of Athens, Athens, Greece

⁵Laboratory for Modelling and Observation of the Earth System (LAMOS), University of Bremen, Bremen, Germany

⁶Climate and Atmosphere Research Center, CARE-C, The Cyprus Institute, Nicosia, Cyprus

⁷Physikalisch-Meteorologisches Observatorium Davos, World Radiation Center, Davos Dorf, Switzerland

⁸Physics Department, Kuwait University, Kuwait, Kuwait

⁹Laser Remote Sensing Laboratory, National Technical University of Athens, Athens, Greece

Correspondence: Myrto Gratsia (mgratsia@noa.gr) and Evangelos Gerasopoulos (egera@noa.gr)

Received: 24 March 2020 – Discussion started: 7 April 2020

Revised: 30 October 2020 – Accepted: 24 November 2020 – Published: 29 January 2021

Abstract. In this study, we report on the retrieval of aerosol extinction profiles from ground-based scattered sunlight multi-axis differential optical absorption spectroscopy (MAX-DOAS) measurements, carried out at Athens, Greece. It is the first time that aerosol profiles are retrieved from MAX-DOAS measurements in Athens. The reported aerosol vertical distributions at 477 nm are derived from the oxygen dimer (O_4) differential-slant-column-density observations at different elevation angles by applying the Bremen Optimal estimation RETrieval for Aerosol and trace gasS (BOREAS) retrieval algorithm. Four case studies have been selected for validation purposes; the retrieved aerosol profiles and the corresponding aerosol optical depths (AODs) from the MAX-DOAS are compared with lidar extinction profiles and with sun-photometric measurements (Aerosol Robotic Network, AERONET, observations), respectively. Despite the different approach of each method regarding the retrieval of the aerosol information, the comparison with the lidar measurements at 532 nm reveals a very good agreement in terms of vertical distribution, with $r > 0.90$ in all cases. The AODs from the MAX-DOAS and the sun pho-

tometer (the latter at 500 nm) show a satisfactory correlation (with $0.45 < r < 0.7$ in three out of the four cases). The comparison indicates that the MAX-DOAS systematically underestimates the AOD in the cases of large particles (small Ångström exponent) and for measurements at small relative azimuthal angles between the viewing direction and the sun. Better agreement is achieved in the morning, at large relative azimuthal angles. Overall, the aerosol profiles retrieved from MAX-DOAS measurements are of good quality; thus, new perspectives are opened up for assessing urban aerosol pollution on a long-term basis in Athens from continuous and uninterrupted MAX-DOAS measurements.

1 Introduction

Tropospheric aerosols originate from both natural and anthropogenic sources. The lifetime of aerosols in the troposphere ranges from a few days to a few weeks, depending on their size and meteorology (e.g. Pandis et al., 1995). They

Abstract. In this study, we report on the retrieval of aerosol extinction profiles from ground-based scattered sunlight multi-axis differential optical absorption spectroscopy (MAX-DOAS) measurements, carried out at Athens, Greece. It is the first time that aerosol profiles are retrieved from MAX-DOAS measurements in Athens. The reported aerosol vertical distributions at 477 nm are derived from the oxygen dimer (O_4) differential slant column density observations at different elevation angles by applying the BOREAS retrieval algorithm. Four case studies have been selected for validation purposes; the retrieved aerosol profiles and the corresponding aerosol optical depths (AODs) from the MAX-DOAS are compared with lidar extinction profiles and with sun photometric measurements (AERONET observations), respectively. Despite the different approach of each method regarding the retrieval of the aerosol information, the comparison with the lidar measurements at 532 nm reveals a very good agreement in terms of vertical distribution, with $r > 0.90$ in all cases. The AODs from the MAX-DOAS and the sun-photometer (the latter at 500 nm) show a satisfactory correlation (with $0.45 < r < 0.7$ in three out of the four cases). The comparison indicates that the MAX-DOAS systematically underestimates the AOD in the cases of large particles (small Ångström exponent) and for measurements at small relative azimuthal angles between the viewing direction and the Sun. Better agreement is achieved in the morning, at large relative azimuthal angles. Overall, the aerosol profiles retrieved from MAX-DOAS measurements are of good quality; thus, new perspectives are opened up for assessing urban aerosol pollution on a long term-basis in Athens from continuous and uninterrupted MAX-DOAS measurements.

4.1 Introduction

Tropospheric aerosols originate from both natural and anthropogenic sources. The lifetime of aerosols in the troposphere ranges from a few days to a few weeks, depending on their size and meteorology (e.g. Pandis et al., 1995). They take part in atmospheric processes through (i) nucleation and interaction with clouds (e.g. Twomey et al., 1977; Rosenfeld et al, 2014), (ii) participation in chemical and photochemical reactions, by providing the required surface for heterogeneous reactions to take place (Andreae & Crutzen, 1997) and (iii) absorption and scattering of incoming solar and earth's IR radiation, affecting atmospheric dynamics and stability (e.g. Dubovik et al., 2002) and the Earth's climate (IPCC, 2001). Significant decrease of UV-Vis irradiance reaching the ground due to urban aerosol pollution has been reported in various cases (e.g. Zerefos et al., 2009; Chubarova et al., 2011).

According to a survey conducted in 25 large European cities, Athens occupies the third position on European level in exceedances of particle pollution regulations (Pascal et al., 2013). Saharan dust transported from the African continent is the main natural source of tropospheric aerosols in Athens (e.g. Kanakidou et al., 2007; Gerasopoulos et al., 2011; Raptis et al., 2020), while common anthropogenic sources are traffic emission and domestic heating (Markakis et al, 2010; Gratsea et al., 2017). Wildfires also contribute to the aerosol mixture in the area occasionally, either from local events (Amiridis et al., 2012) or by long-range transport (Papayannis et al.; 2009, Amiridis et al., 2011; Mona et al., 2012). Whereas emissions of most air pollutants, such as SO_2 , are expected to decrease by more than 80% until the end of the 21st century, the decrease of aerosol emissions is projected to be small (IPCC 2007) and thus aerosols may play an even more critical role in air quality in the future. Therefore, long-term continuous measurements, providing information on the spatial and temporal distribution

of aerosols, are of great importance to urban air pollution assessment and to the understanding of the aerosol contribution to Earth's climate. The knowledge of the vertical distribution of aerosols is necessary for understanding the mechanisms underlying the formation and development of urban smog.

Satellite, airborne and ground-based measurements are widely used to derive aerosol vertical profiles (e.g., Papayannis et al., 2005; Schmid et al., 2006; DeCarlo et al., 2008; Solanki and Singh, 2014); satellite measurements sometimes fail to be accurate in the lower atmosphere, while airborne measurements, although accurate in the lower atmosphere, are temporally restricted. In contrast, ground-based measurements can provide both a very good record of the lower troposphere and a satisfactory temporal resolution. However, since the ground-based profile measurements are mainly relying on lidar systems (e.g., the European Aerosol Research Lidar Network - EARLINET – within the European Research Infrastructure for the observation of Aerosol, Clouds and Trace Gases - ACTRIS), they are costly in terms of setup and operation. An additional option for ground-based observations is the MAX-DOAS technique, which has been gaining ground over the last years (e.g., Wittrock et al., 2004; Heckel et al., 2005; Ma et al., 2013; Schreier et al., 2020) since it can provide low-cost, continuous and uninterrupted measurements without the need for absolute radiometric calibration. The MAX-DOAS technique has also been shown to be very promising for the retrieval of aerosols' vertical distribution (e.g., Sinreich et al., 2005; Lee et al., 2009; Clémer et al., 2010; Wagner et al., 2011). However, its sensitivity at higher altitudes is low and compared to the lidar technique, it provides profiles with much coarser vertical resolution. It also performs only daylight measurements, which can be considered as a limitation of this technique. In some studies, the retrieved aerosol extinction profiles from MAX-DOAS measurements are compared to the corresponding profiles derived from lidar (e.g., Irie et al., 2008; Zieger et al., 2011; Bösch et al., 2018) or Aerosol Robotic Network (AERONET) based measurements (e.g. Wang et al., 2016). For the Athens area, although several studies have been published on aerosol extinction profiles from lidar measurements (e.g. Papayannis et al., 1998; Matthias et al., 2004; Papayannis et al., 2005), vertical trace gas and aerosol profile retrievals from MAX-DOAS have not been published so far.

In the scope of this paper, a retrieval algorithm, recently developed by the Institute of Environmental Physics and Remote Sensing of University of Bremen (Bösch et al., 2018), is employed in order to obtain vertical distributions of aerosol extinction from O_4 MAX-DOAS measurements over the urban environment of Athens. O_4 is an atmospheric absorber with a known concentration profile, therefore measurements of the O_4 column can be used to retrieve the aerosol induced light path changes (Wagner et al., 2004).

For validation purposes the outcomes of our calculations are compared to established techniques; the retrieved profiles are compared to profiles from ground-based lidar measurements (EARLINET station) and the AOD to sun-photometer measurements (AERONET station).

A description of the instruments used in this study (location, instrumentation and data retrieval) along with a brief description of the profile retrieval algorithm are given in section 2. In section 3, we present the derived aerosol vertical distributions for four selected case studies and we compare the MAX-DOAS aerosol extinction coefficient profiles and the AOD with lidar and sun-photometric measurements, respectively. The findings are summarised in section 4, where also the conclusions of this study are provided.

4.2 Methodology

4.2.1 Location

Four mountains surround the city of Athens, forming a basin that is open to the south and southwest. This special topography plays an essential role in the accumulation of atmospheric pollutants over the city under certain meteorological conditions (Kassomenos et al., 1995). Moreover, dust transport episodes from North Africa also contribute to the aerosol load of the city (e.g. Gerasopoulos et al., 2009; Kosmopoulos et al., 2017). In general, the Athens area can be considered as an example of various aerosol types such as dust, local pollution, marine, biomass combustion and their mixtures (Soufiana et al., 2019).

Figure 1 shows the Greater Athens area and the location of each instrument used in this study. The MAX-DOAS instrument is located at the premises of the National Observatory of Athens (NOA, 38.05° N, 23.86° E, 527m a.s.l.), to the north of the city. No strong emission sources are present around the measurement area, which is considered as suburban background. The lidar system performs measurements at the National and Technical University of Athens (NTUA, 37.97 °N, 23.79 °E, 212m a.s.l.) and the site is considered as suburban background. The CIMEL sun-photometer is installed at the premises of NOA at Thissio hill (37° 58' N, 23° 43' E, 150m a.s.l.), which, despite being located in the city centre, is considered as urban background (Paraskevopoulou et al., 2015). Information about the instruments is provided in Table 1.

4.2.2 Instrumentation and data retrieval

4.2.2.1 MAX-DOAS

The MAX-DOAS instrument employed in this study is part of the BREDOM network (Bremian DOAS network for atmospheric measurements, http://www.iup.uni-bremen.de/doas/groundbased_data.htm) and has been operating continuously since October 2012. It comprises a grating spectrometer (LOT 260S, 600 l/mm ruled grating) connected via an optical fiber bundle to a computer-controlled telescope unit. The spectrometer covers a spectral range from 330 to 500 nm with a spectral resolution of approximately 0.7 nm. The detector used is a CCD (Charge-Coupled Device) by Andor Technology, with 2048 x 512 pixel resolution, cooled to -40°C.

The telescope performs intensity measurements at eight elevation angles (-1°, 0°, 1°, 2°, 4°, 8°, 15°, 30°), as well as to the zenith. However, the current retrieval algorithm only considers upward viewing directions, excluding the -1° and 0°. With this choice, little information is available for the profile retrieval below the station altitude, therefore profiles are retrieved and presented only for altitudes above 500 m a.s.l. Measurements in eight azimuthal directions are performed, but in this study, only the S direction - pointing at 52.5° (with respect to South) and associated to the urban atmospheric conditions of the city (Gratsea et al., 2016) - is considered (Fig. 1). The S direction also covers the sun-photometer's location and points close to the lidar's measurement site. The duration of one full

scanning cycle (azimuthal and elevation scanning) is about 15 min, thus about 30 measurement cycles per day are available in winter and 45 in summer.

The spectral measurements are analysed using the DOAS technique; the Beer-Lambert law is considered as the solution of the radiative transfer equation (Platt and Stutz, 2008) and the absorption spectrum is separated into broad and narrow spectral features that show low and high frequency variations, respectively, as a function of wavelength. The narrow spectral features correspond to the unique narrow-band absorption structures of the trace gases, while the broad ones represent the attenuation of solar radiation by scattering processes in the atmosphere as well as the continuum absorption by trace gases and the instrument. For the derivation of the slant column density (SCD, defined as the concentration of the absorber integrated along the light path), a polynomial accounting for the broad spectral features and the laboratory cross-sections of the retrieved species are fitted to the measured optical depth. To determine the optical depth, the logarithm of the ratio of the current horizon measurement (I) and the reference intensity (I_0) is taken.

The SCD of the oxygen dimer (O_4), i.e. the slant optical thickness of the absorber divided by the absorption cross section, measured at different elevations is used as input to the retrieval algorithm for the calculation of the aerosol distribution. The slant column of the O_4 , a weak molecular absorber with a well-known vertical profile (the O_4 concentration is proportional to the square of the O_2), is almost linearly dependent on the average photon pathlengths (Pfeilsticker et al., 1997) and thus can be used as an indicator of the presence of clouds or aerosols in the atmosphere. The SCD_{O_4} is calculated by fitting to the measured optical depth the laboratory spectrum of O_4 (Hermans et al., 2003), NO_2 (Vandaele et al., 1998) and of O_3 (Bogumil et al., 2000) and a polynomial of degree 4 which accounts for the broad spectral features. The fitting spectral window used is 425-490 nm. In order to retrieve the tropospheric SC_{O_4} , the zenith observation, corresponding to each measurement cycle, is used as the reference measurement I_0 , canceling in this way the Fraunhofer lines in the solar spectrum and the stratospheric contributions to the SCD.

Tropospheric vertical column densities (VCD) of NO_2 , shown in section 3.1, can be derived by using air mass factors (AMF) calculated with the SCIATRAN radiative transfer model (Rozanov et al., 2000). To convert the differential tropospheric SCD to the corresponding tropospheric VCD, the differential AMF ($AMF_\alpha - AMF_{90^\circ}$) is required, namely the difference between the AMF at the same elevation α as the SCD measurement and the AMF at the zenith (Eq. 1).

$$VCD = \frac{SCD_\alpha - SCD_{90^\circ}}{(AMF_\alpha - AMF_{90^\circ})} \quad (1)$$

The AMF <https://www.atmos-chem-phys.net/4/955/2004/acp-4-955-2004.pdf> describes the weighting of the absorption as a function of the relative azimuth and the solar zenith angle (SZA) for a given atmospheric profile and at a specific wavelength.

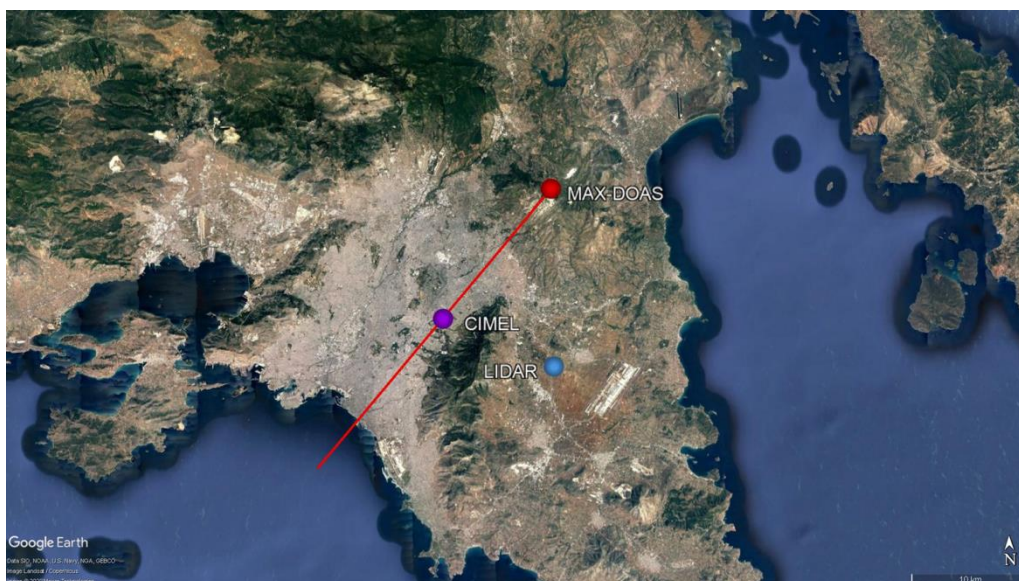


Figure 1. Measurement sites and MAX-DOAS viewing direction (S). The distances between instruments are: MAX-DOAS - sun-photometer (CIMEL) 16 km and MAX-DOAS - lidar 13 km. © Google Earth

Table 1. Instruments and data products used in the present study.

Instrument	Location	Institute	Products
MAX-DOAS	Penteli National Observatory of Athens (38.05°N, 23.86°E, 527 m a.s.l.)	BREDOM network, Institute of Environmental Physics and Remote Sensing, University of Bremen	SCD _{NO2} , VCD _{NO2} , aerosol extinction profile, AOD
EOLE-LIDAR	Zografou (37.97°N, 23.79°E, 212 m a.s.l.)	National Technical University of Athens, Laser Remote Sensing Laboratory (NTUA-LRSU)	Aerosol backscatter profile, aerosol extinction profile, columnar AOD
CIMEL Sun-Sky Radiometer	Thissio (37.96°N, 23.72°E, 150 m a.s.l.)	National Observatory of Athens, Institute for Astronomy, Astrophysics Space Application & Remote Sensing (NOA-IAASARS)	AOD, Inversion data products (ssa, asymmetry factor, refractive index, phase function, size distribution)

4.2.2.2 EOLE lidar system

The six-wavelength Raman-backscatter lidar system (EOLE) operates in Athens since February 2000 as part of the EARLINET network (Pappalardo et al., 2014). The system is designed following the optical set-up of a typical member station (Kokkalis 2017), meeting all the quality assurance requirements of the network. The emission unit is based on a pulsed Nd:YAG laser, emitting high energy pulses at 355, 532 and 1064 nm with a repetition rate of 10 Hz. The optical receiver is based on a Cassegrainian telescope (600 mm focal length and a clear aperture diameter of 300 mm), directly coupled with an optical fiber, to the wavelength separation unit, detecting signals at 355, 387 (N₂ Raman line of

355nm), 407 (H₂O Raman line of 355nm), 532, 607 (N₂ Raman line of the 532nm) and 1064 nm. For every measuring cycle 1000 lidar signal returns are stored (every~1.66). For each case presented in this study, we used hourly averaged profiles, which correspond to approximately 34 individual signal acquisitions (Kokkalis et al., 2012).

During day time operation, the system is capable of providing aerosol backscatter profiles (β_{aer}) at 355, 532 and 1064 nm, based on the standard backscatter lidar technique and employing the Klett inversion method (Klett, 1981). This technique assumes the existence of an aerosol-free region (e.g. upper troposphere) and requires an a-priori assumption of the lidar ratio value (the ratio of the extinction to backscatter coefficient, S_{aer}). A variety of studies revealed a wide range for the lidar ratios, covering values from 20 to 100 sr (Ackermann, 1998; Mattis et al., 2004; Amiridis et al., 2005; Müller et al., 2007; Papayannis et al., 2008; Groß et al., 2011; Giannakaki et al., 2015). When the elastic backscatter lidar technique is used, the assumption of a constant lidar ratio value throughout the laser sounding range, becomes very critical when solving the lidar equation; in this case, the overall uncertainty, including both statistical and systematic errors, on the retrieved β_{aer} -values, is of the order of 20–30% (e.g. Rocadenbosch et al., 2010). In this study, the aerosol extinction profiles have been retrieved under the assumption of three lidar ratio values, 30, 50 and 70 (i.e. 50 ± 20 sr). This range is realistic for pollution and dust cases presented herein (Groß et al., 2013) and it is also in accordance with columnar lidar ratio values (interpolated to 532 nm) obtained by AERONET for the cases of this study, which vary from 48.8 ± 7.5 sr to 59.9 ± 12.1 sr. As a result of this variability (i.e. 50 ± 20 sr), the uncertainties introduced to the aerosol extinction profiles vary from 10 - 40%; the higher uncertainties appear at the upper atmospheric layers, where the signal-to-noise ratio of the system decreases. The corresponding uncertainties of the lidar-derived AOD values due to this assumption were estimated to be up to 11%. All the lidar profiles were obtained with the Single Calculus Chain (SCC) processing platform (D'Amico et al., 2016; Mattis et al., 2016), which is developed in the framework of EARLINET to ensure the high-quality products of the network, by implementing quality checks on both raw lidar data and final optical products.

One of the lidar's main limitations is the distance of full overlap between the laser beam and the receiver's field of view, which makes it difficult for the instrument to obtain useful and accurate aerosol-related information below that height. Wandinger and Ansmann (2002) demonstrated that when not applying overlap correction in lidar signals, the retrieved aerosol extinction coefficient may take even non-physical negative values for heights up to the full overlap. The incomplete overlap effect can be solved by using Raman measurements under night-time conditions. In this study, only daytime measurements are used and therefore no overlap correction is applied on the signals. The geometrical configuration of EOLE results in full overlap distance of 500-800 m above ground (Kokkalis 2017). The aerosol extinction values below the 1000 m a.s.l. height are considered to be inside the overlap region and therefore were omitted from the extinction profile comparison. Nevertheless, in order to calculate the AOD from the lidar profiles, the lowermost trustworthy value of the extinction coefficient was assumed constant (height-independent). During daytime, the upper limit of the planetary boundary layer over Athens ranges between 1500 and 2100 m a.s.l. (Kokkalis et al. 2020), thus the minimum height of lidar profiles at 1000 m a.s.l. is well within the PBL. Our assumption of a well-mixed atmosphere below 1000 m a.s.l. - which means that a constant lidar ratio value is considered for this part of the atmosphere (Wandinger and Ansmann, 2002) - may lead to an underestimation of the AOD at the lowest troposphere, since the city is most probably an additional source of particles. This underestimation cannot be estimated because of the lidar overlap issue.

4.2.2.3 CIMEL sun-photometer

The reported columnar aerosol optical properties have been retrieved by a CIMEL sun-photometer (Holben et al., 1998). The instrument is part of NASA's global sun photometric network, AERONET, and performs automatic measurements of the direct solar radiance at the common wavelengths of 340, 380, 440, 500, 675, 870, 940 and 1020 nm every 15 min and diffuse sky radiance at 440, 675, 870 and 1020 nm. These measurements are further used to provide both optical and microphysical aerosol properties in the atmospheric column (Dubovik et al., 2006). The CIMEL data used in this study are the cloud screened and quality assured level 2.0 data products, providing information about the columnar AOD and the Ångström exponent. The AOD uncertainty is $\leq \pm 0.02$ for UV wavelengths and $< \pm 0.01$ for wavelengths larger than 440 nm (Eck et al., 1999).

4.2.3 BOREAS profile retrieval algorithm

The BRemen Optimal estimation REtrieval for Aerosol and trace gaseS (BOREAS) is an optimal estimation based profile retrieval algorithm developed at the Institute of Environmental Physics, University of Bremen (Bösch et al., 2018). It applies the optimal estimation technique for the retrieval of trace gas concentration profiles, while for our case - the aerosol retrievals - it uses an iterative Tikhonov regularization approach. The main concept of the algorithm for the aerosol retrieval is to minimize the difference between modeled and measured O_4 slant optical depths by applying the iterative Tikhonov technique to varied aerosol extinction profiles. This method uses the difference of the slant optical depth from an a priori state to obtain information on the aerosol concentration that caused this difference through multiple iterations. Slant column densities of trace gases and O_4 from MAX-DOAS measurements at different line of sight (LOS) directions, as well as climatology profile files are used as inputs. The BOREAS algorithm is based on the SCIATRAN radiative transfer model (Rozanov et al., 2005), which is used to calculate box-air-mass-factors (BAMF) and weighting functions, needed for the profile inversion. The BAMF - in contrast to the total AMF - is a function of altitude describing the sensitivity of measurements to the profile at different atmospheric height layers. The aerosol weighting function matrices express the sensitivity of the O_4 measurements to changes in the aerosol extinction coefficient profile. For the radiative transfer model (RTM) calculations, scattered light in a spherical atmosphere (multiple scattering) and atmospheric profiles of pressure and temperature for Athens from the Atmospheric Science Radiosonde Archive of the University of Wyoming (<http://weather.uwyo.edu/upperair/buffraob.shtml>) are considered. The instrument was set to station's altitude and the surface was set at sea level. The aerosol inversion problem is expressed through the minimisation of Eq. (2):

$$\|\Delta\tau(\lambda, \boldsymbol{\Omega}) - \Delta\tilde{\tau}(\lambda, \boldsymbol{\Omega}, N_\alpha(z)) - P(\lambda, \boldsymbol{\Omega})\|^2 \rightarrow \min \quad (2)$$

,where $\Delta\tau$ denotes the measured O_4 differential slant optical thickness, $\Delta\tilde{\tau}$ the simulated differential slant optical thickness, $\boldsymbol{\Omega}$ the measurement geometry (LOS, SZA, relative azimuth), $N_\alpha(z)$ the a priori aerosol number concentration profile which is used as a starting point for the iterations and P a polynomial of lower order which accounts for the attenuation due to scattering processes. Since the relationship between the concentration profile and the O_4 differential slant optical depth is not linear,

the iterative Tikhonov regularisation technique, along with weighting function matrices, is used for the solution of the minimisation problem (Bösch et al., 2018).

The uncertainty associated with each retrieved profile is computed by the algorithm. It is the sum of the noise and smoothing errors, which represent the impact of the measurements and of the a priori profile on the retrieved profile, respectively. These two errors have been calculated for each of our case studies separately and are presented in section 3.2.

The temporal resolution of the measurements is about 15 minutes, which corresponds to the duration of one full scanning cycle through all directions over the city. The vertical sampling of the retrieved profile is 0.05 km, with the bottom layer considered at the sea level and the top layer at 4 km a.s.l. The AOD is calculated by integrating the BOREAS retrieved aerosol extinction coefficient vertically. More details about the values assigned to each parameter are given in section 3.2.

4.3 Results and discussion

4.3.1 Selected case studies

The main objective of this study is to assess the retrieved aerosol profiles from MAX-DOAS measurements by comparing them with well established sun-photometric measurements (CIMEL) and lidar retrievals. Therefore, certain cases had to be selected with available and valid data from all three instruments. Additionally, the selected cases had to coincide with cloud-free days, as all of the used measurement techniques have more substantial uncertainties in the presence of clouds. During the period from January 2015 to June 2016, four cases were found to meet the above conditions, covering winter, summer and spring: i) 05 February 2015 under the influence of a weak dust event, ii) 09 July 2015 with enhanced morning levels of NO_2 for this season (Gratsea et al., 2016) iii) 10 July 2015 with typical levels of pollution and iv) 04 April 2016 with enhanced levels of NO_2 . In order to identify the sources of air masses reaching Athens on the specific dates, 4-day air mass back trajectories at different altitudes, calculated using the NOAA-HYSPLIT (Hybrid Single-Particle Lagrangian-Integrated Trajectory) model (Draxler and Hess, 1997) were used. Potential for Saharan Dust transport below 4 km, which is the highest point of our retrievals, was identified only for case (i) (Fig.2). In the rest of the cases, the air masses below 4 km originate from N/NE directions, and are thus not associated with dust aerosols. The NO_2 levels, measured by MAX-DOAS and presented in Fig. 3, are used as an indicator for the pollution levels over the city. The mean diurnal NO_2 DSCDs for winter and summer months, as reported by Gratsea et al. (2016), range from $6 \cdot 10^{16}$ to $9 \cdot 10^{16}$ and $5 \cdot 10^{16}$ to $11 \cdot 10^{16}$ molec $\cdot\text{cm}^{-2}$, respectively. Thus, enhanced pollution levels are observed during the morning hours in cases (ii) and (iv). The absence of clouds is established using in-situ empirical meteorological observations from the monitoring station of the National Observatory of Athens at the centre of the city and is also verified by the MAX-DOAS retrieved O_4 slant columns throughout the day. The above mentioned cases will henceforth be referred to as cases (i), (ii), (iii) and (iv), respectively and information about each case is summarised in Table 2.

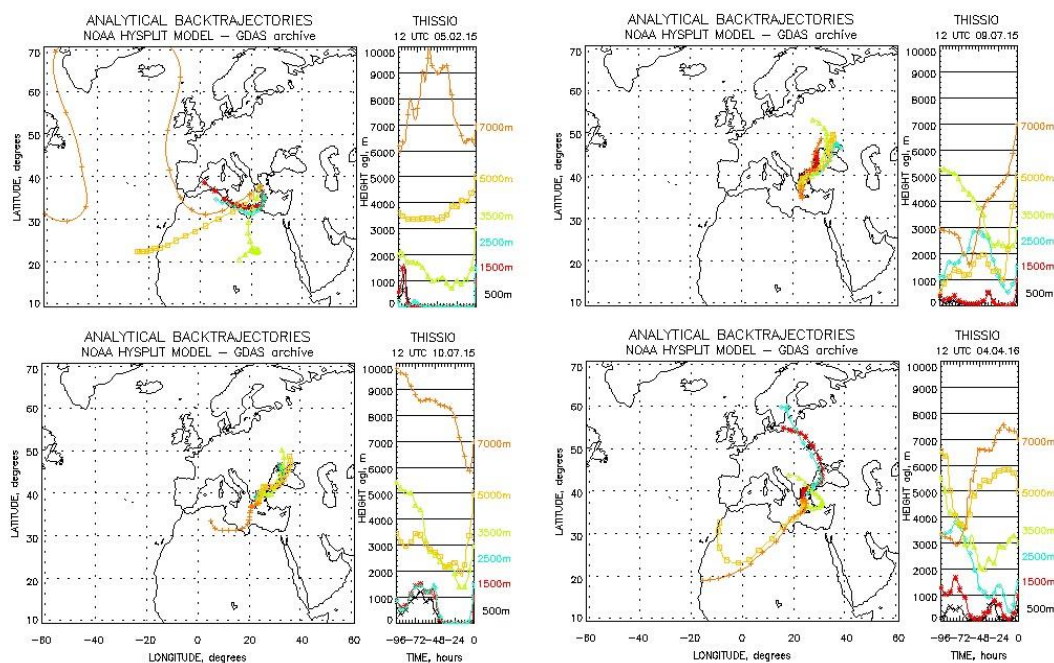


Figure 2. Analytical backtrajectories for Athens as derived from NOAA-HYSPLIT model for the case studies (i) 5Feb15 (top left panel), (ii) 9Jul15 (top right panel), (iii) 10Jul15 (bottom left panel) and (iv) 4Apr16 (bottom right panel).

Table 2. Information about the selected case studies.

	case (i)	case (ii)	case (iii)	case (iv)
Date	5 Feb 15	9 Jul 15	10 Jul 15	4 Apr 16
Atmospheric conditions	weak dust event, low pollution levels	high pollution levels in the morning	typical pollution levels	high pollution levels
Air masses origin below 4 km	S/SW	N/NE	N/NE	N/NE

4.3.2 Aerosol extinction vertical profile retrievals

MAX-DOAS measurements and the BOREAS retrieval algorithm were used for the calculation of the diurnal aerosol extinction vertical distribution over the urban (S) area (Fig. 4) for the selected case studies and for altitudes 0.5-4 km a.s.l. Single scattering albedo (SSA) and phase functions are not retrieved in BOREAS and have to be prescribed. Therefore AERONET measurements are used for specifying SSA (ω) and asymmetry factor (g) values. However, ω and g were not available in AERONET data for case (iv), therefore in this case the algorithm was run using the Henyey-Greenstein phase function with the monthly mean of SSA ($\omega=0.91$) and asymmetry factor ($g=0.68$) from the following year, as derived from the AERONET data (Table 3). Specifically for this case, sensitivity tests with

varying ω and g were carried out. It was found that the variability due to asymmetry factor is small and the impact of SSA negligible. A fixed surface albedo ($\alpha=0.15$), based on a previous study for Athens (Psiloglou et al., 2009), was used in all cases. Table 3 summarises the parameter settings used for the BOREAS retrieval.

Table 3. Settings used for the BOREAS retrieval. The mean daily value of each parameter (ω and g retrieved from AERONET) is mentioned for cases (i), (ii) and (iii). The mean monthly values of ω and g (provided from AERONET for April 2017) were used for case (iv), due to unavailable AERONET daily data around this date.

	case (i)	case (ii)	case (iii)	case (iv)
Surface albedo	0.15	0.15	0.15	0.15
Single scattering albedo (ω)	0.92	0.96	0.93	0.91
Asymmetry factor (g)	0.78	0.65	0.68	0.68
Tikhonov parameter	20	20	20	20

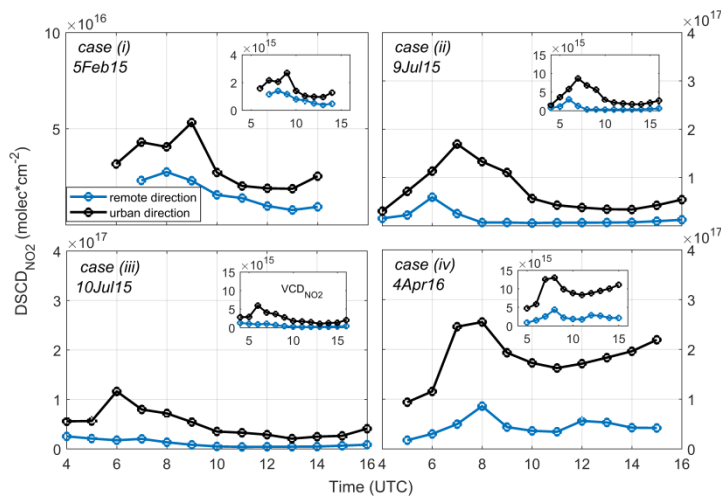


Figure 3. Tropospheric retrievals of diurnal SCD_{NO_2} (elevation angle $+1^\circ$) from MAX-DOAS measurements for the four selected cases studies. The blue and the black curves correspond to the remote (W) and the urban (S) viewing direction, respectively. In the internal panels the corresponding tropospheric VCD_{NO_2} are also shown. Please consider the different scale used in case (i).

The results for case (i) reveal a significant variation of the aerosol distribution in the vertical direction. Although the maximum retrieved extinction values in this case reach almost 0.2 km^{-1} at 1.5 km height in the afternoon, persistent high values are displayed until around local noon (Fig. 4). The temporal variation of the vertical distribution can be attributed to changes in the prevailing wind speed and direction throughout the day; as recorded by NOAA's meteorological monitoring station at Thissio, the prevailing wind direction from 07:00UTC until 10:00UTC (LT=UTC+2 winter time and UTC+3 summer time) was from the south with speed from 1 to $4 \text{ m}\cdot\text{s}^{-1}$, while easterly winds with speed reaching $10 \text{ m}\cdot\text{s}^{-1}$ started blowing at 11:00UTC, efficiently ventilating the Athens basin and removing the dust and atmospheric pollutants. As shown in previous works conducted in the area (e.g Fourtziou et al., 2017), wind speed below $3 \text{ m}\cdot\text{s}^{-1}$ favours the accumulation of pollutants.

The two cases, (ii) and (iii), present an elevated aerosol layer extending up to 3 km between 10:00 and 14:00UTC. Lidar retrievals also show an elevated extinction layer in both cases, as discussed in section 3.3. However, the separation of the two layers could be an artifact which arises from the fact that the MAX-DOAS retrieval's response to a box-like distribution (e.g. a well developed planetary boundary layer - PBL) leads to slight oscillations around this box due to the a priori smoothing. Both cases are related to weak prevailing winds ($<4 \text{ m}\cdot\text{s}^{-1}$), which favour the development of a vertically extended aerosol layer. The higher aerosol load in case (iii) is also corroborated by sun photometric measurements, which are presented and discussed in section 3.4.

Low levels of aerosol extinction (less than 0.1 km^{-1}) are present over the urban area throughout the whole day in case (iv). The highest values of the day (almost 0.14 km^{-1}) are displayed up to 800 m.a.s.l. Given that the NO_2 level, characteristic of anthropogenic pollution, is high during this day (Fig. 3), higher particle pollution levels would be expected.

4.3.3 MAX-DOAS aerosol extinction profiles evaluation

The BOREAS retrieved aerosol extinction profiles from the MAX-DOAS measurements at 477 nm, between 0.5 km (station's elevation) and 4 km height, are compared with the lidar aerosol extinction coefficient measurements at 532 nm, between 1 and 4 km height, for the selected case studies (Fig. 6). Representative morning and afternoon snapshots during each day have been chosen to be presented and discussed. The lack of morning profiles for some days is due to the absence of lidar data, thus, both morning and evening data is available only for cases (i) and (ii). The lidar profile presented in each figure is the result of the mean lidar signal, averaged between the starting and the ending time of the corresponding MAX-DOAS profiles. The uncertainty in the lidar extinction profiles increases substantially for altitudes below 1000 m.a.s.l. due to the loss of overlap between the telescope field of view and the laser beam (Wandinger and Ansmann, 2002; Kim et al., 2008, Papayiannis et al., 2008); hence the lidar data for altitudes below 1000 m a.s.l. is not presented and only measurements above 1000 m a.s.l. are considered for the calculation of the correlation between the two instruments. Another point that has to be considered when comparing the results from the two instruments is that the lidar profiles are characterised by high vertical and temporal resolution and degradation to the sensitivity of the MAX-DOAS profiles is necessary in order to have a meaningful comparison to the MAX-DOAS data. According to the method described by Rodgers and Connor (2003), the degraded lidar profile x_f can be estimated by applying the equation

$$x_f = x_a + AK \cdot (x - x_a) \quad (3)$$

with x_a being the a priori profile used in the algorithm calculations, x the initial lidar profile and AK the averaging kernel from the BOREAS retrieval. The averaging kernel (Fig. 5) denotes the sensitivity of the retrieved profile to the true atmospheric profile for each layer and in fact it represents the smoothing of the true profile in the retrieval. The lidar profile, degraded to 50 m vertical resolution, represents the MAX-DOAS profile that would have been retrieved, if the true extinction profile was x . Last, but not least, the horizontal distance (13 km) between the two measurement sites and the different operation principles of the two instruments should be noted. The lidar system retrieves information

from the air mass right above the measurement site, while MAX-DOAS probes air masses along the line of sight of the telescope pointing from the top of a hill towards the city centre; hence the retrieved aerosol profiles from the two instruments correspond to different air masses and are not expected to fully agree, especially when the aerosol pollution is not horizontally homogeneous over the Athens basin. Thus, the comparison is mainly focused on a qualitative basis.

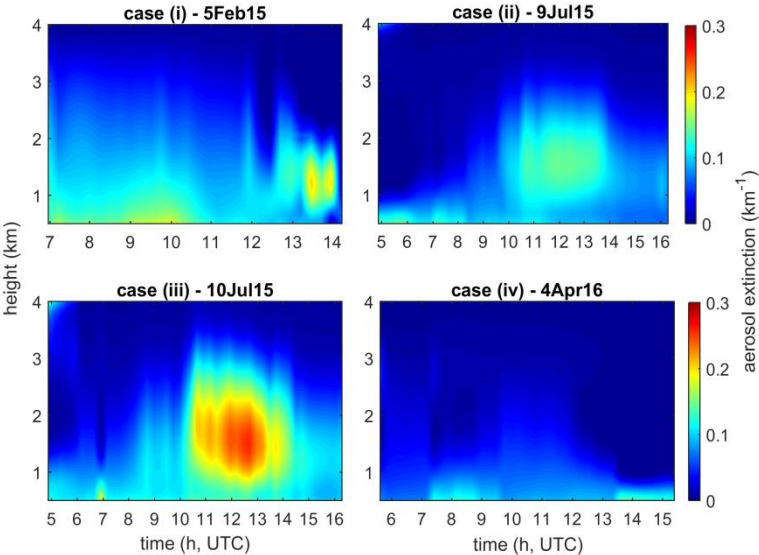


Figure 4. MAX-DOAS retrieved aerosol extinction vertical distributions (from instrument’s height up to 4 km a.s.l.) for the four case studies over the urban area (S). The spatial and vertical resolution of the retrievals is 50 m and 15 min, respectively.

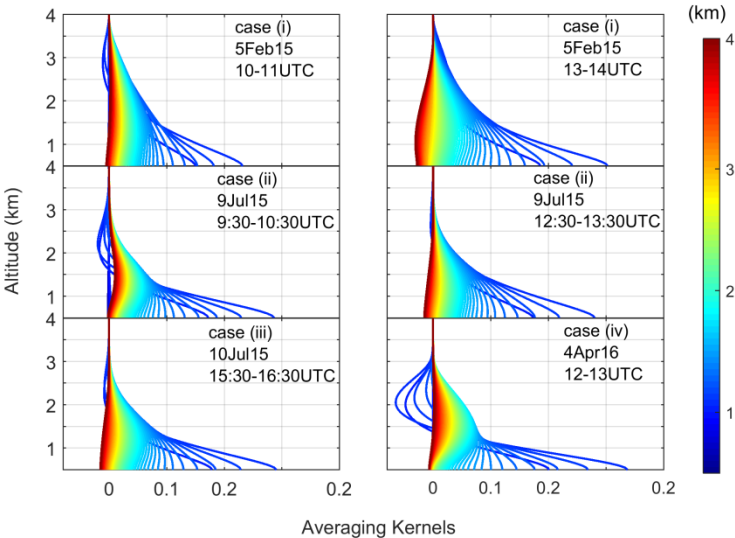


Figure 5. Averaging kernels of the aerosol retrievals for the four case studies. For cases (i) and (ii), the left and right panel corresponds to the morning and afternoon profiles, respectively. The colour bar represents the height of the atmospheric layers.

Each case is examined separately. Comparison information is given in the form of performance statistics - correlation coefficient (r), median lidar/MAX-DOAS ratio, root mean square error (RMSE) and fractional gross error (FGE) – and is shown in Table 4. This set of statistics has been chosen as

suitable to provide a detailed view of the algorithm performance; it has been proposed (Morris et al., 2005) that a FGE less than or equal to 0.75 is a criterion to evaluate good performance of an algorithm, therefore, any FGE>0.75 is used as indicator of a relatively poor performance in this study. In order to perform the statistical calculations we averaged the four MAX-DOAS profiles comprising each case. Thus, all performance statistics have been calculated using the temporally averaged MAX-DOAS profile for each case and the corresponding degraded lidar profile, so that both profiles are of the same temporal and vertical resolution. In all cases, 61 data points are used for the derivation of the statistics. The average smoothing and noise errors for the MAX-DOAS retrievals are given for each case study separately in Table 5. In all cases, the noise error ranges between about 1 and 5%. In cases (i)-mor, (ii) and (iii), the smoothing error is about 15%. The large smoothing errors in cases (i)-aft and (iv) are due to the very small extinction values at higher altitudes.

Case study (i) - 5 February 15

In case (i), the two instruments seem to be in excellent agreement in terms of correlation, with a very high correlation coefficient ($r>0.95$). In the afternoon, a peak in aerosol extinction ($\sim 0.15 \text{ km}^{-1}$) between 1 and 1.5 km is captured by both instruments. The large discrepancy between the original and the degraded lidar profile is attributed to the fact that the AKs of the afternoon retrievals illustrate low sensitivity of the retrieved profile to the true atmospheric profile for altitudes up to 2.5 km (Fig. 5).

It should be mentioned that this is the only case in the present study, where high aerosol load is found in the upper levels (free troposphere) in the original lidar profiles due to transboundary transport of aerosols at higher altitudes. The fact that, at these altitudes, the MAX-DOAS only agrees with the degraded lidar profiles (which means after including the AK information) suggests more significant errors in the a priori aerosol profiles and the reduced capacity of the MAX-DOAS to capture the characteristic inhomogeneity at higher atmospheric layers during aerosol transport episodes. Nevertheless, an overall satisfactory performance of the algorithm is indicated for the morning measurements by the FGE (0.31).

Table 4. Quantitative performance statistics of MAX-DOAS aerosol extinction calculations (BOREAS algorithm) compared to lidar measurements.

Performance Measure	case (i)-mor	case (i)-aft	case (ii)-mor	case (ii)-aft	case (iii)	case (iv)
r	0.97	0.96	0.92	0.95	0.97	0.90
median ratio (lidar/MAXDOAS)	1.37	1.11	0.91	0.60	0.99	1.58
RMSE (km^{-1})	0.03	0.03	0.02	0.04	0.01	0.02
FGE	0.31	0.80	0.37	0.54	0.20	0.61

Table 5. The MAX-DOAS average smoothing and noise errors (%) for each case study.

Uncertainties (%)	case (i)-mor	case (i)-aft	case (ii)-mor	case (ii)-aft	case (iii)	case (iv)
smoothing error	15.59	90.52	16.69	13.61	17.46	53.65
noise error	3.94	2.03	2.69	1.93	2.25	5.53

Case study (ii) - 9 July 15

The retrieved MAX-DOAS profiles agree quite well with the degraded lidar profiles; they both show an aerosol layer extending up to about 2.5 km and the correlation coefficient is very high ($r \approx 0.95$), during both morning and afternoon measurements. In the afternoon, however, the MAX-DOAS measurements result in higher extinction levels by almost 65% compared to the degraded lidar profile. As shown in Fig. 6 (middle row panels), in this case MAX-DOAS tends to overestimate the lidar extinction levels mainly at higher altitudes, a fact that can be attributed to the smoothing effect of the retrieval procedure on the true profile; given that a MAX-DOAS profile algorithm cannot retrieve sharp edges, the underlying narrow high altitude enhancement in the afternoon propagates through the retrieval into a smoother and broader aerosol peak. The FGE, ranging from 0.35 to 0.55, indicates a good performance of the algorithm.

Case study (iii) - 10 July 15

The two instruments seem to correlate very well ($r=0.97$). The MAX-DOAS coincides well with the aerosol extinction levels from the degraded lidar profile; the lidar to MAX-DOAS ratio is equal to 0.99. Nevertheless, when the original lidar profile is considered, a clear discrepancy in the extinction levels is present; the lidar peak value (0.16 km^{-1}) is enhanced by a factor of two. The discrepancy between the original and the degraded lidar profile results from the low sensitivity of the averaging kernels for heights up to about 2 km (Fig. 5, case (iii)), which plays significant role in the degradation (smoothing) of the lidar retrieval. The RMSE is small (0.01 km^{-1}) and the low FGE (0.20) indicates good performance of the algorithm.

Case study (iv) - 4 April 16

The profiles resulting from both instruments display an aerosol layer extending from the lower atmospheric layers up to 1.5 km height. The MAX-DOAS and degraded lidar profile shapes are very similar and highly correlated ($r=0.90$). However, the MAX-DOAS underestimates by almost 30% the lidar aerosol extinction (median lidar/MAX-DOAS ratio=1.58). Although the correlation is high and the RMSE is small (0.02), the FGE (0.61) indicates a moderate performance of the algorithm for the specific case. This FGE value, however, results from the high median ratio of the two profiles, which in turn results from the low extinction levels, since the absolute difference between the two profiles is not that large.

Overall, the correlation between lidar and MAX-DOAS measurements is very good ($0.90 < r < 0.97$) in all cases and a good agreement in the profile shape and altitude of the peak extinction level is also observed. The failure of the MAX-DOAS to capture clearly distinguished aerosol layers is attributed to

the smoothing effect due to the presence of a priori constraints during the retrieval procedure. The RMSE ranges from 0.01 to 0.04 km⁻¹ in all cases. A high FGE (0.80) has been calculated only in the case of measurements at small relative azimuthal angles between the viewing direction and the Sun and in parallel presence of large particles. Due to the different operation principles of each instrument (active/passive remote sensing), the different wavelengths and the different air masses probed by each instrument, a full agreement in the derived profiles would not be expected. In particular, the lidar profiles represent the aerosols which are directly over the measurement site, whereas the MAX-DOAS profiles are representative of the atmosphere at a distance of several kilometres along the line of sight of the instrument. Another conclusion arising from these four cases is that the MAX-DOAS fails to detect part of the urban aerosol pollution when the pollution levels are low (e.g. case(iv)) and also fails to capture the inhomogeneity at higher altitudes in case of aerosol transport episodes.

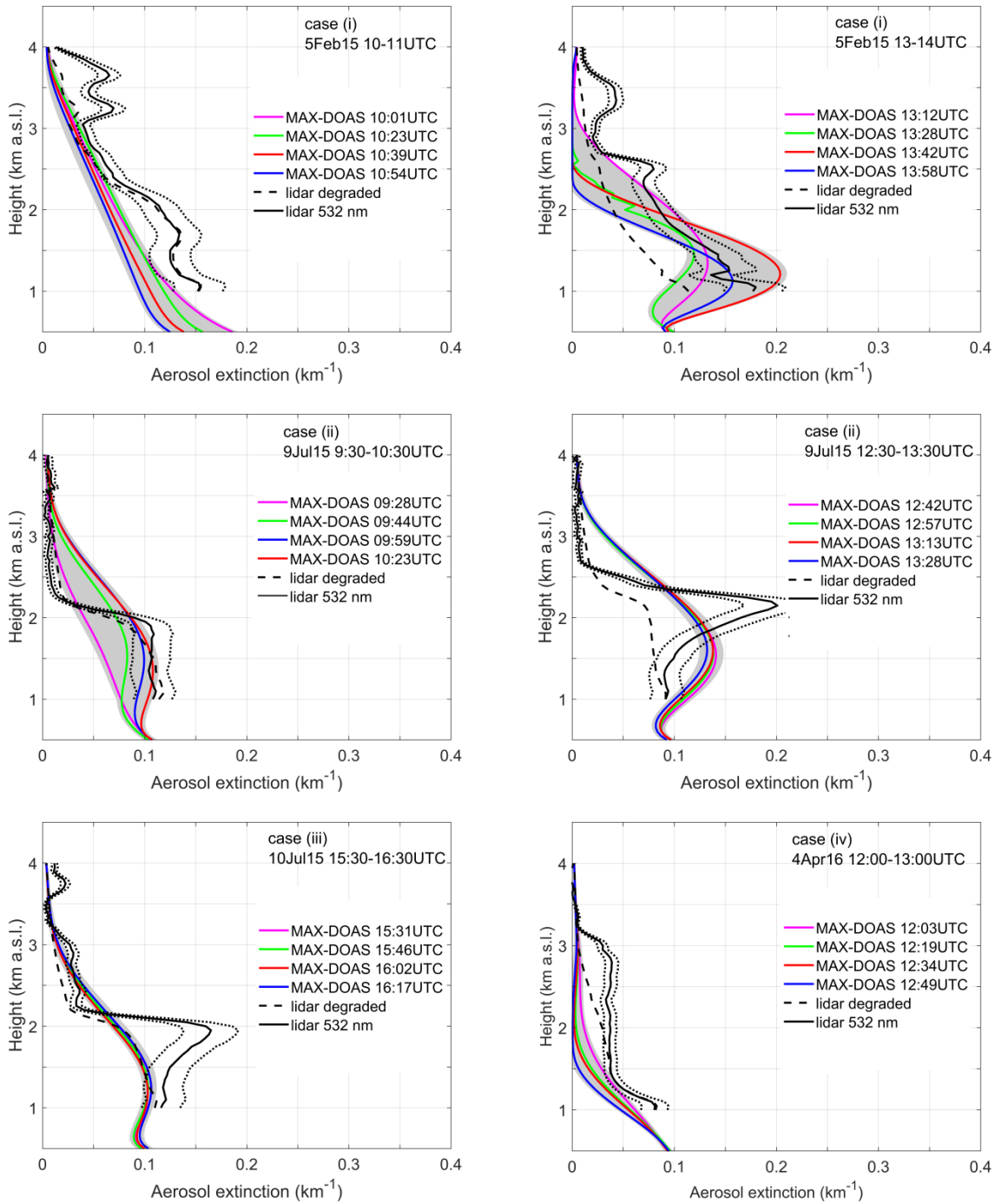


Figure 6. Comparison of retrieved MAX-DOAS aerosol extinction profiles at 477 nm (multicoloured curves), lidar aerosol extinction coefficient vertical profile at 532 nm (black curve) and the corresponding degraded lidar profile (dashed black curve) for the selected case studies. The lidar profile used in each case is the average profile retrieved between the starting and the ending time of the MAX-DOAS retrievals and the light dashed black curves are the lidar-derived aerosol extinction uncertainty obtained by the lidar assumption of 50 ± 20 sr. The grey shaded area represents the corresponding MAX-DOAS uncertainty.

4.3.4 AOD evaluation

In the previous section, lidar measurements were used for the evaluation of the aerosol extinction profiles obtained from MAX-DOAS. However, a conclusive evaluation of MAX-DOAS aerosol optical depth (AOD) cannot be done strictly with lidar-derived AOD values mainly due to the lidar blind range (overlap height), resulting in AOD underestimation. Therefore, in this section, we focus on the comparison between the retrieved AOD from MAX-DOAS measurements at 477 nm and from CIMEL measurements at two wavelengths (440 nm and 500 nm), during the aforementioned case studies (Fig. 7). For the MAX-DOAS AOD calculation, the missing values in the extinction coefficient profiles below 500 m are set to a constant value (equal to the retrieved value at 500 m). This assumes that the atmosphere is well-mixed below 500 m, which probably results in an underestimation of the calculated AOD in case of enhanced surface aerosol layer. When looking at the figures, one should consider that the CIMEL AOD uncertainty is estimated to be approximately 0.01 for wavelengths > 400 nm (Eck et al., 1999). The MAX-DOAS AOD uncertainties are shown in the figures. The Ångström exponent, derived from the CIMEL measurements (400 - 870 nm), is also taken into account, as a qualitative indicator of aerosol particle size, in order to investigate the origin of the aerosols (natural-dust or anthropogenic sources) and the performance of the MAX-DOAS retrievals for different aerosol types and sizes. An overview of the comparison statistics (described in section 3.3), representative of the degree of agreement between MAX-DOAS and CIMEL measurements at 500 nm, is presented in Table 6. The calculations were made on hourly basis to achieve uniform results regarding the air masses. Although this section is focused on the comparison with the AOD from CIMEL, the AOD from lidar measurements (calculated by integrating the aerosol extinction coefficient from ground up to the identified reference height of 4 km a.s.l.) is also presented indicatively. Nevertheless, as a complementary analysis, the comparison between lidar and MAX-DOAS AOD for the common altitude (1-4 km) - along with the corresponding uncertainties - is presented in Table 7.

Case study (i) - 5 February 15

The very small Ångström exponent, ranging between 0.05 and 0.13 throughout the day, indicates the dominance of coarse particles in the aerosol distribution. Given the cloud-free sky conditions and the potential for dust transport found for this day by the NOAA-HYSPLIT (Fig. 2), these particles are probably associated with the presence of dust in the atmosphere. The correlation between the two instruments is moderate ($r=0.47$) and the calculated AOD levels from the MAX-DOAS measurements underestimate by about 20% the CIMEL measurements (median ratio CIMEL/MAX-DOAS = 1.22). The daily averaged AOD values are $0.33 (\pm 0.02)$ and $0.39 (\pm 0.03)$ for MAX-DOAS and CIMEL, respectively, and are much higher than the climatological monthly average value (0.27 ± 0.03) for February in Athens, as reported in Gerasopoulos et al. (2011). The RMSE is 0.07, however the FGE, which is small (0.17) implies excellent performance of the algorithm. The moderate correlation results may arise from the fact that CIMEL performs direct sun measurements, whereas MAX-DOAS measurements - and the subsequent AOD retrieval - are performed at a fixed azimuthal direction. Thus, the CIMEL measurements are highly affected by variations in the temporal and spatial distribution of the aerosols. The AOD from the lidar measurements at 10:00 and 13:00UTC (0.37 and 0.35, respectively) coincides well both with CIMEL and MAX-DOAS measurements.

Case study (ii) - 9 July 15

In this case, the large values of the Ångström exponent ($\alpha \geq 2$) are indicative of the presence of fine mode aerosols that are associated with urban pollution (Westphal and Toon, 1991, Eck et al., 1999, Gerasopoulos et al., 2011). The considerable levels of NO_2 measured during this day (Fig. 3), indicate the presence of anthropogenic pollution. The two instruments are again moderately correlated ($r=0.67$), however if the afternoon measurements - after 16:00LT - are excluded, the correlation becomes very good ($r=0.87$). The median ratio (0.85) indicates that the MAX-DOAS overestimates the AOD levels measured by the CIMEL. However, the overestimation is more profound during the morning, while in the afternoon the MAX-DOAS slightly underestimates the measured AOD by about 20%, a fact that can be attributed to inaccuracies in the radiative transfer calculation for the forward scattering geometry. The daily averaged AOD values are 0.20 and 0.19 for MAX-DOAS and CIMEL, respectively. The small values of both the RMSE (0.07) and the FGE (0.26) are indicators of very good performance of the algorithm. The gaps in the CIMEL data in this case, as well as in case (iii), are probably due to saturation of the instrument. The lidar AOD in this case (0.21 at 10:00UTC and 0.26 at 13:00UTC) agrees well with the CIMEL measurements at 500 nm, but is lower than the AOD from the MAX-DOAS; the difference is more considerable in the afternoon.

Case study (iii) - 10 July 15

In the third case study, the measurements from the two instruments seem to be in better agreement during morning hours. Overall, the MAX-DOAS AOD levels coincide well with CIMEL (median CIMEL/MAX-DOAS ratio is 0.95), however the underestimation due to light scattering geometry after 13:00UTC is about 35%. The moderate results with respect to correlation ($r=0.53$) are due to the large discrepancy between the two instruments during the afternoon. If only the measurements until 13:00UTC are considered, the correlation is considerably improved ($r=0.75$). Despite the non-satisfactory correlation, the calculated FGE (0.28) indicates a very good performance of the algorithm. The lidar-derived AOD in the afternoon is higher than the MAX-DOAS measurement. Unfortunately, no CIMEL or lidar data are available around noon in order to validate the aerosol plume captured by MAX-DOAS. It should be noted, though, that case studies (ii) and (iii) (both summer days in July) exhibit the same diurnal pattern; lower values in the morning, steadily increasing throughout the day and then slightly declining in the afternoon. A similar diurnal AOD pattern was found for summer in Athens by Gerasopoulos et al., 2011 and this pattern has been associated with local urban or industrial sources (Smirnov et al., 2002).

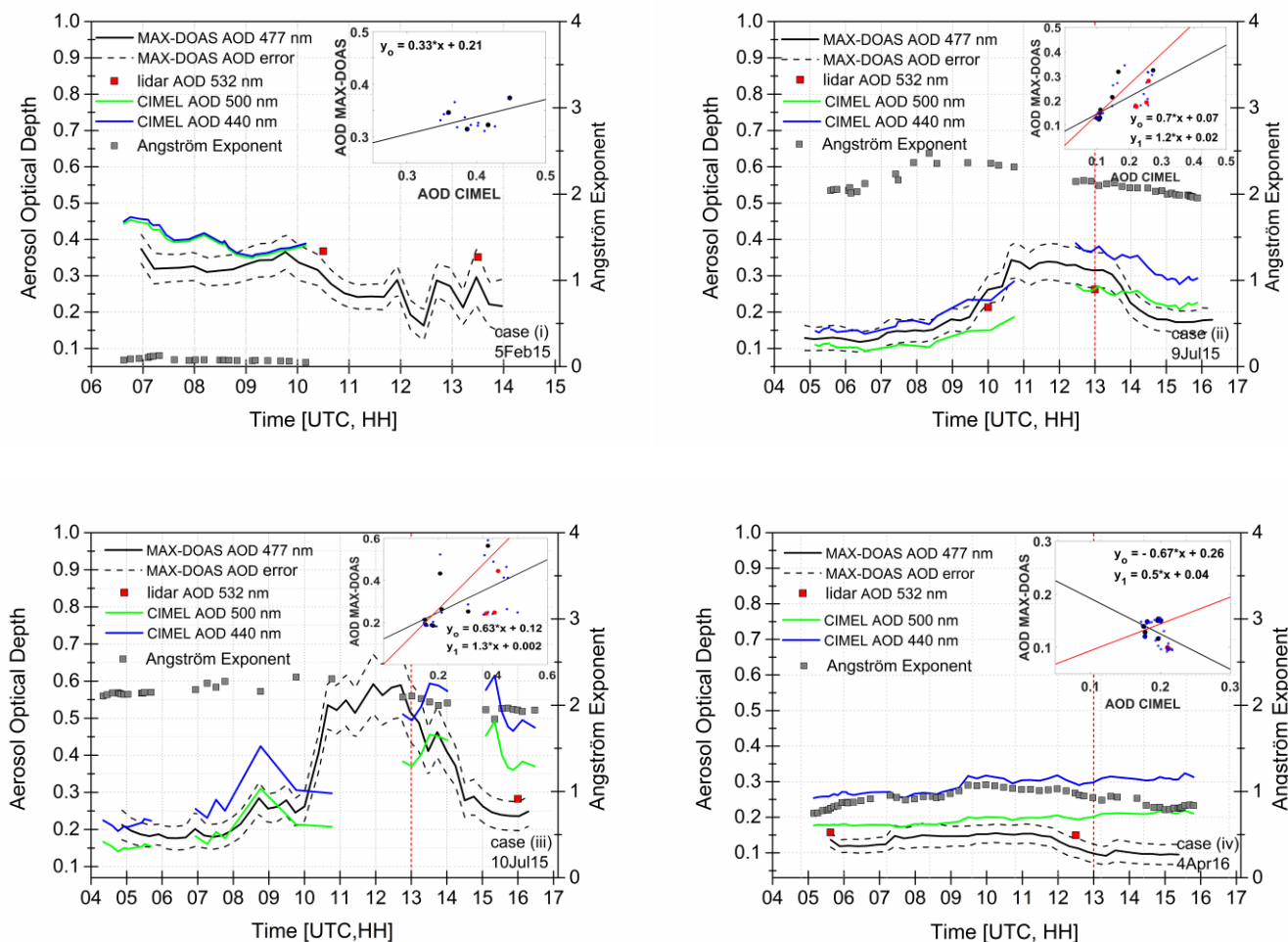


Figure 7. AOD as derived from MAX-DOAS (black curve) and CIMEL at 440 nm and 500 nm (green and blue curve, respectively). The grey and the red square markers represent the Angström exponent derived from 400 and 870 nm and the lidar derived AOD, respectively. The dashed black curves represent the MAX-DOAS AOD uncertainties. The scatter plots between hourly AOD calculated from MAX-DOAS measurements and hourly AOD from CIMEL at 500 nm are shown in the internal panels; the red points correspond to measurements after 13:00UTC. Accordingly, y_0 is the linear regression equation with all the data points included and y_1 is the linear regression equation when the data points after 13:00UTC have been excluded. The smaller blue points are the raw data points. The vertical red dashed line separates the measurement data before and after 13:00UTC

Table 6. Quantitative performance statistics of MAX-DOAS AOD calculations (BOREAS algorithm) at 477 nm compared to CIMEL measurements at 500 nm .

Performance Measure	case (i)	case (ii)	case (iii)	case (iv)
r	0.47	0.67	0.53	-0.42
median ratio (CIMEL/MAXDOAS)	1.22	0.85	0.95	1.37
RMSE	0.07	0.06	0.11	0.07
FGE	0.17	0.26	0.28	0.40

Case study (iv) - 4 April 16

The Ångström exponent in this case ($\alpha \approx 1$) indicates the presence of coarse aerosols ($\text{radii} \geq 0.5 \mu\text{m}$) in the atmosphere (Westphal and Toon, 1991, Eck et al., 1999). The NOAA HYSPLIT backtrajectories show the potential for African dust transport to Athens, however, at higher altitudes of up to 5 km. Nevertheless, despite the presence of coarse particles, the AOD levels are low; the daily averaged AOD values are 0.13 and 0.19 for MAX-DOAS and CIMEL, respectively. The MAX-DOAS underestimates the AOD with respect to CIMEL by about 25% (and by 50% if only the afternoon measurements are considered), the RMSE is 0.07 and the FGE is 0.40, yet it seems that the two measurement techniques are not correlated ($r = -0.42$). However, the comparison in terms of correlation, results in better outputs if only the morning measurements are considered; in this case the correlation coefficient is 0.75. It seems that MAX-DOAS, in this case, fails to detect the accumulation of coarse particles. Nevertheless, the AOD lidar measurements agree very well with the MAX-DOAS measurements (Table 7).

Overall, a systematic underestimation of the AOD, by 20 to 35%, by the MAX-DOAS is observed in the afternoon measurements, when the relative azimuthal angle between the MAX-DOAS viewing direction and the Sun is small. Better agreement is achieved at large relative azimuthal angles in the morning. This finding has also been reported by Frieß et al. (2016) when comparing different retrieval algorithms with sun photometer measurements. Considering that i) the sun-photometer is located downtown (150 m a.s.l.), at lower altitude than the MAX-DOAS (527 m a.s.l.) and thus more sensitive to aerosols in the lower troposphere and ii) the absence of real measurements from MAX-DOAS for altitudes below 500 m a.s.l., an underestimation of the contribution of the urban pollution to the retrieved by MAX-DOAS AOD would be expected. Nevertheless, the MAX-DOAS seems to detect well the typical urban aerosols in the boundary layer; the mean AOD difference (CIMEL minus MAX-DOAS) of all the measurements is 0.03 with standard deviation 0.08. Furthermore, CIMEL is a direct sun photometer, which means that in each measurement different air masses are detected, while the MAX-DOAS always points at the same direction; this operational difference is reflected in the non-satisfactory correlation. When fixed values of SSA and asymmetry factor (instead of AERONET data) are used by BOREAS, it seems that MAX-DOAS fails to detect accumulated coarse particles (e.g. case (iv)), leading to underestimation in case of small Ångström exponent values (< 1). Frieß et al. (2016) have also come to this conclusion during the CINDI-2 campaign. However, the underestimation could also be attributed to the high altitude aerosol layer detected by the lidar (Fig. 6); the MAX-DOAS' sensitivity at higher altitudes is low and the calculated AOD is limited up to 4 km, while the AOD from CIMEL refers to the total atmospheric column. In addition, the presence of aerosol layers above 4 km that could contribute to the AOD was examined by using the lidar signals and no significant aerosol load was observed above this height. It should also be noted that the standard AERONET version 2 algorithm uses an NO_2 climatology with a spatial resolution much coarser than the area of the city of Athens (Giles et al., 2019), hence in certain cases the difference between the MAX-DOAS and the higher CIMEL AOD levels at 440 nm could result from additional NO_2 content in the atmosphere, which is the case of highly polluted days. The lidar-derived AOD levels coincide well with the MAX-DOAS measurements.

Table 7. MAX-DOAS (477 nm) and lidar (532 nm) AOD calculations for the atmospheric layer 1-4 km.

AOD (1-4 km)	case (i)-mor	case (i)-aft	case (ii)-mor	case (ii)-aft	case (iii)	case (iv)
lidar	0.24 ± 0.04	0.21 ± 0.03	0.13 ± 0.03	0.19 ± 0.03	0.19 ± 0.03	0.09 ± 0.01
MAX-DOAS	0.16 ± 0.03	0.15 ± 0.06	0.18 ± 0.04	0.27 ± 0.05	0.19 ± 0.04	0.07 ± 0.03

4.4 Summary and conclusions

An assessment of the retrieval of aerosol extinction profiles and AOD from MAX-DOAS measurements is presented for the first time for the urban environment of Athens. The profiling results are compared to lidar extinction profiles and to AODs obtained from sun photometric measurements. The intercomparison results are very promising, showing that the MAX-DOAS measurements provide a good estimation of the aerosol vertical profile over Athens. Although this intercomparison is of great importance for the validation of the MAX-DOAS retrieval, the different operation, characteristics and measurement principles of each instrument, in addition to some comparison restrictions, have to be considered.

Regarding the spatial characteristics, (i) the measurements with the MAX-DOAS technique represent an area that includes the AERONET and the lidar locations, but it is not limited to them. Regarding the vertical aerosol information, (ii) the MAX-DOAS retrievals are representative for 500-4000 m a.s.l., while the lidar profiles are valid for altitudes higher than 1000 m above the station and finally (iii) the AOD AERONET measurements describe the columnar aerosol properties representative of an area ranging from few up to 10 km radius above the Athens area, depending on solar elevation. Also, (iv) the sun-photometer AOD observations probe the extinction in the full atmospheric column while MAX-DOAS retrievals are sensitive only to the lowest kilometers, leading to differences in the presence of aerosol layers at altitudes above 4 km. Nevertheless, despite the comparison restrictions and the differences of the three instruments, the comparison of the retrieved profiles and the AODs shows that the MAX-DOAS measurements bode well for the future of aerosol measurements and they are able to provide a good estimation of the aerosol vertical distribution over Athens.

The vertical profiles retrieved by BOREAS profiling algorithm applied to the MAX-DOAS measurements are qualitatively in good agreement with the lidar profiles smoothed with the MAX-DOAS averaging kernels; there is good agreement in aerosol layer shape and aerosol extinction levels, except in cases of inhomogeneity at higher altitudes, characteristic of aerosol dust transport episodes. Very good correlation ($r > 0.90$) was found in all cases. A satisfactory fractional gross error ($0.20 < FGE < 0.54$) has been calculated in all cases with fine aerosol particles (urban pollution), indicating a good performance of the BOREAS profiling algorithm in these cases. In some cases, the observed underestimation of the aerosol extinction (by 20 to 35%) by the MAX-DOAS at small relative azimuth angles can be attributed to the geometry of Mie scattering in relation to the location and viewing geometry of MAX-DOAS, resulting in MAX-DOAS' failure to detect part of the urban aerosol pollution. Overall, the agreement between the two instruments is encouraging, especially when considering the different nature of each technique and the different instrument locations, suggesting that the MAX-DOAS can accurately enough represent the aerosol vertical distribution.

The MAX-DOAS retrieved AODs show satisfactory agreement with the sun photometric measurements, in terms of AOD levels. The MAX-DOAS underestimates the AOD in the presence of coarse particles; CIMEL/MAX-DOAS ratio > 1 coincides with Ångström exponent values < 1 . A systematic underestimation by MAX-DOAS is observed in the afternoon measurements due to MAX-DOAS' viewing geometry. Overall, the MAX-DOAS can be considered as an effective mean for measuring the aerosol levels in Athens; the average AOD difference of all measurements between the two instruments is 0.03. It is important to note that in Athens, a highly populated and polluted area, horizontal gradients, especially in anthropogenic aerosols, are very likely to occur, resulting in different air masses detected by each instrument and subsequently in discrepancies between MAX-DOAS and CIMEL measurements.

This intercomparison is of great importance for the validation of the MAX-DOAS retrieval. Despite the already mentioned limitations due to different operation, characteristics and measurement principles of each instrument, this work demonstrates that the MAX-DOAS measurements in Athens and the BOREAS algorithm can provide a good estimation of the aerosol vertical structure of the urban atmosphere, on a continuous and long-term basis, offering a reliable data set for scientific studies. There is certainly more work to be conducted in future studies in order to understand the sensitivity of the MAX-DOAS aerosol measurements based on different aspects of urban pollution evolution and long range transported aerosols.

Data availability

All data sets used and produced for the purposes of this work are freely available and can be requested from the corresponding author.

Author contribution

MG, PK and AR conceived the presented idea. MG performed the analysis and prepared the manuscript. TB developed the profile retrieval algorithm and provided guidance to MG on the algorithm calculations and parameterization. AR provided guidance to MG on MAX-DOAS data retrieval and profile calculations. MG designed the figures with support from PK and TB. AR and SK advised MG on the results interpretation. PK, AP and MM provided the lidar data. VA provided the sun-photometer measurements. AT made comments on the sun-photometer/max-doas comparison. AR, EG, SK, NM and MV provided critical feedback. All authors provided comments that helped shape the manuscript.

Competing interests

Andreas Richter and Vassilis Amiridis are members of the editorial board of the journal.

Acknowledgments

We acknowledge support of this work by the project “PANhellenic infrastructure for Atmospheric Composition and climatE change” (MIS 5021516), which is implemented under the Action “Reinforcement of the Research and Innovation Infrastructure”, funded by the Operational Programme “Competitiveness, Entrepreneurship and Innovation” (NSRF 2014-2020) and co-financed by Greece and the European Union (European Regional Development Fund).

The combined effect of reduced fossil fuel consumption and increasing biomass combustion on Athens' air quality, as inferred from long term CO measurements

To evaluate the role of increasing biomass combustion emissions and the reduced use of fossil fuel as a result of the economic recession in Greece, carbon dioxide (CO) atmospheric concentrations from five stations of the National Air Pollution Monitoring Network of the Ministry of Environment in Athens, spanning the period 2000-2015, in conjunction with black carbon (BC) concentrations from the NOA (National Observatory of Athens) station at Thissio were analysed. The contribution of different sources to the diurnal cycle of these pollutants is evident and is reflected in two peak concentrations: one morning peak (09:00 LT) attributed to vehicle traffic and one afternoon peak (22:00 LT) attributed both to fossil fuel combustion (traffic plus central heating) and biomass combustion.

The interannual changes in the relative contribution of biomass and fossil fuel combustion were estimated through the calculation of morning (06:00-10:00 LT) and afternoon (16:00-05:00 LT) integrals of CO concentrations for the last 15 years. The results of this analysis demonstrated that:

i) CO concentrations during morning rush hours have been steadily declining over the years (total reduction of around 50% since 2000) and during all seasons. This demonstrates the decline in fossil fuel use over the last 15 years, which can be attributed to the gradual renewal of the vehicle fleet (along with other measures adopted under European legislation towards reducing emissions) and to reduced anthropogenic activities in the most recent years as a response to the financial crisis.

(ii) The impact of biomass burning becomes dominant during winter months since 2011, when the economic crisis affected the price of oil: an increase of 23%-78% (depending on the measurement site) in the winter afternoon integrals since 2012, provides evidence of the significant contribution of biomass combustion, which has prevailed over fossil fuel for domestic heating.

In addition, CO emitted by wood burning was found to contribute almost 50% to the total CO emissions during night time (16:00-5:00), suggesting that emissions from biomass combustion have gained an increasing role in atmospheric pollution levels in Athens.

Overall, it is deduced that the shift of Athens' habitants to wood burning, as major fuel for heating purposes, has significant impact on Athens' air quality (as revealed by the CO levels), which is to the opposite direction of the impact from reduced fossil fuel consumption.

The importance of this study lies on the fact that it quantifies the diachronic changes in air pollution in Athens and associates it with several socioeconomic factors (e.g. measures, economic crisis, behavioural changes), while it can serve as reference in the future for assessing and evaluating expected mitigation measures.

The text of this study, published in the international peer-reviewed journal Science of the Total Environment, is attached.



Contents lists available at ScienceDirect

Science of the Total Environment

journal homepage: www.elsevier.com/locate/scitotenv

The combined effect of reduced fossil fuel consumption and increasing biomass combustion on Athens' air quality, as inferred from long term CO measurements



Myrto Gratsea^{a,b}, Eleni Liakakou^a, Nikos Mihalopoulos^{a,b}, Anastasios Adamopoulos^c, Eirini Tsilibari^c, Evangelos Gerasopoulos^{a,*}

^a Institute for Environmental Research and Sustainable Development, National Observatory of Athens, Greece

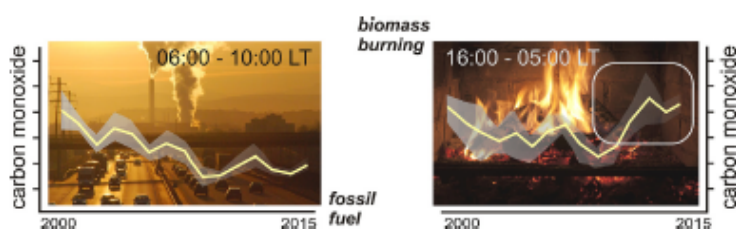
^b Environmental Chemical Processes Laboratory, Department of Chemistry, University of Crete, Greece

^c Ministry of the Environment & Energy, Dept. of Air Quality, Athens, Greece

HIGHLIGHTS

- BC and long term CO measurements to evaluate the increasing role of biomass combustion
- Morning CO peaks decreased by 50% reflect reduction of fossil fuels use.
- Winter evening CO peaks increased by 37%–78% since 2012 reflect intense wood burning.
- CO_{wb} contributes 50% to the total CO emissions during night time.

GRAPHICAL ABSTRACT



ARTICLE INFO

Article history:

Received 22 November 2016

Received in revised form 14 February 2017

Accepted 5 March 2017

Available online xxxxx

Editor: D. Barcelo

Keywords:

Urban atmosphere
Biomass combustion
Carbon monoxide
Black carbon
Athens
Economic recession

ABSTRACT

To evaluate the role of biomass burning emissions, and in particular of residential wood heating, as a result of the economic recession in Greece, carbon monoxide (CO) atmospheric concentrations from five (5) stations of the National Air Pollution Monitoring Network in Athens, spanning the period 2000–2015, in conjunction with black carbon (BC) concentrations from the NOA (National Observatory of Athens) station at Thessio were analysed. The contribution of the different sources to the diurnal cycle of these two pollutants is clear, resulting to a morning peak, mainly due to traffic, and a late evening peak attributed both to fossil fuel (traffic plus central heating) and biomass combustion. Calculated morning and evening integrals of CO peaks, for the investigated period, show consistent seasonal modulations, characterised by low summer and high winter values. The summer and winter morning CO peak integrals demonstrate an almost constant decreasing trend of CO concentrations over time (by almost 50% since 2000), attributed to the renewal of passenger car fleet and to reduced anthropogenic activities during the last years. On the other hand, an increase of 23%–78% (depending on the monitoring site) in the winter evening integrals since 2012, provides evidence of the significant contribution of biomass combustion, which has prevailed over fossil fuel for domestic heating. CO emitted by wood burning was found to contribute almost 50% to the total CO emissions during night time (16:00–5:00), suggesting that emissions from biomass combustion have gained an increasing role in atmospheric pollution levels in Athens.

© 2017 Elsevier B.V. All rights reserved.

* Corresponding author.

E-mail address: egera@noagr (E. Gerasopoulos).

Abstract. To evaluate the role of biomass burning emissions, and in particular of residential wood heating, as a result of the economic recession in Greece, carbon monoxide (CO) atmospheric concentrations from five (5) stations of the National Air Pollution Monitoring Network in Athens, spanning the period 2000-2015, in conjunction with black carbon (BC) concentrations from the NOA (National Observatory of Athens) station at Thissio were analysed. The contribution of the different sources to the diurnal cycle of these two pollutants is clear, resulting to a morning peak, mainly due to traffic, and a late evening peak attributed both to fossil fuel (traffic plus central heating) and biomass combustion. Calculated morning and evening integrals of CO peaks, for the investigated period, show consistent seasonal modulations, characterised by low summer and high winter values. The summer and winter morning CO peak integrals demonstrate an almost constant decreasing trend of CO concentrations over time (by almost 50% since 2000), attributed to the renewal of passenger car fleet and to reduced anthropogenic activities during the last years. On the other hand, an increase of 23%-78% (depending on the monitoring site) in the winter evening integrals since 2012, provides evidence of the significant contribution of biomass combustion, which has prevailed over fossil fuel for domestic heating. CO emitted by wood burning was found to contribute almost 50% to the total CO emissions during night time (16:00-5:00), suggesting that emissions from biomass combustion have gained an increasing role in atmospheric pollution levels in Athens.

5.1 Introduction

The economic recession that has engulfed Europe since 2008 had great impact on air quality in several European countries. The impact on air quality has been evaluated in several studies using in-situ (e.g. Cusack et al., 2013 and Lyamani et al., 2011) and satellite measurements (Castellanos and Boersma, 2012), revealing significant reduction of air pollutants attributed to reduced fuel consumption. The subsequent reduction of industrial activities and traffic emissions resulted in pollution reduction, while on the other hand, the extended use of biomass instead of oil for domestic heating, have resulted in severe smog episodes during winter (e.g Puxbaum et al. 2007; Favez et al., 2009 and references therein).

In Greece, the economic recession has vastly affected the general productivity, inducing changes in the field of air pollution, mainly in large cities. It has also led to changes in consumers' behaviour regarding the level and type of fuel consumption. For Athens in particular, Vrekoussis et al. (2013), using satellite observations, showed a 30-40% reduction in NO₂ tropospheric columns since 2008. Since 2011, when the economic crisis in Greece affected the price of oil, a great part of the population of Athens have been gradually relying on the use of wood stoves and fireplaces during winter months, as primary domestic heating devices. In addition, the use of biomass as fuel for central heating in Athens became legal in 2011, according to ministerial decision. The most recent survey from the Hellenic Statistical Authority conducted in 2011-12, reported that the main sources of heating in Greece are: fossil fuel (oil, 64%), biomass (12%), electricity (12%) and natural gas (9%). Additionally, 32% of those who use fossil fuel, they also burn wood in fireplaces. Fireplaces exist mainly in new buildings (constructed after 2000), the geographical distribution of which is mainly in Athens' northern and southern suburbs. However, wood stoves are used extensively in all areas (especially in poorer parts of the city), where

the wood quality has been widely questioned (e.g. furniture). The smoke from wood burning during night time in combination with Athens' special topography (surrounded by three mountains to the North, West and Northeast favoring the accumulation of atmospheric pollutants) and shallow nocturnal atmospheric boundary layer (Kallos et al., 1993, Kassomenos et al., 1995, Fourtziou et al., 2016) gave rise to severe smog episodes. Similar episodes due to biomass burning have also been reported in the second most populated city of Greece, Thessaloniki (Saffari et al., 2013). Such smog episodes may have severe health impacts on population as it has been revealed by the relationship between human lung cancer and the long-term high concentrations of certain pollutants abundant in smog (Beeson et al., 1998). Air pollution in general is a major environmental risk, affecting human health (e.g. Voutsas et al., 2015, Dimitriou et al., 2013, Kampa and Castanas 2008).

To track biomass burning activities, several tracers have been introduced. Fourtziou et al. (2016) evaluated a number of them for the case of Athens, including black carbon (BC) and carbon monoxide (CO). BC consists of pure carbon in several linked forms and it is formed through the incomplete combustion of fossil fuels, biofuel and biomass. It is a strong absorber of visible solar radiation in the atmosphere and therefore its concentration and distribution in the atmosphere has a positive impact on the radiation budget. Its lifetime in the atmosphere is several days to weeks. CO is produced by partial oxidation of hydrocarbons and its significant role in tropospheric chemistry makes it an important trace gas of the atmosphere (Crutzen and Zimmermann, 1991). CO and especially BC are good indicators for combustion processes (e.g. Saurer et al. 2009). In the urban environment of Athens the main sources of CO and BC are traffic (Chaloulakou et al., 2003) and more recently biomass burning (Paraskevopoulou et al., 2014). An emission inventory constructed for Greece and the Greater Athens Area by Fameli and Assimakopoulos (2016) showed that regarding residential emissions, 67% of the emitted CO in Greece originates from fireplaces.

Overall, Athens is a megacity characterised by great abundance of atmospheric pollutants and frequent pollution episodes. The atmospheric environment of Athens has been the subject of several studies (e.g. Ziomas et al., 1998, Kalabokas et al., 1999) throughout time. Vehicle exhausts, industry and central heating during winter months are the main sources of air pollution in the city (Lalas et al., 1982). Reduction of pollution has been reported during 1984-1993 due to measures adopted for improving city's air quality (Fenger et al., 2013) and a following stabilisation until 2008, when the global economic crisis arose. The latter induced on one hand cut down of industrial activities and vehicle's use and on the other hand an increase of residential wood burning.

To our knowledge, the relative contribution ratio of wood burning and fossil fuel combustion to Athens' air quality is not known. In this work we used long-term CO measurements from three urban, two urban background and one suburban station in Athens, to assess the impact of biomass burning and to relate it with the evolution of air quality and the economic recession in Greece. In addition simultaneous CO and BC measurements were performed at an urban background station during two winters period (2012-2013 and 2014-2015) to validate our use of CO as an efficient wood burning tracer. Section 2 provides a short description of the measurement sites and the instruments used. Section 3 presents the results of the statistical analysis including wood burning episodes identification, measurement sites intercomparison and assessment of the interannual variability. The development

of a simple algorithm for distinguishing CO emitted from wood burning and fossil fuel combustion is also described. Finally, in section 4 the main conclusions are presented.

5.2 Methodology

5.2.1 Sampling

Data used in this study were obtained from in-situ measurements of the National Observatory of Athens (NOA) at Thissio station (37° 58' N, 23° 43' E) and five more stations - Marousi (38° 01' N, 23° 47' E), N.Smyrni (37° 55' N, 23° 42' E), Athinas (37° 58' N, 23° 43' E), Geoponiki (37° 59' N, 23° 42' E) and Piraeus (37° 56' N, 23° 43' E) - of the National Air Pollution Monitoring Network (NAPMN), which is part of the Ministry of Environment and Energy network. Athinas, is located in the centre of the city near to a busy road and it is characterized as an urban traffic station. Marousi and N.Smyrni are urban background stations and are located in the northeast and south area of Athens, respectively (Fig. 1). Geoponiki is an industrial-suburban station and Piraeus (port) is in the south and is an urban traffic station.

Thissio sampling site is located on top of a hill in the historic centre of Athens, surrounded mostly by a pedestrian zone and some densely populated neighbourhoods, and it is considered as urban background station reflecting the average pollution of the city (Paraskevopoulou et al., 2015). The major sources of air pollution affecting the site are expected to be vehicular emissions and residential heating. In general, several particulate and gaseous components are being continuously monitored since December 2013 at Thissio station during intensive campaigns in winter, either by online in-situ monitoring or by sampling and subsequent chemical analysis at the laboratory (e.g. Fourtziou et al., 2017). Each of the intensive campaigns (winter 2013-2014 and 2014-2015) lasted for a period of approximately two months, from mid-December until mid-February.

BC measurements at Thissio station were obtained using a portable Aethalometer (AE-42, Magee Scientific) operating at 7 wavelengths (370, 470, 520, 590, 660, 880 and 950 nm) and a Multi Angle Absorption Photometer (MAAP 5012 Thermo company). CO was monitored by a Horiba APMA-360 series automatic gas analyser (scale: 0-10 ppmv, lower detectable limit: 0.2 ppmv, precision: ± 0.2 ppmv). The NAPMN network consists of 15 stations in Athens area providing data of atmospheric pollutant concentrations since 1983. CO is measured at five NAPMN stations and is determined using a Horiba APMA-360 series automatic gas analysers (NDIR technique, scale: 0-20 ppmv, lower detectable limit: 0.05 ppmv). The CO analysers provide 1-min concentrations. In situ calibration of automatic analyzers is carried out on a monthly basis using a dynamic dilution system, while intermediate checks are performed according to EN 14626 and EN 14211. The mass flow controllers of the dynamic dilution system are calibrated every year at the premises of the Ministry of the Environment & Energy in agreement with the quality assurance programmes of the National Reference Laboratory for Air Quality. The linearity, zero drift and repeatability are main parameters, among

others, that are checked for all analysers according to the relevant EN standards. CO cylinders are used for the in situ calibration of the gas analysers. These cylinders have been initially checked by a static dilution system in agreement with the National Reference Laboratory for Air Quality. The Laboratory of Air Quality is accredited according to EN ISO 17025, inter alia, for the performance of calibration of gas flow and determination of the composition of gas mixtures of CO using the static volumetric method. Meteorological data from NOA's station at Thissio was additionally retrieved.

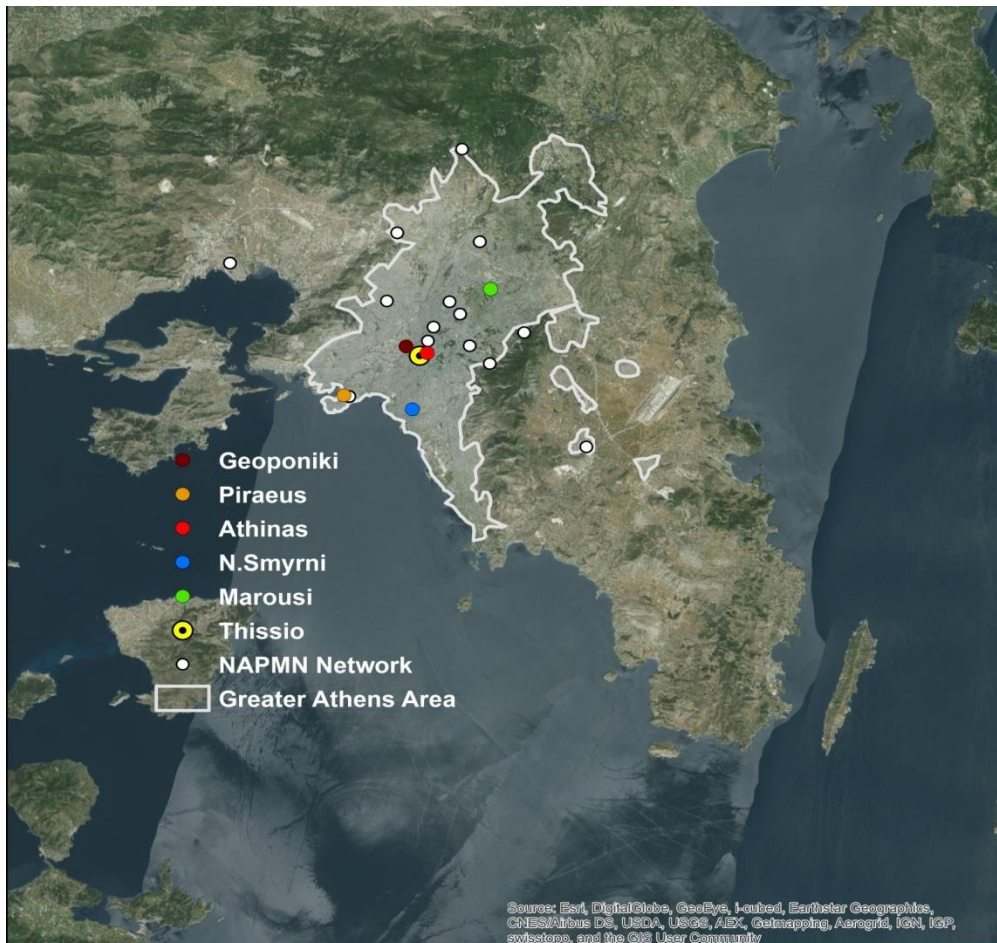


Figure 1. Map of the Athens area. Locations of the NAPMN monitoring sites and Thissio station. The Greater Area of Athens is marked.

5.2.2 Data analysis

Data sets of 1-hour averaged CO concentrations for the time period 2000-2015 were used for the analysis. Continuous BC measurements were performed at Thissio station from December 2013 to February 2014 and from November 2014 to February 2015. To discriminate between BC associated with fossil fuel (BC_{ff}) and wood burning (BC_{wb}) processes, a technique and corrections for multiple scattering and shadowing effects - as described in previous works (Sciare et al., 2011; Favez et al., 2010, Collaud Coen et al., 2010, Weingartner et al., 2003) has been applied.

5.3 Results and discussion

5.3.1 Biomass burning episodes identification

Winter time (November 2014 – February 2015) concentrations of CO, BC and BC_{wb} measured at the Thissio station are presented in Figure 2, where severe spikes can be clearly seen. High values of BC, coinciding with BC_{wb} peaks, have been recorded during night time reaching in some cases 18 µg/m³ mass concentrations. Minimum values are recorded before sunrise. In similar studies conducted for urban areas in Canada and Beijing, hourly BC concentrations varied from 0.1µg/m³ to 7µg/m³ and from 2.7 µg/m³ to 6.1 µg/m³, respectively (Sharma et al., 2002 and Wang et al., 2009). In Paris, biomass combustion has been estimated to contribute almost 20% of the total BC mass, at a representative for particulate pollution station at the centre of Paris (Crippa et al., 2013). A study conducted at an urban background station in Athens from 2008 to 2013 reveals an elevation of elemental carbon (EC) in the PM_{2.5} fraction since 2011, reaching maximum daily concentrations higher than 3 µg/m³ (Paraskevopoulou et al., 2014). Florou et al. (2016), report that domestic wood burning in Athens is in general a more significant organic aerosol (OA) source compared to traffic accounting for almost 40% of the OA versus 10% of the traffic. Finally, Fourtziou et al. (2016) show that during biomass burning episodes PM1 is consisted mainly of OA (more than 80%).

An obvious coincidence of BC and CO peaks can be seen in Figure 2. CO concentrations range from 200 to 3500 ppb. The 8-hour limit value for CO, 10 mg m⁻³ (~ 8000 ppb), has not been exceeded (Table 1). The peak values for both BC and CO appear in late evening and night when the use of fireplaces and wood stoves for heating purposes is more intense.

Table 1. BC and CO basic statistics (hourly resolution) from November 2014 until February 2015. The corresponding values for winter 2013-14 are also reported in brackets.

	Average	Median	Minimum	Maximum
BC (µg/µ ³)	2.95 ± 3.25 (2.93 ± 3.28)	2.05 (1.60)	0.09 (0.18)	18.09 (26.84)
CO (ppb)	556 ± 525 (606 ± 609)	368 (340)	106 (97)	4326 (3544)

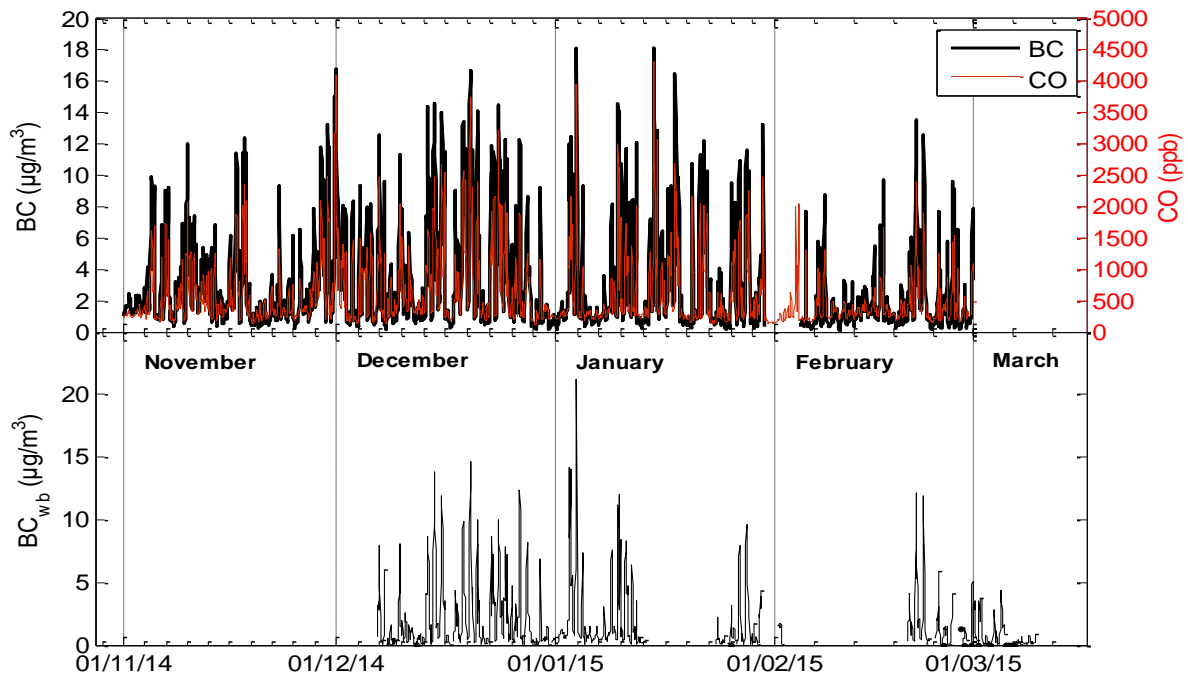


Figure 2. Time series of 1-hour averaged concentrations of CO (red line) and BC (black line, MAAP 5012) (upper panel) and BC_{wb} (lower panel, AE-42) at Thissio monitoring station.

To follow the related to biomass burning, late evening buildup of CO and BC, during the transition from autumn to winter and the gradual restoration of normal concentrations towards spring, the mean diurnal cycles, calculated for each winter month separately at Thissio station, are used. (Fig.3a & 3b). The diurnal variation of both species depicts two characteristic peaks: one in the morning (around 09:00 LT) which is due to traffic (morning rush hour) and the second one in the evening (around 22:00 LT) which is mainly attributed to wood burning. The morning peak is in consistency with other studies which have shown that the morning rush hours in Athens are from 8:00 LT until 11:00 LT (Katsoulis 1996, Kourtidis et al., 1999). Both CO and BC start building up at 06:00 LT reaching a maximum at 09:00 LT and then they decrease towards noon. Thereafter, low values are maintained until 16:00 LT when they start building up again reaching a maximum at 22:00 LT. The slow decrease after midnight, when wood burning emissions are expected to be lower, could be attributed to the poor ventilation of the Athens basin during night time, in combination with a shallow nocturnal boundary layer (Kassomenos et al., 1995), leading to entrainment of pollution.

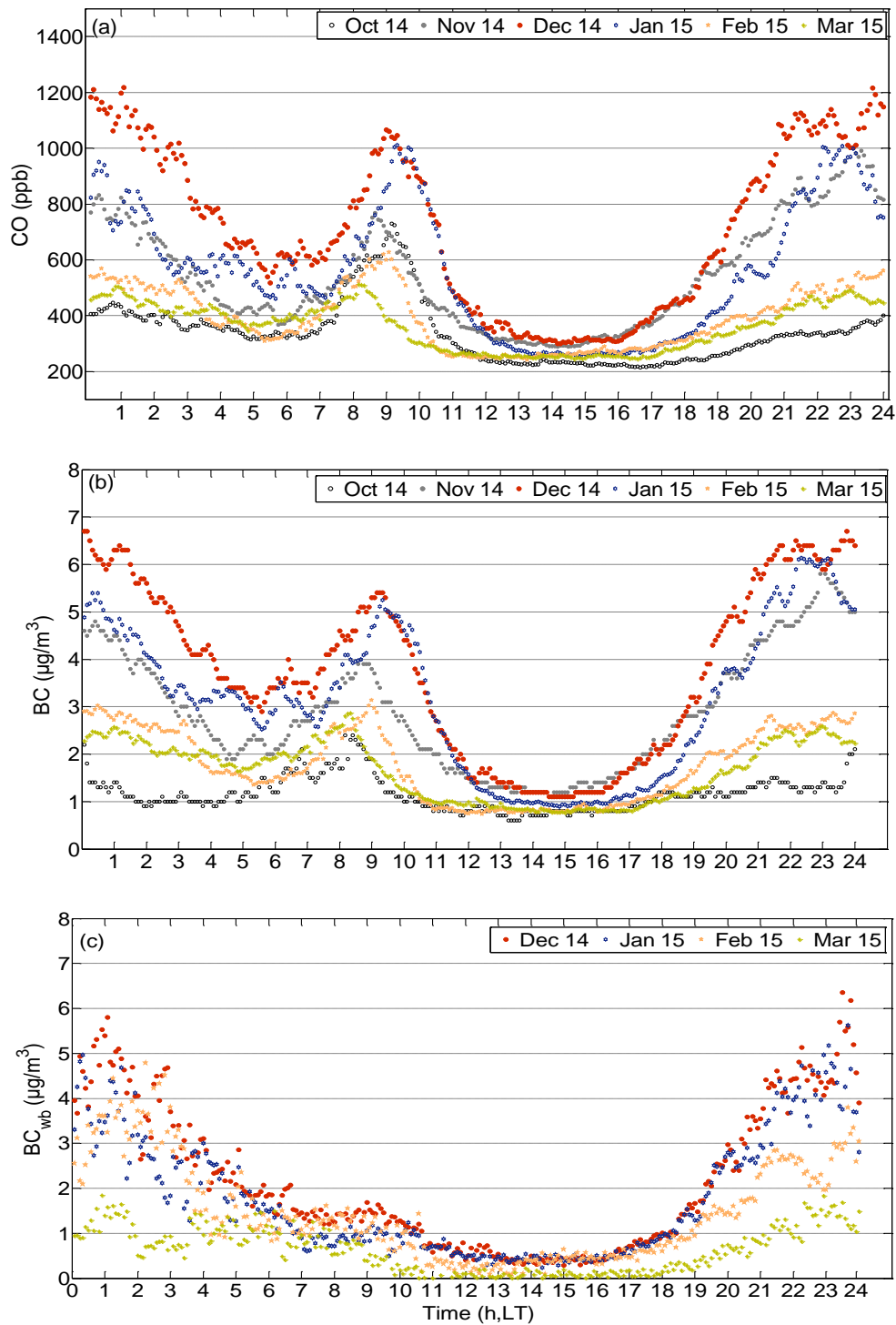


Figure 3. Mean diurnal variation per month for CO (a), BC (b) and BC_{wb} (c) concentration measurements at Thissio station.

Studies focusing on wood burning in Athens have showed that smog episodes are related to low wind speed, absence of precipitation (Fourtziou et al., 2016) and low nocturnal mixing layer height (Gerasopoulos et al., 2016). In this study, the influence of the meteorological conditions and the subsequent local circulation patterns on the BC concentrations measured at Thissio is investigated for

the particular period covered in Fig. 2. Wind speed and wind direction data, from the meteorological station at Thissio, are used and presented in Fig.4. High BC concentrations are encountered during low wind speed conditions ($u < 3$ m/s), both during day time and night time, highlighting the important role of ventilation and internal city air mass transport patterns to air quality. During evening and night time (17:00-04:00LT) BC concentrations exceed daytime concentrations and this finding does not depend on the direction of the air masses under low speed conditions.

The CO and BC morning peaks in December and January are almost 50% higher compared to November's and February's peak. The evening peaks in November, December and January are increased by a factor of 2 compared to February. Although November also exhibits significant BC concentrations, December and January are colder months (mean temperatures 12.7 °C and 9.9 °C, respectively) compared to November (14.9°C) and subsequently more representative of wintertime conditions. The high peaks in January are probably linked to extensive periods of stationary anticyclonic conditions, usually occurring in Athens during January (Van Dop & Kallos, 2012), leading to poor dispersion conditions. Indeed, according to surface analysis charts from UKMO (United Kingdom Met Office, www.metoffice.gov.uk), until at least January 21st the peaks are linked to anticyclonic conditions.

The BC_{wb} concentration shows a characteristic diurnal variability (Fig. 3c). In contrast to CO and BC, the diurnal variation of BC_{wb} depicts only one peak at around 22:00 LT (which coincides with the evening peak of CO and BC), due to biomass combustion emissions during night time. The peaks in December and January are, just like in the CO and BC case, increased by a factor of 2 compared to February and March.

Considering the above findings, it can be deduced that smog episodes are more intense and frequent during December and January; therefore these two months are hereafter considered as the typical winter months for the analysis following in the next sections.

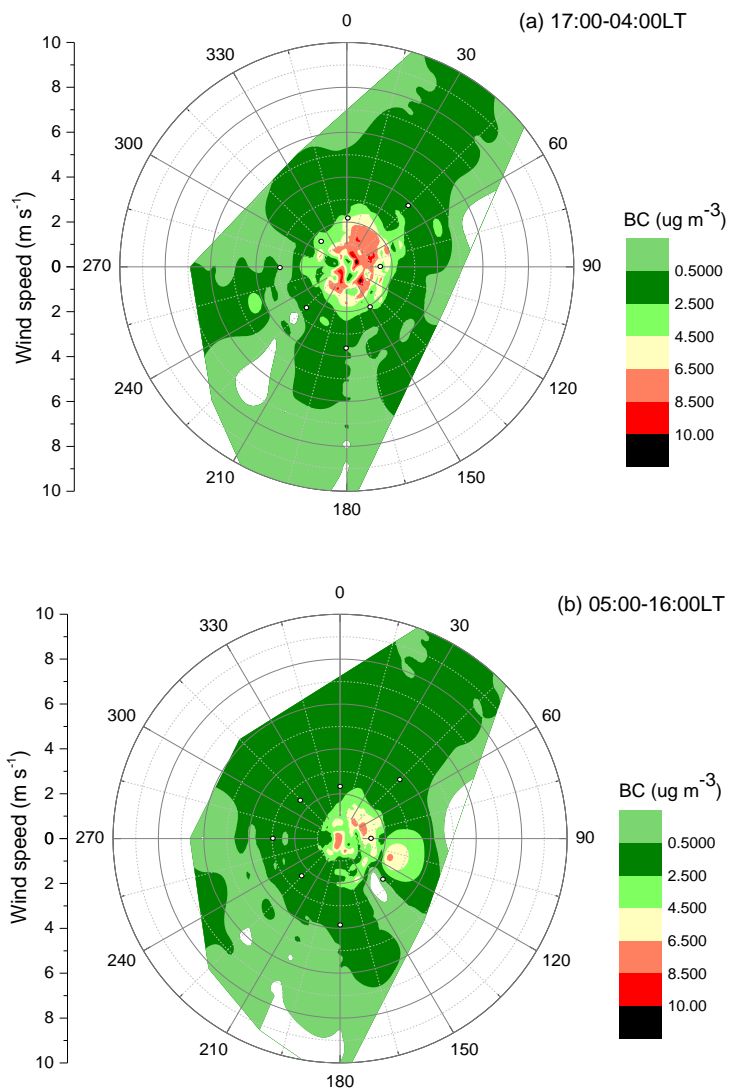


Figure 4. Hourly BC concentration values as a function of wind direction and wind speed for 17:00-04:00LT (a) and 05:00-16:00LT (b). White spots represent the mean wind speed per direction.

5.3.2 Contribution of biomass burning to evening CO concentrations

The contribution of wood burning to air pollution loads could be assessed by distinguishing the sources (fossil fuel versus wood burning) which contribute to the CO load in the atmosphere. Although the wood burning contribution to BC concentrations (particulate matter pollutant) has already been calculated, as discussed in section 2.2, there is no direct way to distinguish CO sources from the existing measurements. An indirect method is proposed here, to enable an overview of the contribution of the different sources to CO as well.

Making the assumption that the influence of wood burning in the atmosphere during morning hours is insignificant, we considered that the recorded CO morning values are attributed entirely to fossil fuel burning. Linear regression analysis is applied on CO and BC_{ff} morning (07:00-10:00) data for the

period December 2014-February 2015 (Fig. 5 a), revealing a significant correlation ($R^2=0.89$, $N=336$). The regression equation ($y=241.6(\pm 3.6)x$, setting y -intercept=0) is then applied to evening BC_{ff} data (21:00-00:00 LT) calculating in that way the evening CO_{ff} (Carbon Monoxide from fossil fuel combustion). Subtracting the calculated CO_{ff} from the measured CO, CO emitted by wood burning (CO_{wb}) is finally obtained. A qualitative validation of the obtained CO_{wb} is performed using the BC_{wb} measurements (Fig. 5 b). The results indicate a significant correlation ($R^2=0.76$, $y=(72.0\pm 2.9)x+170(\pm 14)$).

This analysis reveals a contribution of CO_{wb} to the total CO up to approximately 50% on average during night (21:00-00:00 LT), showing once more the increasing role of the biomass combustion in the levels and diurnal variability of pollutants in Athens.

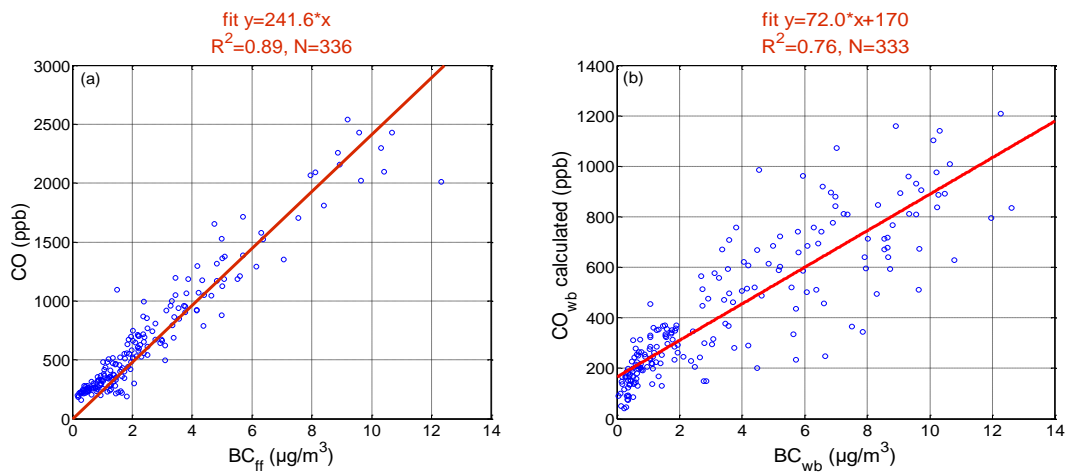


Figure 5. Scatter plot between BC_{ff} and CO morning (07:00 – 10:00) measurements at Thissio station for the period December 2014-February 2015 (left panel). Scatter plot between calculated BC_{wb} evening (21:00-00:00) measurements and calculated CO_{wb} for the same time period (right panel).

Given that CO and BC at Thissio station are very well correlated ($R^2=0.94$, $N=2756$), we have focused on CO measurements in order to study the trends during the last 15 years. CO is also well correlated with BC_{wb} ($R^2=0.80$, $N=1169$). CO is a good indicator for traffic emissions during morning hours and also a good indicator for both fossil fuel and biomass burning during night time. In this study, CO has been chosen over BC for the analysis, due to the long-term availability of its monitoring in Athens.

5.3.3 Comparison of CO measurements: site representativeness

Data from the Thissio station has been analysed and presented so far. Hence, it is important to examine whether the specific monitoring station can be considered as representative of the air quality in Athens.

For this, the CO measurements at Thissio station were compared to observations from NAPMN stations (Marousi, N.Smyrni, Athinas, Geoponiki, Piraeus), during one winter period (2013-2014). Indicatively, the scatter plot of CO concentrations at Thissio versus Athinas, for the period December 2013-January 2014, is shown in Fig. 6. Athinas and Thissio measurements are significantly correlated ($R^2=0.78$, $N=1077$), which is expected given the vicinity of the two sites. However, CO concentrations observed at Athinas, compared to Thissio station, are higher by almost a factor of 2, which is explained by the type of the sites (Athinas-urban traffic, Thissio-central but away from immediate exposure to traffic sources). Similarly, Marousi and N.Smyrni CO measurements are also significantly correlated with Thissio ($R^2=0.63$, $N=1076$ and $R^2=0.76$, $N=1077$, respectively) and the recorded concentrations are correspondingly 55% and 75% higher than the measurements at Thissio. The correlation is also significant for Geoponiki and Piraeus ($R^2=0.58$, $N=1074$ and $R^2=0.59$, $N=1075$, respectively) with 65% and 120% higher CO concentrations, respectively, when compared to Thissio. The correlation coefficients (R) between CO measurements in all stations are shown in Table 2. The high correlation between the five NAPMN sites and Thissio, as well as the relative difference in absolute levels, support the characterisation of Thissio as an urban background site, non-intensively affected by local traffic.

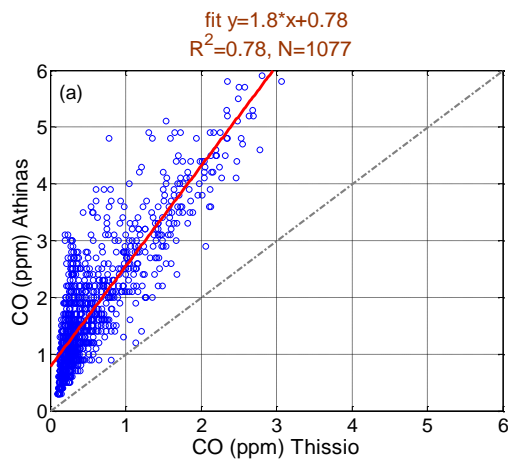


Figure 6. Scatter plot between CO measurements at Thissio station and CO measurements at Athinas station, for winter (December-January) 2013-14.

Table 2. Correlation matrix of CO for all monitoring stations.

Monitoring stations	Thissio	Athinas	Marousi	N.Smyrni	Geoponiki	Piraeus
Thissio		0.882	0.791	0.875	0.759	0.766
Athinas	0.882		0.758	0.805	0.743	0.808
Marousi	0.791	0.758		0.745	0.755	0.678
N.Smyrni	0.875	0.805	0.745		0.727	0.753
Geoponiki	0.759	0.743	0.755	0.727		0.754
Piraeus	0.766	0.808	0.678	0.753	0.754	

5.3.4 Analysis of interannual variability

For achieving interpretable results for the CO trend during the last 15 years and for estimating the effect of the wood burning on this trend, the integrals of the morning and evening peaks for each day and for each season separately were calculated. The integrals are calculated between 06:00 LT and 10:00 LT in the morning and 16:00 LT and 05:00 LT in the evening. The area below the peak, defined by these two points and the x-axis, is considered as background value and is subtracted (Fig. 7). The mean integrals for winter (December-January) and summer months (July-August) for the five NAPMN stations representing urban and urban background environment, are presented in Figure 8.

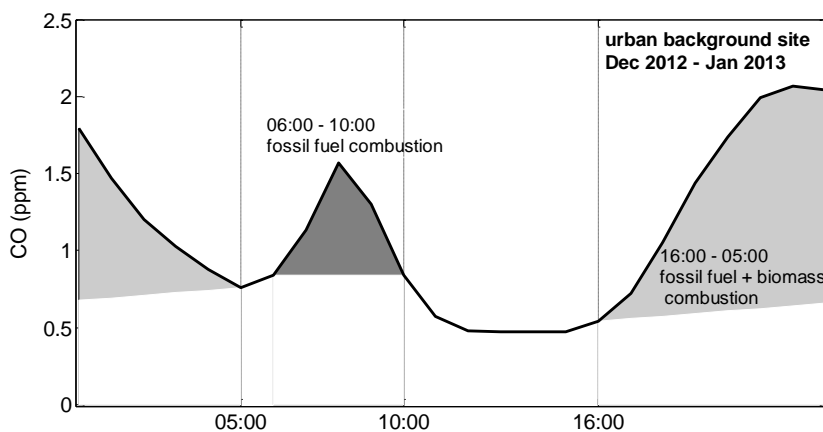


Figure 7. CO winter (December 2012 - January 2013) diurnal variability for N.Smyrni station. The calculated morning integral (dark grey) and evening integral (light grey) are here shown as a typical example of the methodology followed.

During summer, CO is released into the atmosphere of Athens mainly via fossil fuel combustion processes (e.g. vehicle exhausts). The low summer values (Fig. 8 a) are attributed to photochemistry (oxidation by OH radicals), reduced traffic (vacation period) and more efficient dispersion of the pollutants due to deep mixing heights and strong thermal circulations that lead to better ventilation conditions (Kassomenos et al. 1995). Winter morning values are enhanced by a factor of 3 (Fig. 8 c) compared to summer and this can be attributed to i) the extensive use of central heating, ii) decreased photochemistry, iii) shallower boundary layer and iv) poor dispersion due to stationary conditions.

The gradual decrease over the years, both in winter and summer morning peak integrals, is most likely resulting from the gradual replacement of old vehicles with new ones (catalytic converters), along with the economic recession starting in 2008. Faneli and Assimakopoulos (2016) estimated that CO traffic emissions were decreased by 40% during the period 2006-2012. In this study, the winter morning integrals are approximately 50% decreased during the period 2000-2010 and from 2010 on, no further decrease is observed. Low integral values are also observed in the summer evening peaks (Fig. 8 b), along with a gradual decrease over the years, once more attributed to reduced traffic and depollution strategies. Since 2012, biomass burning has prevailed over fossil fuel for domestic heating purposes and this can be clearly seen in the winter evening integrals (Fig. 8 d). The increasing over time values of the winter evening integrals of CO, during this period, indicates a dominant influence of wood burning during nighttime in all five stations. This is also supported by the fact that the more recent winter months were not characterised by lower temperature values compared to previous years. More specifically, the mean winter temperature, for the months considered in this analysis, is 10.5°C for the period 2000-2011 and 10.7°C for the rest of the time period. The mean value (7.3) of the winter evening integrals at Athens station during the last 4 years is 78% higher than the mean value (4.1) of the previous years. The corresponding percentages for Marousi, N.Smyrni, Geoponiki and Piraeus are 59% (8.9 versus 5.6 mean value), 37% (8.2 vs 6.0 mean value), 37% (7.0 vs 5.1 mean value) and 23% (5.4 vs 4.4 mean value) respectively.

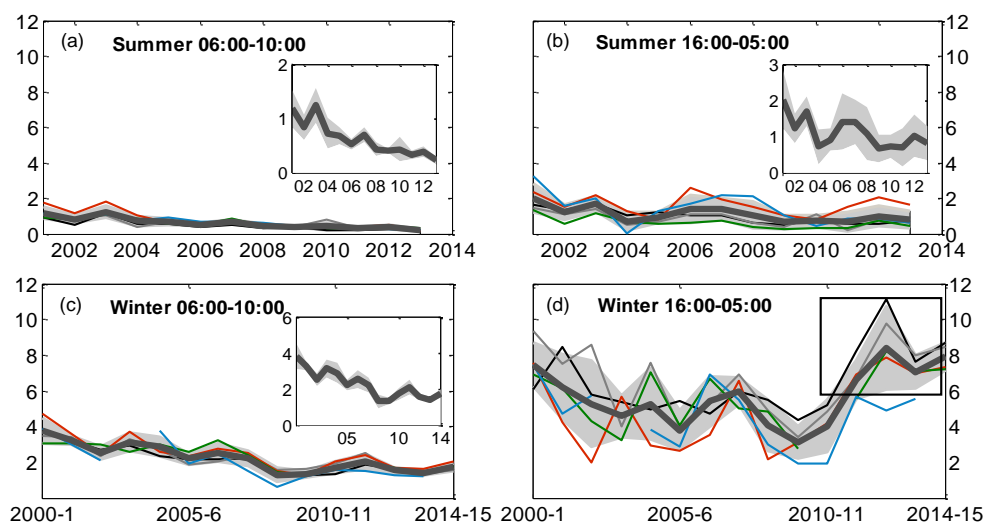


Figure 8. Mean integrals of the morning and evening CO peaks for summer (top panels) and winter months (bottom panels) calculated for Marousi (black line), N.Smyrni (light grey line), Athens (red line), Geoponiki (green line) and Piraeus (blue line) stations (please consider the different scale used in each case). The dark grey curve

corresponds to the mean value of all five stations and the grey shaded area represents the standard deviation (1σ). In the internal panels in (a), (b) and (c) the mean value is reproduced in different scale to highlight the existing trend over time.

In order to highlight the relative competition between the reduction of CO due to traffic and its late evening increase due to wood burning, we have calculated the ratio of CO_{ev}/CO_{mor} using the peak value at 09:00 LT for CO_{mor} and the peak value at 22:00 LT for CO_{ev} . In Figure 9, the interannual trend of the mean ratio of CO_{ev}/CO_{mor} for wintertime is presented. The ratio subtracts the influence of fossil fuel and what it remains mainly highlights the impact of wood burning. The mean ratio was calculated from the daily ratios. Since the CO_{ev} peak is mostly controlled by changes in wood burning, while the morning peak is due to traffic emissions (traffic rush hour), the ratio of CO_{ev}/CO_{mor} actually subtracts the influence of fossil fuel and thus it could serve as an additional good indicator of the increasing importance of wood burning in Athens.

The increase of biomass burning during evening and night time since 2012 (along with the stabilisation of morning CO values during the same period) leads to a gradual enhancement of the CO_{ev}/CO_{mor} ratio. The increase is more obvious at the urban background stations: 41% (mean ratio=1.61 until 2012 & 2.27 from 2012 on) and 33% (mean ratio=1.45 until 2012 & 1.93 from 2012 on) for Marousi and N.Smyrni stations, respectively. However, at Athinas monitoring station, the increased biomass combustion is partly counterbalanced by the generally elevated traffic emissions, resulting in slighter increase (22%) of the CO_{ev}/CO_{mor} ratio (mean ratio=0.98 until 2012 & 1.20 from 2012 on). These results demonstrate once more the increasing role of biomass combustion in the air quality of Athens' basin.

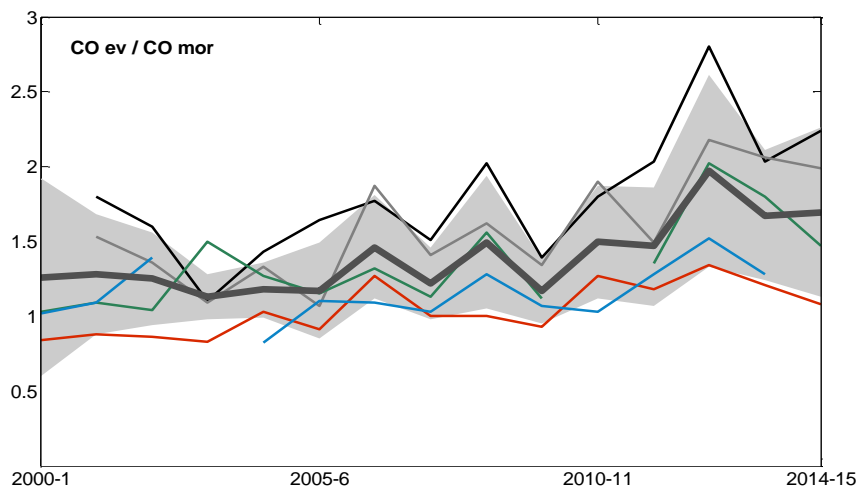


Figure 9. Mean annual evolution of the CO_{ev}/CO_{mor} ratio in winter for Marousi (black line), N.Smyrni (grey line), Athinas (red line), Geoponiki (green line) and Piraeus (blue line) stations. The dark grey curve corresponds to the mean value of all five stations and the grey shaded area on either side of the mean curve represents the standard deviation (1σ).

5.4 Summary and conclusions

15 years of surface CO observations from five monitoring stations in Athens, along with simultaneous BC and CO measurements during two intense winter campaigns (Dec 13-Feb 14 & Dec14-Feb15) at Thissio station (urban station), were analysed in this study, in an attempt to shed light on the relative contribution of biomass burning versus fossil fuel combustion in Athens' air quality and to reveal the enhancement of wood burning during the more recent years of the economic crisis in Greece.

Both CO and BC follow identical diurnal patterns characterised by two distinct peaks: a morning peak (around 09:00 LT) attributed to the traffic rush hour and an evening peak (around 22:00 LT) consistent with the increased contribution of biomass combustion during night time. The deconvolution of BC to its components, namely wood burning (BC_{wb}) and fossil fuel combustion (BC_{ff}), allows us to understand the current contributions of the two processes in BC levels. However, since BC measurements are available only during the last years, the aforementioned relation between BC and CO, was used to go back in time.

The interannual changes of the relevant contribution of wood burning and fossil fuel combustion were revealed via calculation of morning (06:00-10:00 LT) and evening (16:00-05:00 LT) integrals of the CO concentrations for the last 15 years. The results of this analysis demonstrate that:

(i) CO concentrations during the morning traffic peak decrease constantly over time (by almost 50% since 2000) and during both seasons (summer, winter). This reflects the decrease of fossil fuel combustion during the last 15 years, which can be attributed both to the gradual renewal of the vehicles fleet (or other countermeasures adopted to achieve EU cut of pollutant emissions), and to the economic crisis during the last years. The latter has been evidenced in Greece as a general cut down on industrial activity and vehicles use.

(ii) The impact of biomass burning becomes dominant during winter since 2011, when the price of oil was affected by the financial crisis. This is evident by the respective significant increase of winter evening CO integrals. The competition between activities cut down due to the crisis and the increase of wood burning use is shown via the ratio between evening CO peak values to morning values, which has been constantly increasing during the last four years (41% increase at urban background stations).

The decomposition of CO to CO_{wb} and CO_{ff} , showed that CO_{wb} contribution is about 50% during night time (21:00-00:00 LT), suggesting that emissions from biomass combustion have indeed gained an increasing role in night time atmospheric pollution levels in Athens.

Overall, it is deduced that the shift of Athens' habitants to wood burning, as major fuel for heating purposes, has significant impact on Athens' air quality (as revealed by the CO levels), which is to the opposite direction of the impact from reduced fossil fuel consumption. The importance of this study lies on the fact that it quantifies the diachronic changes in air pollution in Athens and links it with several socioeconomic factors (e.g. measures, economic crisis, behavioural changes), while it can serve as reference in the future for assessing and evaluating expected mitigation measures. The intensive campaigns that have taken place in Athens during the last few winters provide significant information

and details about the physical and chemical characteristics of wood burning in Athens, and will support the increasing evidence of the impacts of residential wood burning not only in Greece but also in Europe as a whole.

Conclusions

Photochemical smog and smog formed under strong stationary emissions during evening hours, are the most common air pollution phenomena in the urban environment of Athens. In order to study the smog phenomena and apply appropriate measures to minimise them, regular monitoring and studying of the spatio-temporal variability of air pollutants is required. For this purpose, ground-based remote sensing methods were used, mainly the MAX-DOAS technique, which fills the gap between the local character of in-situ measurements and the small spatial analysis of satellite measurements. Additionally, the telescope's multiple viewing directions made it possible to study both the horizontal and vertical distribution of the pollutants under study. This technique has the advantage of continuously recording absorption spectra resulting in the acquisition of long-term data series, which are necessary for observing the evolution over time of the atmosphere, as well as evaluating the results of the measures taken from time to time to improve air quality. Lidar active remote sensing system - part of the EARLINET network - and the CIMEL photometer - part of NASA's AERONET network - were used for auxiliary measurements. However, since the MAX-DOAS system is unable to perform measurements after sunset, it was deemed necessary to use in-situ measurements (intensive experimental campaigns of NOA and long-term measurements from the monitoring station network of the Ministry of Environment), in order to study the increased biomass combustion, which is the main reason for the frequent smog episodes at nights. This phenomenon has a strong presence from 2011 onwards, when the Greek economic crisis began.

The compounds used in the present work as indicators for the study of the urban smog are nitrogen dioxide, formaldehyde, glyoxal, particulate matter, black carbon and carbon monoxide.

During the first MAX-DOAS measurements in Athens, the slant column densities (SCDs) of NO_2 , HCHO, CHOCHO and O_4 were calculated for eight elevation angles and for eight different azimuth viewing directions, covering the entire area of Athens. The measurements at low elevation angles, characterised by high sensitivity to the concentration of absorbing trace species close to the surface, provided important information for the study of the horizontal distribution of atmospheric pollutants in Attica. Overall, the spatio-temporal distribution of NO_2 , HCHO and CHOCHO was captured, reaching the following conclusions:

- ❖ On a seasonal and daily basis, the study of NO_2 SCDs showed a clear seasonal variation, with 145% higher levels during winter compared to the summer levels, and also, a clear diurnal cycle with a morning and an afternoon peak. Moreover, reduced levels by 30-50% were recorded during weekends. These time variations are related to anthropogenic NO_2 emissions.

The corresponding analysis for formaldehyde and glyoxal also resulted in seasonal variation with the difference that the maximum values appear in the summer months, due to the photochemical formation of the specific trace gases. The diurnal cycle of formaldehyde during summer is characterized by a peak at 12:00LT, as a result of photochemical activity, and during

winter by a wide afternoon peak only in the urban areas of Athens, which implies a relation to anthropogenic activities. Glyoxal also presents a peak at 12:00LT in the summer and a gradual increase starting in the morning until 14:00LT in winter. These observations are related to photochemical processes. During weekends, formaldehyde and glyoxal levels are reduced by 3-17% and 3-33%, respectively, a result that is expected for VOCs with significant biogenic emissions. Additional analyses confirmed the effect of the Etesian winds on the levels of atmospheric pollutants by efficiently removing them. The dominant role of photochemistry during summer months was highlighted.

- ❖ The contribution of local urban emissions to the total NO_2 levels in the urban area of Athens was found to be 45% and 60% for winter and summer respectively, without significant daily variation. The contribution of urban HCHO sources is 5% in the morning and 15% during the rest of the day. The corresponding contribution of CHOCHO is 25-30% in the morning and 15-20% in the afternoon. Therefore, the presence of NO_2 in the atmosphere of the urban area of Athens is more related to anthropogenic activities and fossil fuel combustion, compared to hydrocarbons such as formaldehyde and glyoxal.
- ❖ Wind direction was not found to significantly affect SC_{HCHO} and $\text{SC}_{\text{CHOCHO}}$ levels in the urban area. On the contrary, lower levels of SC_{NO_2} were recorded when north-northeast winds prevailed and higher values under westerly winds. These findings can be attributed to the topography of the city and the emission sources of the pollutants in relation to the instrument location.

To sum up, the spatio-temporal distribution of the studied pollutants demonstrated (i) the dominant role of anthropogenic sources on NO_2 levels, (ii) the significantly active role of photochemistry in Athens and (iii) the fact that HCHO and CHOCHO levels in Athens are mainly determined by photochemical processes.

Regarding the retrieval and evaluation of the vertical distribution of tropospheric aerosols using MAX-DOAS measurements, it is the first time that this takes place in Athens. Therefore, the study focuses primarily on evaluating the results and secondarily on their interpretation. The profile retrieval for four selected case studies, was based on O_4 MAX-DOAS measurements and the BOREAS retrieval algorithm, developed in the frame of the SCIATRAN radiative transfer model using the Tikhonov iterative regularization technique. For the evaluation of the results, lidar and CIMEL measurements were used. Due to the different operation principles of each instrument and the different air masses probed by each instrument, a full agreement between the measurements are not expected.

Overall, the following conclusions can be drawn:

- ❖ The vertical profiles retrieved from the MAX-DOAS measurements are qualitatively in good agreement with the lidar profiles. A very good correlation ($r > 0.90$) was found indicating a good agreement in aerosol layer shape. Regarding the aerosol extinction levels, MAX-DOAS performs well in presence of fine particles; however, it fails to detect part of the urban aerosol pollution at small relative azimuth angles (underestimation by 20 to 35%). Furthermore, in case of dust transport, it does not adequately capture the spatial inhomogeneity at high altitudes.

- ❖ The MAX-DOAS retrieved AODs is in good agreement with the corresponding measurements of the CIMEL photometer, both in terms of levels and variation, and seems to capture quite satisfactorily the urban particulate pollution in the lower layers of the atmosphere. MAX-DOAS underestimates the AOD in the presence of coarse particles (Angström coefficient <1), as well as in the afternoon measurements, due to MAX-DOAS' viewing geometry.

Summarising, it has been shown that the MAX-DOAS measurements in Athens and the BOREAS algorithm can provide a good estimation of the AOD and the vertical structure of the aerosols on a continuous and long-term basis, offering new perspectives for continuous and reliable datasets in Athens. Although there is certainly more work to be conducted in future studies in order to understand the sensitivity of the MAX-DOAS aerosol measurements, this study could be treated as a reference point for MAX-DOAS ability to record urban particulate pollution in Athens.

In order to study the industrial smog evolution related to the intensification of biomass combustion in recent years, an attempt was made to quantify the relative contribution of biomass combustion versus fossil fuel combustion in Athens' air quality and to reveal the enhancement of wood burning during the more recent years of the economic crisis in Greece. Long-term in-situ CO measurements from five monitoring stations in Athens, along with simultaneous BC and CO measurements during two intense winter campaigns carried out at the Thissio station, were used. The analyses came to the following conclusions:

- ❖ Both CO and BC follow identical diurnal patterns characterised by two distinct peaks (a morning peak at 09:00 LT and an evening peak at 22:00 LT during wintertime). Therefore, both of these compounds can be used alternatively or in addition to each other to study the industrial smog.
- ❖ CO concentrations during the morning traffic peak have decreased by almost 50% since 2000, as a consequence of the gradual renewal of the vehicles fleet, as well as the economic crisis during the last years, which has led to a reduced industrial activity and vehicles use.
- ❖ The impact of biomass burning becomes dominant during winter since 2011, when the price of oil was affected by the financial crisis. This is evident by the respective significant increase of winter evening CO levels and the almost 40% increase of the evening to morning CO concentration ratio during 2011-2015.
- ❖ The decomposition of CO to CO emitted from wood burning and CO emitted from fossil fuel combustion, indicated the increased contribution of wood burning emissions to the atmospheric pollution levels in Athens; the contribution was found about 50% during night time (21:00-00:00 LT).

Overall, it is deduced that the shift of Athens' habitants to wood burning, as major fuel for heating purposes, has had a significant negative impact on Athens' air quality. This finding is towards the

opposite direction of the improvement since the beginning of the economic crisis, which had led to reduced fossil fuel consumption and thus, to reduced anthropogenic emissions. The importance of the results lies on the fact that it quantifies the diachronic changes in air pollution in Athens and links it with socioeconomic factors, such as the economic crisis, environmental measures and behavioural changes. The present study can serve as reference in the future for assessing and evaluating the effectiveness of air pollution mitigation measures to be implemented.

The MAX-DOAS instrument provides a unique opportunity for stand-alone routine measurements to study the spatiotemporal variability of aerosols and certain trace gases affecting urban photochemistry. The position of the instrument at an elevated (500 m a.s.l.) station, scanning a 5-million population city is challenging in terms of the retrieval processes, but also provides a unique opportunity for a spatiotemporal characterization of the area. A network combining the MAX-DOAS instrument with other instruments (sun-photometric, lidar, in situ) at different city locations can provide the opportunity for a well-determined 4D characterization of the urban air pollution along with linked implications to photochemistry, health and emission policies. The western countries have raised awareness to the local authorities to reduce emissions and control the pollution and in this frame, such a network could be of substantial importance.

REFERENCES

- Ackermann, J.: *The extinction-to-backscatter ratio of tropospheric aerosol: A numerical study*, *J. Atmospheric Ocean. Technol.*, 15(4), 1043–1050, 1998
- Akimoto H.: *Global air quality and pollution*, *Science*, 302, 5651, 1716-1719, doi:10.1126/science.1092666, 2003
- Amanatidis G.T., Viras L.G., Kotzias D., Bartzis J.G. : *Carbonyl levels in Athens during a winter air pollution episode*, *Fresenius Environment Bulletin*, 6(7-8), 372-377, 1997
- Amiridis, V., Balis, D. S., Kazadzis, S., Bais, A., Giannakaki, E., Papayannis, A. and Zerefos, C.: *Four-year aerosol observations with a Raman lidar at Thessaloniki, Greece, in the framework of European Aerosol Research Lidar Network (EARLINET)*, *J. Geophys. Res.*, 110(D21), doi:10.1029/2005JD006190, 2005
- Amiridis, V., Balis, D., Giannakaki, E., Kazadzis, S., Arola, A., Gerasopoulos, E.: *Characterization of the aerosol type using simultaneous measurements of the lidar ratio and estimations of the single scattering albedo*, *Atmospheric research*, 101(1-2), pp.46-53, 2011
- Amiridis, V., Zerefos, C., Kazadzis, S., Gerasopoulos, E., Eleftheratos, K., Vrekoussis, M., Stohl, A., Mamouri, R.E., Kokkalis, P., Papayannis, A., Eleftheriadis, K.: *Impact of the 2009 Attica wild fires on the air quality in urban Athens*, *Atmospheric Environment*, 46, pp. 536-544, 2012
- Andreae, M.O., Crutzen, P.J.: *Atmospheric aerosols: Biogeochemical sources and their role in atmospheric chemistry*, *Science*, 276, 1052–1058, 1997
- Andreae M.O. and Merlet P.: *Emission of trace gases and aerosols from biomass burning*, *Global Biochemical Cycles*, 15(4), 955-966, 2001
- Arlander D. W., Brunind D., Schmidt U., Ehhalt D. H. : *The tropospheric distribution of formaldehyde during tropoz-ii*, *Journal of Atmospheric Chemistry*, 22, 251-269, 1995
- Atkinson R. : *Atmospheric chemistry of VOCs and NOx*, *Atmospheric Environment*, 34, 2063-2101, 2000
- Avdikos G., Tsaknakis G., Papayannis A., Kalabokas P., Zanis P., Eleftheratos K., Ziomas I., *Systematic measurements of air pollution in the city of Athens, Greece, using a DOAS system Final Symposium of Cost 720, Applications of Atmospheric Profiles in Research and Operations, Toulouse, France, 15-18 May 2006*
- Bakeas E., Argyris D., Siskos P. : *Carbonyl compounds in the urban environment of Athens, Greece*, *Chemosphere*, 52, 805-813, 2003
- Bakeas E., Siskos P. : *Volatile Hydrocarbons in the atmosphere of Athens, Greece*, *Environmental Science and Pollution Research* 9(4), 234-240, 2002
- Barde J., Button K. : *Transport policy and the environment, six case studies*, Earthscan Publications Ltd, ISBN 1 85383 075 5, 1990
- Beeson W.L., David, E.A., Knutsen, F.: *Long-term concentrations of ambient air pollutants and incident lung cancer in California adults: results from the AHSMOG study*, *Environ. Health Perspect.*, 106 (12), 813–823, 1998
- Bigi A., Harrison M. : *Analysis of the air pollution climate at a central urban background site*, *Atmospheric Environment*, 44, 2004-2012, doi:10.1016/j.atmosenv.2010.02.028, 2010
- Bogumil, K., Orphal, J., Burrows, J.P.: *Temperature dependent absorption cross sections of O₃, NO₂, and other atmospheric trace gases measured with the SCIAMACHY spectrometer*, *Proc. ERS-Envisat Symposium Gothenburg*, 2000

- Bösch, T., Rozanov, V., Richter, A., Peters, E., Rozanov, A., Wittrock, F., Merlaud, A., Lampel, J., Schmitt, S., de Haij, M., Berkhout, S., Henzing, B., Apituley, A., den Hoed, M., Vonk, J., Tiefengraber, M., Müller, M., Burrows, J. P.: BOREAS - a new MAX-DOAS profile retrieval algorithm for aerosols and trace gases, *Atmos. Meas. Tech.*, 11, 6833-6859, doi:10.5194/amt-11-6833-2018, 2018
- Bond T.C., Doherty S.J., Fahey D.W., Forster P.M., Berntsen T., DeAngelo B.J., Flanner M.G., Ghan S., Karcher B., Koch D., Kinne S., Kondo Y., Quinn M.C., Sarofim M.C., Schultz G., Schulz M., Venkataraman C., Zhang S., Bellouin N., Guttikunda S.K., Hopke P.K., Jacobson M.Z., Kaiser J.W., Klimont Z., Lohmann U., Schwartz J.P., Shindell D., Storelvmo T., Warren S.G.: Bounding the role of black carbon in the climate system: A scientific assessment, *JGR Atmospheres*, 118, 5380-5552, doi:10.1002/jgrd.50171, 2013
- Bösch, T., Peters, E., Richter, A., Wittrock, F., Rozanov, V., Burrows, J. P.: Introduction into IUP Bremen's new MAX-DOAS profile retrieval algorithm BOREAS. 8th International DOAS Workshop, Yokohama, Japan, September 2017
- Brewer A.W., McElroy C.T., Kerr J.B. : Nitrogen dioxide concentrations in the atmosphere, *Nature*, 246(5429), 129-133, doi: 10.1038/246129a0, 1973
- Calvert J.G., Atkinson R., Kerr J.A., Madronich S., Moortgat G.K., Wallington T.J., Yarwood G.: *The Mechanisms of Atmospheric Oxidation of the Alkenes*, Oxford University Press, New York, 2000
- Carlton A G., Wiedinmyer C., Kroll J.H.: A review of Secondary Organic Aerosol (SOA) formation from isoprene, *Atmos. Chem. Phys.*, 9(14), 4987–5005, doi:10.5194/acp-9-4987-2009, 2009
- Castellanos, P., and K. F. Boersma: Reductions in nitrogen oxides over Europe driven by environmental policy and economic recession, *Sci. Rep.*, 2, 265, doi:10.1038/srep00265. D, 2012
- Chaloulakou A., Kassomenos P., Spyrellis N., Demokritou P., Koutrakis P.: Measurements of PM10 and PM2.5 particle concentrations in Athens, Greece, *Atmospheric Environment* 37, 649-660, 2003
- Chaloulakou A., Mavroidis I., Gavriil I. : Compliance with the annual NO₂ air quality standard in Athens. Required NO_x levels and expected health implications, *Atmospheric Environment*, 42(3), 454-465, 2008
- Chen, D., Zhou, B., Beirle, S., Chen, L. M., and Wagner, T.: Tropospheric NO₂ column densities deduced from zenith-sky DOAS measurements in Shanghai, China, and their application to satellite validation, *Atmos. Chem. Phys.*, 9, 3641–3662, doi:10.5194/acp-9-3641-2009, 2009.
- Chou M.D., Suarez M.: Parameterizations for cloud overlapping and shortwave single-scattering properties for use in general circulation and cloud ensemble models, *Journal of Climate*, 11, 202-214, 1998
- Chubarova N.Y., Sviridenkov M.A., Smirnov A., Holben B.N.: Assessments of urban aerosol pollution in Moscow and its radiative effects, *Atmos. Meas. Tech.*, 4, 367-378, doi:10.5194/amt-4-367-2011, 2011
- Clémer, K., Van Roozendaal, M., Fayt, C., Hendrick, F., Hermans, C., Pinardi, G., Spurr, R., Wang, P., De Maziere, M.: Multiple wavelength retrieval of tropospheric aerosol optical properties from MAXDOAS measurements in Beijing, *Atmos. Meas. Tech.*, 3, 863-878, doi:10.5194/amt-3-863-2010, 2010
- Collaud Coen M.: Minimizing light absorption measurement artifacts of the aethalometer: Evaluation of five correction algorithms, *Atmospheric Measurement Techniques*, 3, 457-474, doi:10.5194/amt-3-457-2010, 2010
- Crippa M., DeCarlo P.F., Slowik J.G., Mohr C., Heringa M.F., Chirico R., Poulain L., Freutel F., Sciare J., Cozic J., Di Marco C.F., Elsassé M., Nicolas J.B., Marchand N., Abidi E., Wiedensohler A., Drewnick F., Schneider J., Borrmann S., Nemitz E., Zimmermann R., Jaffrezo J.L., Prévot A.S.H., Baltensperger

- U.: Wintertime aerosol chemical composition and source apportionment of the organic fraction in the metropolitan area of Paris, *Atmospheric Chemistry and Physics*, 13, 961-981, doi:10.5194/acp-13-961-2013, 2013
- Crutzen, P.J. : *The role of NO and NO₂ in the chemistry of the troposphere and stratosphere*, *Annu. Rev. Earth Planet. Sci.*, 7, 443– 472. Environmental Protection Agency (1998), *National air quality and emissions trends report 1998*, Rep. EPA 454/R-00-003, 1979
- Crutzen, P.J., Zimmermann, P.H.: *The changing photochemistry of the troposphere*, *Tellus* 43, 136–151, 1991
- Cusack M., Pérez N., Pey J, Alastuey A., Querol X.: *Source apportionment of fine PM and sub-micron particle number concentrations at a regional background site in the western Mediterranean: a 2.5 year study*, *Atmos. Chem. Phys.*, 13, 2013, pp. 5173–5187
- Dahlback A, Stamnes K.: *A new spherical model for computing the radiation field available for photolysis and heating at twilight*, *Planet. Space Sci.*, 39, 671-683, 1991
- D'Amico, G., Amodeo, A., Mattis, I., Freudenthaler, V., Pappalardo, G.: *EARLINET Single Calculus Chain – technical – Part 1: Pre-processing of raw lidar data*, *Atmos. Meas. Tech.*, 9, 491-507, doi:10.5194/amt-9-491-2016, 2016
- DeCarlo, P.F., Dunlea, E.J., Kimmel, J.R., Aiken, A.C, Sueper, D., Crouse, J., Wennberg, P.O., Emmons, L., Shinozuka, Y, Clarke, A., Zhou, J., Tomlinson, J., Collins, D.R., Knapp, D., Weinheimer, A.J., Montzka, D.D., Campos, T., Jimenez, J.L.: *Fast airborne aerosol size and chemistry measurements above Mexico City and Central Mexico during the MILAGRO campaign*, *Atmospheric Chemistry and Physics*, 8 (14), 4027-4048, 2008
- Draxler, R.R., Hess, G.D.: *Description of the HYSPLIT_4 modeling system*, NOAA Tech. Memo ERL ARL-224, 24, NOAA, Silver Spring, Md, 1997
- Dubovik, O., Holben, B. Eck, T.F., Smirnov, A., Kaufman, Y.J., King, M.D, Tantré, D., Slutsker, I.: *Variability of absorption and optical properties of key aerosol types observed in worldwide locations*, *Journal of the Atmospheric Sciences*, 59, 590-608, doi:10.1175/1520-0469(2002)059, 2002
- Dubovik, O., Sinyuk, A., Lapyonok, T., Holben, B. N., Mishchenko, M., Yang, P., Eck, T. F., Volten, H., Muñoz, O., Veihelmann, B., van der Zande, W. J., Leon, J.-F., Sorokin, M. and Slutsker, I.: *Application of spheroid models to account for aerosol particle nonsphericity in remote sensing of desert dust*, *J. Geophys. Res. Atmospheres*, 111(D11), D11208, doi:10.1029/2005JD006619, 2006
- Dimitriou K., Paschalidou A.K., Kassomenos P.A.: *Assessing air quality with regards to its effect on human health in the European Union through air quality indices*, *Ecol. Indic.* 27:108–115, <http://dx.doi.org/10.1016/j.ecolind.2012.11.023>, 2013
- Dockery D. W., Pope C. A. III, Xu X., Spengler J. D., Ware J. H., Fay M. E., Ferris B. G. Jr., Speizer F.E.: *An association between air pollution and mortality in six U.S. cities*, *New England J. Med.*, 329, 1753-1759, 1993
- Dubovik O., Smirnov A., Holben B. N., King M. D., Kaufman Y. J., Eck T. F., Slutsker I.: *Accuracy assessments of aerosol optical properties retrieved from Aerosol Robotic Network (AERONET) Sun and sky radiance measurements*, *J. Geophys. Res.*, 105(D8), 9791–9806, 2000
- Dubovik, O., Sinyuk, A., Lapyonok, T., Holben, B. N., Mishchenko, M., Yang, P., Eck, T. F., Volten, H., Muñoz, O., Veihelmann, B., van der Zande, W. J., Leon, J.-F., Sorokin, M. and Slutsker, I.: *Application of spheroid models to account for aerosol particle nonsphericity in remote sensing of desert dust*, *J. Geophys. Res. Atmospheres*, 111(D11), D11208, doi:10.1029/2005JD006619, 2006

- Duncan B. N., Bey I.: A modeling study of the export pathways of pollution from Europe: Seasonal and interannual variations (1987–1997), *J. Geophys. Res.*, 109, D08301, doi:10.1029/2003JD004079, 2004
- Eck T.F., Holben B.N., Dubovik O., Smirnov A., Slutsker I., Lobert J.M., Ramanathan V.: Column-integrated aerosol optical properties over the Maldives during the northeast monsoon for 1998–2000, *Journal of Geophysical Research*, 106 (D22), 28555–28566, 2001
- Eck T. F., Holben B. N., Reid J. S., Dubovik O., Smirnov A., O’Neill N. T., Slutsker I., Kinne S.: Wavelength dependence of the optical depth of biomass burning, urban, and desert dust aerosols, *J. Geophys. Res. Atmospheres*, 104(D24), 31333–31349, doi:10.1029/1999JD900923, 1999
- Fameli K., Assimakopoulos V.: The new open Flexible Emission Inventory for Greece and the Greater Athens Area (FEI-GREGAA): Account of pollutant sources and their importance from 2006–2012, *Atmospheric Environment*, 137, 17–37, doi:10.1016/j.atmsenv.2016.04.004, 2016
- Favez O., El Haddad I., Piot C., Borave A., Abidi E., Marchand N., Jaffrezo J.-L., Besombes J.-L., Personnaz M.-B., Sciare J., Wortham H., George C., D’Anna B.: Inter-comparison of source apportionment models for the estimation of wood burning aerosols during wintertime in an Alpine city (Grenoble, France), *Atmospheric Chemistry and Physics*, 10(12), 5295–5314, 2010
- Fenger J., Hertel O., Palmgren F.: *Urban Air Pollution – European Aspects*, Environmental Pollution, Springer Science & Business Media, ISBN 978-90-481-5147-9, doi:10.1007/978-94-015-9080-8
- Finlayson B.J. and Pitts J.N. : *Photochemistry of the polluted troposphere*, Science, 192, 111–119, 1976
- Finlayson B.J. and Pitts J.N. : *Upper and lower atmosphere*, Academic Press, San Diego, 2000
- Florou K., Papanastasiou D., Pikridas M., Kaltsonoudis C., Louvaris E., Gkatzelis E., Patoulias D., Mihalopoulos M., Pandis S.: The contribution of wood burning and other pollution sources to wintertime organic aerosol levels in two Greek cities, *Atmospheric Chemistry and Physics Discussion*, doi:10.5194/acp-2016-721, 2016
- Fourtziou, L., Liakakou, E., Stavroulas, I., Theodosi, C., Zarbas, P., Psiloglou, B., Sciare, J., Maggos, T., Bairachtari, K., Bougiatioti, A., Gerasopoulos, E., Sarda, R., Bonnaire, N., Mihalopoulos, N.: Multi-tracer approach to characterize domestic wood burning in Athens (Greece) during wintertime, *Atmos. Environ*, 148, 89–101, doi:10.1016/j.atmsenv.2016.10.01, 2017
- Frieß U., Monks P. S., Remedios J. J., Rozanov A., Sinreich R., Wagner T., Platt U.: MAX-DOAS O₄ measurements: A new technique to derive information on atmospheric aerosols: 2. Modeling studies, *J. Geophys. Res.*, 111, D14203, doi:10.1029/2005JD006618, 2006
- Frieb, U., Klein Baltink, K., Beirle, S., Clémer, K., Hendrick, F., Henzing, B., Irie, H., de Leeuw, G., Li, A., Moerman, M., van Roozendaal, M., Shaiganfar, R., Wagner, T., Wang, Y., Xie, P., Yilmaz, S., Zieger, P.: Intercomparison of aerosol extinction profiles retrieved from MAX-DOAS measurements, *Atmos. Meas. Tech.*, 9, 3205–3222, doi:10.5194/amt-9-3205-2016, 2016
- Gerasopoulos E., Kouvarakis G., Babasakalis P., Vrekoussis M., Putaud J.P., Mihalopoulos N.: Origin and variability of particulate matter (PM₁₀) mass concentrations over the eastern Mediterranean, *Atmospheric Environment*, 40, 4679–4690, doi:10.1016/j.atmosenv.2006.04.020, 2006
- Gerasopoulos, E., Kokkalis, P., Amiridis, V., Liakakou, E., Perez, C., Haustein, K., Eleftheratos, K., Andreae, M.O., Andreae, T.W., Zerefos, C.: Dust specific extinction cross-section over the Eastern Mediterranean using the BSC-DREAM model and sun-photometer data: the case of urban environments, *Ann. Geophys.*, 27, 2903–2912, 2009
- Gerasopoulos E., Amiridis V., Kazadzis S., Kokkalis P., Eleftheratos K., Andreae M.O., Andreae T.W., El-Askary H., Zerefos C.S.: Three-year ground based measurements of aerosol optical depth over the

- Eastern Mediterranean: the urban environment of Athens, Atmos. Chem. Phys.*, **11**, 2145-2159, doi:10.5194/acp-11-2145-2011, 2011
- Gerasopoulos E., Liakakou E., Psiloglou V., Stavroulas J., Fourtziou L., Roukounakis N., Lianou M., Kappos N., Zampas P., Kambezidis H., Sciare J., Mihalopoulos N. : *Smog events over Athens during winter 2013-2014: Pollution measurements and chemical characterization, Geophysical Research Abstracts, Vol.16, EGU2014-12764-1, 2014*
- Gerasopoulos E., Gratsea M., Liakakou E., Lianou M., Psiloglou B., Kappos N., Kambezidis H., Mihalopoulos N.: *An overview of biomass burning impacts on Athens air quality and analysis of its increasing significance, 13th International Conference on Meteorology, Climatology and Atmospheric Physics, COMECAP 2016*
- Giannakaki, E., Pfüller, A., Korhonen, K., Mielonen, T., Laakso, L., Vakkari, V., Baars, H., Engelmann, R., Beukes, J. P., Van Zyl, P. G., Josipovic, M., Tiitta, P., Chiloane, K., Piketh, S., Lihavainen, H., Lehtinen, K. E. J. and Komppula, M.: *One year of Raman lidar observations of free-tropospheric aerosol layers over South Africa, Atmospheric Chem. Phys.*, **15**(10), 5429–5442, doi:10.5194/acp-15-5429-2015, 2015
- Giles, D.M., Sinyuk, A., Sorokin, M.G., Schafer, J.S, Smirnov, A., Slutsker, I., Eck, T.F., Holben, B.N., Lewis, J.R., Campbell, J.R., Welton, E.J., Korkin, S.V., Lyapustin, A.I.: *Advancements in the Aerosol Robotic Network (AERONET) Version 3 database – automated near-real-time quality control algorithm with improved cloud screening for Sun photometer aerosol optical depth (AOD) measurements, Atmos. Meas. Tech.*, **12**, 169-209, doi:10.5194/amt-12-169-2019, 2019
- Groß, S., Tesche, M., Freudenthaler, V., Toledano, C., Wiegner, M., Ansmann, A., Althausen, D. and Seefeldner, M.: *Characterization of Saharan dust, marine aerosols and mixtures of biomass-burning aerosols and dust by means of multi-wavelength depolarization and Raman lidar measurements during SAMUM 2, Tellus B*, **63**(4), doi:10.3402/tellusb.v63i4.16369, 2011
- Groß, S., Esselborn, M., Weinzierl, B., Wirth, M., Fix, A., and Petzold, A.: *Aerosol classification by airborne high spectral resolution lidar observations, Atmos. Chem. Phys.*, **13**, 2487–2505, <https://doi.org/10.5194/acp-13-2487-2013>, 2013
- Grosjean D., Grosjean E., Gertler A.W.: *On-road emissions of carbonyls from light-duty and heavy-duty vehicles, Environ. Sci. Technol.*, **35**, 45 – 53, 2001
- Guerova G., Bey I., Attle J.-L., Martin R V., Cui J., Sprenger M.: *Impact of transatlantic transport episodes on summertime ozone in Europe, Atmos. Chem. Phys.*, **6**, 2057–2072, 2006
- Gurjar B.R., Butler T.M., Lawrence M.G., Lelieveld J.: *Evaluation of emissions and air quality in megacities, Atmospheric Environment*, **42**, 1593-1606, 2008
- Heckel A., Richter A., Tarsu T., Wittrock F., Hak C., Pundt I., Junkermann W., Burrows J.P.: *MAX-DOAS measurements of formaldehyde in the Po-Valley, Atmos. Chem. Phys.*, **5**, 909-918, doi:10.5194/acp/2005-5-909, 2005
- Hermans, C., Vandaele, A.C., Fally, S., Carleer, M., Colin, R., Coquart, B., Jenouvrier, A., Merienne, M.F.: *Absorption cross-section of the collision-induced bands of oxygen from the UV to the NIR. In: Camy-Peyret, C., Vigasin, A.A. (Eds.), Proceedings of the NATO Advanced Research Workshop, Weakly Interacting Molecular Pairs: Unconventional Absorbers of Radiation in the Atmosphere, Fontevraud, France, 24 April-2 May 2002, NATO Science Series IV Earth and Environmental Sciences, Vol. 27. Kluwer Academic Publishers, Boston, pp. 193-202, 2003*
- Ho K.F., Lee S.C., Louie P., Zou S.C., *Seasonal variation of carbonyl compound concentrations in urban area of Hong Kong, Atmospheric Environment*, **36** (8), 1259-1265, 2002

- Holben, B. N., Eck, T. F., Slutsker, I., Tanré, D., Buis, J. P., Setzer, A., Vermote, E., Reagan, J. A., Kaufman, Y. J., Nakajima, T., Lavenu, F., Jankowiak, I. and Smirnov, A.: AERONET—A Federated Instrument Network and Data Archive for Aerosol Characterization, *Remote Sens. Environ.*, 66(1), 1–16, doi:10.1016/S0034-4257(98)00031-5, 1998
- Hönninger G., Von Friedeburg C., Platt U.: Multi Axis Differential Optical Absorption Spectroscopy (MAX-DOAS), *Atmospheric Chemistry and Physics*, 4, 231-254, doi:1680-7324/acp/2004-4-231, 2004
- Husar R.B., Tratt D.M., Schichtel B.A., Falke S.R., Li F., Jaffe D., Gasso S., Gill T., Lanlainen N. S., Lu F., Reheis M.C., Chun Y., Westphal D., Holben B. N., Gueymard C., McKendry I., Kuring N., Feldman G.C., McClain C., Frouin R.J., Merrill J., DuBois D., Vignola F., Murayama T., Nickovic S., Wilson W.E., Sassen K., Sugimoto N., and Malm W.C.: Asian dust events of April 1998, *J. Geophys. Res.*, 106, 18 317–18 330, 2001
- Intergovernmental Panel on Climate Change (IPCC) (2001), *Climate Change 2001: The Science of Climate Change, Technical Summary of the Working Group I Report*, Cambridge Univ. Press, New York
- IPCC: *Climate Change 2007: The Physical Science Basis. Contribution of working group I to the Fourth Assessment Report of the Intergovernmental Panel on Climate Change*, edited by: Solomon S., Qin D., Manning M., Chen Z., Marquis M., Averyt K.B., Tignor M. and Miller H.L., Cambridge University Press, Cambridge, United Kingdom and New York, NY, USA, 2007
- Jacobson M.: Strong radiative heating due to the mixing state of black carbon in atmospheric aerosols, *Nature* 409, 695-697, doi:10.1038/35055518, 2001
- Kalabokas P., Hatzianestis J., Bartzis J., Mimikos N. : Seasonal and diurnal variation of carbonyl compounds concentration levels in the atmosphere of the Athens basin, *Fresenius Environment Bulletin* 6: 172-177, 1997
- Kalabokas P., Bartzis J. : Photochemical air pollution characteristics at the station of NCSR-Demikritos, during the MEDCAPHOT-TRACE campaign in Athens, Greece, *Atmospheric Environment*, 32(12), 2123-2139, doi:1352-2310/98, 1998
- Kalabokas P., Papayannis A., Tsaknakis G., Avdikos G., Eleftheratos K., Balis, D., Ziomas I., Georgoussis G., Paliatsos A. and Tsamalis C., Atmospheric concentrations of SO₂, NO₂ and O₃ in Athens, Greece measured by DOAS and DIAL techniques, *IGAC 10th International Conference "Bridging the scales in Atmospheric Chemistry: Local to Global"*, Annecy, France, 7-12 September, 2008
- Kalabokas P., Repapis C. : A climatological study of rural surface ozone in central Greece, *Atmos. Chem. Phys.*, 4, 1139-1147, doi:10.5194/acp-4-1139-2004, 2004
- Kalabokas P., Viras L., Repapis C. : Analysis of the 11-year record (1987-1997) of air pollution measurements in Athens, Greece. Part I: Primary air pollutants. *Global Nest: the Int. J. Vol 1 No 3: 157-167*, 1999
- Kalabokas P. D., Papayannis A. D., Tsaknakis G., Ziomas I. : Study on the atmospheric concentrations of primary and secondary air pollutants in the Athens basin performed by DOAS and DIAL measuring techniques, *The Science of the Total Environment*, 414, 556-563, 2012
- Kallos G., Kassomenos P., Pielke R.A. : Synoptic and mesoscale weather conditions during air pollution episodes in Athens, Greece, *Boundary-Layer Meteorology*, 62, 163-184, 1993
- Kampa M., Castanas E.: Human health effects of air pollution, *Environmental Pollution*, 151(2), 362-367, doi:10.1016/j.envpol.2007.06.012, 2008

- Kanakidou M., Mihalopoulos N., Kalivitis N., Tsigaridis K., Kouvarakis G., Koulouri E., Gerasopoulos E., Vrekoussis M., Myriokefalitakis S.: *Natural contributions to particulate matter levels over Europe - the experience from Greece*, In: CEST2007: A-585-592, 2007
- Kanakidou M., Mihalopoulos N., Kindap T., Im U., Vrekoussis M., Gerasopoulos E., Dermitzaki E., Unal A., Kocak M., Markakis K., Melas D., Kouvarakis G., Youssef A., Richter A., Hatzianastassiou N., Hilboll A., Ebojie F., Wittrock F., Savigny C., Burrows J., Ladstatter-Weibenmayer A. : *Megacities as hot spots of air pollution in the East Mediterranean*, *Atmospheric Environment* 45(6), 1223-1235, 2011
- Kassomenos P., Kotroni V., Kallos G.: *Analysis of climatological and air quality observations from greater Athens area*, *Atmospheric Environment* 29(24), 3671-3688, 1995
- Katsoulis B.: *The relationship between synoptic, mesoscale and microscale meteorological parameters during poor air quality events in Athens, Greece*, *The Science of the Total Environment* 181, 13-24, 1996
- Kim, S.W., Berthier, S., Raut, J.C., Chazette, P., Dulak, F., Yoon, S.C.: *Validation of aerosol and cloud layer structures from the space-borne lidar CALIOP using ground-based lidar in Seoul, Korea*, *Atmos. Chem. Phys.*, 8, 3705-3720, 2008
- Kirchstetter, T. W., Harley, R. A., Kreisberg, N. M., Stolzenburg, M. R., and Hering, S. V.: *On-road measurement of fine particle and nitrogen oxide emissions from light- and heavy-duty motor vehicles* *Atmos. Environ.*, 33, 2955–2968, 1999
- Klemm, O., Ziomas, I.C., Balis, D., Suppan, P., Slemr, J., Romero, R., Vyras, L.G.: *A summer air-pollution study in Athens, Greece*, *Atmospheric Environment* 32 (12), 2071–2087, 1998
- Klett, J. D.: *Stable analytical inversion solution for processing lidar returns*, *Appl. Opt.*, 20(2), 211, doi:10.1364/AO.20.000211, 1981
- Knote, C., Hodzic, A., Jimenez, J. L., Volkamer, R., Orlando, J. J., Baidar, S., Brioude, J., Fast, J., Gentner, D. R., Goldstein, A. H., Hayes, P. L., Knighton, W. B., Oetjen, H., Setyan, A., Stark, H., Thalman, R., Tyndall, G., Washenfelder, R., Waxman, E., and Zhang, Q.: *Simulation of semi-explicit mechanisms of SOA formation from glyoxal in aerosol in a 3-D model*, *Atmospheric Chemistry and Physics*, 14, 6213–6239, doi:10.5194/acp-14-6213-2014, 2014
- Koch D., Bond T C., Streets D., Unger N., van der Werf G. R.: *Global impacts of aerosols from particular source regions and sectors*, *J. Geophys. Res.*, 112, D02205, doi:10.1029/2005JD007024, 2007
- Kokkalis, P., Papayannis, A., Mamouri, R. E., Tsaknakis, G., Amiridis, V.: *The EOLE lidar system of the National Technical University of Athens*, in *Reviewed and revised papers presented at the 26th International Laser Radar Conference*, pp. 25–29., 2012
- Kokkalis, P.: *Using paraxial approximation to describe the optical setup of a typical EARLINET lidar system*, *Atmos. Meas. Tech.*, 10, 3103–3115, <https://doi.org/10.5194/amt-10-3103-2017>, 2017
- Kokkalis, P., Alexiou, D., Papayannis, A., Rocadenbosch, F., Soupiona, O., Raptis, P.I., Mylonaki, M., Tzani, C.G., Christodoulakis, J.: *Application and Testing of the Extended-Kalman-Filtering Technique for Determining the Planetary Boundary-Layer Height over Athens, Greece*, *Boundary-Layer*
- Kosmopoulos, P. G., Kazadzis, S., Taylor, M., Athanasopoulou, E., Speyer, O., Raptis, P. I., Marinou, E., Proestakis, E., Solomos, S., Gerasopoulos, E., Amiridis, V., Bais, A., Kontoes, C.: *Dust impact on surface solar irradiance assessed with model simulations, satellite observations and ground-based measurements*, *Atmos. Meas. Tech.*, 10, 2435-2453, <https://doi.org/10.5194/amt-10-2435-2017>, 2017

- Kourtidis K.A., Ziomas I.C., Rappenglueck B., Proyou A., Balis D.: *Evaporative traffic hydrocarbon emissions, traffic CO and speciated HC traffic emissions from the city of Athens, Atmospheric Environment* 33, 3831-3842, 1999
- Lalas D.P., Veirs V.R., Karras G., Kallos G.: *An analysis of the SO₂ concentration levels in Athens, Greece, Atmospheric Environment* 16, 531-544, 1982
- Lalas D., Assimakopoulos D., Deligiorgi D., Helmis C.: *Sea breeze circulation and photochemical pollution in Athens, Greece, Atmospheric Environment*, 17(9), 1621-1632, 1983
- Lee, Y.-N., et al.: *Atmospheric chemistry and distribution of formaldehyde and several multioxygenated carbonyl compounds during the 1995 Nashville/Middle Tennessee Ozone Study, J. Geophys. Res.*, 103, 22, 449–22, 462, 1998
- Lee, H., Irie, H., Kim, Y., Noh, Y., Lee, C., Kim, Y., Chun, K.: *Retrieval of Aerosol Extinction in the Lower Troposphere Based on UV MAX-DOAS Measurements, Aerosol, Sci. Tech.*, 43, 502–509, doi:10.1080/02786820902769691, 2009
- Leigh R.J., Corlett G.K., Frieb U., Monks P.S. : *Spatially resolved measurements of nitrogen dioxide in an urban environment using concurrent multi-axis differential optical absorption spectroscopy, Atmospheric Chemistry and Physics*, 7, 4751-4762, 2007
- Lelieveld J., Berresheim H., et al.: *Global air pollution crossroads over the Mediterranean, Science* 298, 794-799, 2002
- Leue C., Wenig M., T. Wagner, O. Klimm, U. Platt, Jahne B.: *Quantitative analysis of NO_x emissions from Global Ozone Monitoring Experiment satellite image sequences, J. Geophys. Res.*, 106(D6), 5493–5505, 2001
- Levy H. : *Normal atmosphere: Large radical and formaldehyde concentrations predicted, Science*, 173, 141-143, 1971
- Liu L., Flatoy F., Ordóñez C., Braathen G.O., Hak C., Junkermann W., Andreani-Aksoyoglu S., Mellqvist J., Galle B., Prévot A.S.H. & Isaksen I.S.A. : *Photochemical modelling in the Po basin with focus on formaldehyde and ozone, Atmos. Chem. Phys.*, 7, 121-137, 2007.
- Logan J.A., Prather M.J., Wofsy S.C., McElroy M.B.: *Tropospheric chemistry: A global perspective, Journal of Geophysical Research*, doi:10.1029/JC086iCO8p07210, 1981
- Lowe D., Schmidt U.: *Formaldehyde (HCHO) measurements in the nonurban atmosphere, Journal of Geophysical Research*, 88 (C15), 10844-10858, 1983
- Lyamani H., Olmo F.J., Foyo I., Alados-Arboleds L.: *Black carbon aerosols over an urban area in south-eastern Spain: Changes detected after the 2008 economic crisis, Atmospheric Environment* 45, 6423-6432, 2011
- Ma, J.Z., Beirle, S., Jin, J.L., Shaiganfar, R., Yan, P., Wagner, T.: *Tropospheric NO₂ vertical column densities over Beijing: results of the first three years of ground-based MAX-DOAS measurements (2008-2011) and satellite validation, Atmos. Chem. Phys.*, 13, 1547-1567, doi:10.5194/acp-13-1547-2013, 2013
- Mage D., Ozolins G., Peterson P., Webster A., Orthofer R., Vandeweerd V., Gwynne M.: *Urban air pollution in megacities in the world, Atmospheric Environment*, 30 (5), 681-686, 1996
- Markakis K., Poupkou A., Melas D., Tzoumaka P., Petrakakis M. : *A computational approach based on GIS technology for the development of an anthropogenic emission inventory for air quality applications in Greece, Water Air and Soil Pollution*, 207, 157-180, doi:10.1007/s11270-009-0126-5, 2010

- Marquard L., Platt U.: AMFTRAN: A new Monte Carlo radiative transfer model for calculating air mass factors, *Atmospheric Ozone Dynamics Observations in the Mediterranean Region*, NATO ASI Ser. I, vol. 53, edited by C. Varotsos, 231-241, Springer New York, 1997
- Marquard L.C., Wagner T., Platt U.: Improved air mass factor concepts for scattered radiation differential optical absorption spectroscopy of atmospheric species, *Journal of Geophysical Research*, 105 (D1), 1315-1327, 2000
- Matthias, V., Balis, D., Bösenberg, J., Eixmann, R., Iarlori, M., Komguem, L., Mattis, I., Papayannis, A., Pappalardo, G., Perrone, M.R., Wang, X.: Vertical aerosol distribution over Europe: Statistical analysis of Raman lidar data from 10 European Aerosol Research Lidar Network (EARLINET) stations, *Journal of Geophysical Research*, 109, D18201, doi:10.1029/2004JD004638, 2004
- Mattis, I., Ansmann, A., Müller, D., Wandinger, U., Althausen, D.: Multiyear aerosol observations with dual-wavelength Raman lidar in the framework of EARLINET: MULTIYEAR AEROSOL PROFILING IN EUROPE, *J. Geophys. Res. Atmospheres*, 109(D13), n/a-n/a, doi:10.1029/2004JD004600, 2004
- Mattis, I., D'Amico, G., Baars, H., Amodeo, A., Madonna, F., Iarlori, M.: EARLINET Single Calculus Chain – technical – Part 2: Calculation of optical products, *Atmos. Meas. Tech.*, 9, 3009-3029, doi:10.5194/amt-9-3009-2016, 2016
- Mavroidis I., Chaloulakou A.: Long-term trends of primary and secondary NO₂ production in the Athens area. Variation of the NO₂/NO_x ratio, *Atmospheric Environment*, 45 (38), doi:10/1016/j.atmosenv.2010.11.006, 2011
- Menut L., Goussebaile A., Bessagnet B., Khvorostiyannov D., Ung A. (2012) Impact of realistic hourly emission profiles on air pollutants concentration modelled with CHIMERE. *Atmospheric Environment* (49):233-244. doi: 10.1016/j.atmosenv.2011.11.057
- Mitsakou C., Kallos G., Papantoniou N., Spyrou C, Solomos S., Astitha M., Housiadas C.: Saharan dust levels in Greece and received inhalation doses, *Atmos. Chem. Phys.*, 8, 7181-7192, 2008
- Mona, L., Müller, D., Omar, A., Papayannis, A., Pappalardo, G., Sugimoto, N., Vaughan, M.: Lidar measurements for desert dust characterization: A Review, *Advances in Meteorology (Special Issue: Desert Dust Properties, Modelling, and Monitoring)* ID356265, doi:10.1155/2012/356265, 2012
- Morris, R., Koo, B., McNally, D., et al.: Application of Multiple Models to Simulation Fine Particulate in the Southeastern U.S. Presented at the National Regional Planning Organizations Modeling Meeting, Denver, CO, 2005
- Müller, D., Ansmann, A., Mattis, I., Tesche, M., Wandinger, U., Althausen, D. and Pisani, G.: Aerosol-type-dependent lidar ratios observed with Raman lidar, *J. Geophys. Res.*, 112(D16), doi:10.1029/2006JD008292, 2007
- Moussiopoulos N., Sahm P., Kessler Ch.: Numerical simulation of photochemical smog in Athens, Greece—A case study. *Atmos. Environ.*, 29, 3619–3632, 1995
- Moussiopoulos P., Sahm P., Karatzas K., Papalexiou S., Kragiannidis A. : Assessing the impact of the new Athens airport to urban air quality with contemporary air pollution models, *Atmospheric Environment*, 31(10), 1497-1511, 1997
- Noxon J.F. : Tropospheric NO₂, *J. Journal of Geophysical Research*, 83,3051-3057, 1978
- Noxon J.F., Whipple E.C., Hyde R.S.: Stratospheric NO₂, observational method and behavior at midlatitudes, *J. Geophys. Res.*, 84, 5047-5076, 1979
- Palmer, P. I., Jacob D.J., Fiore A.M., Martin R.V., Chance K., and Kurosu T.P.: Mapping isoprene emissions over North America using formaldehyde column observations from space, *J. Geophys. Res.*, 108(D6), 4180, doi:10.1029/2002JD002153, 2003

- Pandis, S., Wexler, A., Seinfeld, J.: Dynamics of tropospheric aerosol, *J. Phys. Chem*, 99, 9646-9659, 1995
- Pappalardo, G., Amodeo, A., Apituley, A., Comeron, A., Freudenthaler, V., Linné, H., Ansmann, A., Bösenberg, J., D'Amico, G., Mattis, I., Mona, L., Wandinger, U., Amiridis, V., Alados-Arboledas, L., Nicolae, D. and Wiegner, M.: EARLINET: towards an advanced sustainable European aerosol lidar network, *Atmos. Meas. Tech.*, 7(8), 2389–2409, doi:10.5194/amt-7-2389-2014, 2014
- Papayannis, A., Balis, D., Bais, A., Van Der Bergh, H., Calpini, B., Durieux, E., Fiorani, L., Jaquet, L., Ziomas, I., Zerefos, C.S.: Role of urban and suburban aerosols on solar UV radiation over Athens, Greece, *Atmospheric Environment*, 32 (12), 2193-2201, 1998
- Papayannis A., Balis D., Amiridis V., Chourdakis G., Tsaknakis G., Zerefos C., Castanho D.A., Nickovic, Kazadzis S., Grabowski J.: Measurements of Saharan dust aerosols over the Eastern Mediterranean using elastic backscatter-Raman lidar, spectrophotometric and satellite observations in the frame of the EARLINET project, *Atmospheric Chemistry and Physics*, 5 (8), 2065-2079, 2005
- Papayannis, A., Amiridis, V., Mona, L., Tsaknakis, G., Balis, D., Bösenberg, J., Chaikovski, A., De Tomasi, F., Grigorov, I., Mattis, I., Mitev, V., Müller, D., Nickovic, S., Pérez, C., Pietruczuk, A., Pisani, G., Ravetta, F., Rizi, V., Sicard, M., Trickl, T., Wiegner, M., Gerding, M., Mamouri, R. E., D'Amico, G. and Pappalardo, G.: Systematic lidar observations of Saharan dust over Europe in the frame of EARLINET (2000–2002). *J. Geophys. Res. Atmospheres*, 113(D10), D10204, 2008
- Papayannis, A., Mamouri, R.E., Amiridis, V., Kazadzis, S., Pérez, C., Tsaknakis, G., Kokkalis, P.: Systematic lidar observations of Saharan dust layers over Athens, Greece in the frame of EARLINET project (2004-2006), *Annalesgeophysicae*, 27, 3611-3620, 2009
- Papayannis A., Mamouri R.E., Remoundaki E., Bourliva A., Tsaknakis G., Amiridis V., Kokkalis P., Veselovskii I., Kazadzis S., Kolgotin A., Nenes A., Fountoukis C. : Optical – microphysical properties and chemical characterization of Saharan dust aerosols using a multi – wavelength Raman lidar, in situ sensors and modelling, *Atmos. Chem. Phys.*, 12, 4011-4032, 2012
- Paraskevopoulou D., Liakakou E., Gerasopoulos E., Mihalopoulos N. : Sources of atmospheric aerosol from long-term measurements (5 years) of chemical composition in Athens, Greece, *Science of The Total Environment*, Vol. 527-528, 165-178, doi: 10.1016/j.scitotenv.2015.04.022, 2015
- Pascal M., Corso M., Chanel O., Declercq C., Bandaloni C., Cesaroni G., Henschel S., Meister K., Haluza D., Martin-Olmedo P., Medina S.: Assessing the public health impacts of urban air pollution in 25 European cities: Results of the Aphekom project, *Science of The Total Environment* , 449, 390-400, 2013
- Petzold A. and Schönlinner M.: Multi-angle absorption photometry – A new method for the 695 measurement of aerosol light absorption and atmospheric black carbon, *J. Aerosol Sci.*, 35, 421–441, doi:10.1016/j.jaerosci.2003.09.005, 2004.
- Perner, D. and U. Platt, Detection of nitrous acid in the atmosphere by differential optical absorption, *Geophys. Res. Lett.*, 7, 1053-1056, 1979
- Perner D., Platt U. : Absorption of light in the atmosphere by collision pairs of oxygen (O₂)₂, *Geophysical Research Letters*, 7, 1053-1056, doi:10.1029/GL007i012p01053, 1980
- Pezzoli A. : Observation and analysis of etesian wind storms in the Saroniko Gulf, *Advances in Geosciences*, 2, 187-194, 2005
- Pfeilsticker K., Erle F., Platt U. : Absorption of solar radiation by atmospheric O₄, *Journal of the Atmospheric Sciences*, Vol. 54, 1997
- Pinardi G., Van Roozendaal M., Abuhassan N., Adams C., Cede A., Clémer K., Fayt C., Frieb U., Gil M., Herman J., Hermans C., Hendrick F., Irie H., Merlaud A., Navarro Comas M., Peters E., Piters A.J.M.,

- Puenteadura O., Richter A., Schönhardt A., Shaiganfar R., Spinei E., Strong K., Takashima H., Vrekoussis M., Wagner T., Wittrock F., Yilmaz S.: MAX-DOAS formaldehyde slant column measurements during CIND: intercomparison and analysis improvement, *Atmos. Meas. Tech.*, 6, 167-185, doi:10.5194/amt-6-167-2013, 2013
- Platt U., Perner D., Pätz W. : Simultaneous measurement of atmospheric CH₂O, O₃ and NO₂ by differential optical absorption, *Journal of Geophysical Research*, Vol. 84, NO. C10, 1979
- Platt, U., "Differential optical absorption spectroscopy (DOAS)", *Chem. Anal. Series*, 127, 27 - 83, 1994.
- Platt, U., Stutz, J.: *Differential Optical Absorption Spectroscopy: Principles and Applications*, Springer, Berlin, Heidelberg, Germany, 2008.
- Pleijel H., Klingberg J., Bäck E.: Characteristics of NO₂ pollution in the city of Gothenburg, South-West Sweden-relation to NO_x and O₃ levels, photochemistry and monitoring location, *Water, Air and Soil Pollution: Focus*, 9, 1525, 2009
- Possanzini, M., Di Palo, V., Petricca, M., Fratarcangeli, R., Brocco, D. : Measurements of lower carbonyls in Rome ambient air,. *Atmospheric Environment* 30 (22), 3757–3764, 1996
- Psiloglou, B.E., Kambezidis, H.D.: Estimation of the ground albedo for the Athens area, Greece, *Journal of Atmospheric and Solar-Terrestrial Physics*, 71 (8-9), 943-954, doi:10.1016/j.jastp.2009.03.017,2009
- Psiloglou B., Larissi I., Petrakis M., Paliatsos A., Antoniou A., Viras L. : Case studies on summertime measurements of O₃, NO₂ and SO₂ with a DOAS system in an urban semi-industrial region in Athens, Greece, *Environ. Monit. Assess.*, doi:10.1007/s10661-013-3134-2, 2013
- Puxbaum, H., Caseiro, A., Sánchez-Ochoa, A., Kasper-Giebl, A., Claeys, M., Gelencsér, A., Legrand, M., Preunkert, S., & Pio, C. A., Levoglucosan levels at background sites in Europe for assessing the impact of biomass combustion on the European aerosol background, *Journal of Geophysical Research: Atmospheres*, 112(23), 2007.
- Ramanathan V., Carmichael G.: Global and regional climate changes due to black carbon, *Nature Geoscience*, 1, 221-227, doi: 10.1038/ngeo156, 2008
- Ren X., Harder H., Martinez M., Leshner R., Oligier A., Simpas J.B., Brune W., Schwab J.J., Demerjian K.L., He Y., Zhou X., Gao H.: OH and HO₂ chemistry in the urban atmosphere of New York, *Atmospheric Environment*, 37 (26), 3639-3651, doi:10.1016/S1352-2310(03)00459-X, 2003
- Rappenglück B., Fabian P., Kalabokas P., Viras L.G., Ziomias I.C. : Quasi-continuous measurements of non-methane hydrocarbons (NMHC) in the greater Athens area during the MEDCAPHOT-TRACE, *Atmospheric Environment* 32(12), 2103-2121, 1998
- Raptis P., Kazadzis S., Amiridis V., Gkikas A., Gerasopoulos E., Mihalopoulos N.: A decade of aerosol optical properties measurements over Athens, Greece, *Atmosphere*, 11(2), 154, doi:10.3390/atmos11020154, 2020
- Retalis A., Cartalis C., Athanasiou E.: Assessment of the distribution of aerosols in the area of Athens with the use of Landsat Thematic Mapper data, *International Journal of Remote Sensing*, Vol. 20 (5), 939-945, doi:10.1080/014311699213000, 1999
- Roscoe H.K., Brough N., Jones A.E., Wittrock F., Richter A., Van Roozendael M., Hendrick F. : Characterisation of vertical BrO distribution during events of enhanced tropospheric BrO in Antarctica, from combined remote and in-situ measurements, *Journal of Quantitative Spectroscopy & Radiative Transfer*, 138, 70-81, doi:10.1016/j.jqsrt.2014.01.026, 2014
- Rocadenbosch, F., Reba, M. N. M., Sicard, M. and Comerón, A.: Practical analytical backscatter error bars for elastic one-component lidar inversion algorithm, *Appl. Opt.*, 49(17), 3380–3393, 2010

- Rodgers, C. and Connor, B.: Intercomparison of remote sounding instruments, *J. Geophys. Res.*, **108**, 4116–4229, doi:10.1029/2002JD002299, 2003
- Rozanov, V., Diebel D., Spurr R., Burrows J.: Gometran: A radiative transfer model for the satellite project GOME: The plane parallel version, *J. Geophys. Res.*, **102**, 16683-16697, 1997
- Rozanov, A., Rozanov, V., Burrows, J.P.: Combined differential-integral approach for the radiation field computation in a spherical shell atmosphere: Nonlimb geometry, *J. Geophys. Res.*, **105**, D18, 22, 937, 2000
- Rozanov, A., Rozanov, V., Buchwitz, M., Kokhanovsky, A., Burrows, J.P.: SCIATRAN 2.0 – A new radiative transfer model for geophysical applications in the 175-2400 nm spectral region, *Advances in Space Research*, **36**, 1015-1019, 2005
- Rozanov, A., Bovensmann, H., Bracher, A., Hrechanyy, S., Rozanov, V., Sinnhuber, M., Strohm, F., Burrows, J.P.: NO₂ and BrO vertical profile retrieval from SCIAMACHY limb measurements: Sensitivity studies, *Advances in Space Research*, **36**, 846-854, doi:10.1016/j.asr.2005.03.013, 2005
- Rosenfeld, D., Sherwood, S., Wood, R., Donner, L.: Climate effects of aerosol-cloud interactions, *Science*, **343** (6169), 379-380, doi:10.1126/science.1247490, 2014
- Saffari A., Daher N., Samara C., Voutsas D., Kouras A., Manoli E., Karagiozidou O., Vlachokostas C., Moussiopoulos N., Shafer M., Schauer J., Sioutas C.: Increased biomass burning due to economic crisis in Greece and its adverse impact on wintertime air quality in Thessaloniki, *Environ. Sci. Technol.*, **47**(23), 13313-13320, 2013, doi:10.1021/es403847h
- Sander S. P., Golden D.M., Kurylo M.J., Moortgat G.K., Wine P.H., Ravishankara A.R., Kolb C.E., Molina M.J., Finlayson-Pitts B.J., Huie R.E., Orkin V.L.: *Chemical Kinetics and Photochemical Data for Use in Atmospheric Studies*, Evaluation Number 15, JPL Publication 06-02, Jet Propulsion Laboratory, Pasadena, Calif., 2006
- Saurer M., Prevot A.S.H., Dommen J., Sandradewi J., Baltensperger U., Siegwolf T.H.: The influence of traffic and wood combustion on the stable isotopic composition of carbon monoxide, *Atmos. Chem. Phys.*, **9**, 3147-3161, 2009
- Schwartz J., Spix C., Wichmann H.E., Malin E. : Air pollution and acute respiratory illness in five German communities, *Environmental Research*, **56**(1), 1-14, doi:10.1016/S0013-935(05)80104-5, 1991
- Sciare J., D'Argouges O., Sarda-Estve R., Gaimoz C., Dolgorouky C., Bonnaire N., Favez O., Bonsang B., Gros V.: Large contribution of water-insoluble secondary organic aerosols in the region of Paris (France) during wintertime, *Journal of Geophysical Research:Atmospheres*, **116**(22), 2011
- Schmid, B., Ferrare, R., Flynn, C., Elleman, R., Covert, D., Strawa, A., Welton, E., Turner, D., Jonsson, H., Redemann, J., Eilers, J., Ricci, K., Hallar, A.G., Clayton, M., Michalsky, J. Smirnov, A., Holben, B., Barnard, J.: How well do state-of-the-art techniques measuring the vertical profile of tropospheric aerosol extinction compare?, *JGR Atmospheres*, doi:10.1029/2005JD005837, 2006
- Schreier, F.S., Richter, A., Peters, E., Ostendorf, M., Schmalwieser, A.W., Weihs, P., Burrows, J.P.: Dual ground-based MAX-DOAS observations in Vienna, Austria: Evaluation of horizontal and temporal NO₂, HCHO and CHOCHO distributions and comparison with independent data sets, *Atmospheric Environment:X*, **5**, 100059, doi:10.1016/j.aeaoa.2019.100059, 2020
- Seinfeld, J. H., and S. N. Pandis, *Atmospheric Chemistry and Physics: From Air Pollution to Climate Change*, John Wiley & Sons, New York, 1998
- Seinfeld J., Pandis S. : *Atmospheric chemistry and physics from air pollution to climate change*, John Wiley and Sons, ISBN-13:978-0-471-72018-8, 2006
- Serway R., Moses C., Moyer C.: *Modern Physics*, Saunders College Publishing, 1989

- Seyler A., Wittrock F., Kattner L., Mathieu-Üffing B., Peters E., Richter A., Schmolke S., Burrows J.P.: Monitoring shipping emissions in the German Bight using MAX-DOAS measurements, *Atmos. Chem. Phys.*, 17, 10997-11023, doi:10.5194/acp-17-10997-2017, 2017
- Sharma S., Brook J.R., Cachier H., Chow J., Gaudenzi A., Lu G.: Light absorption and thermal measurements of black carbon in different regions of Canada, *Journal of Geophysical Research*, 107(D24), AAC 11-1-AAC 11-11, doi: 10.1029/2002JD002496, 2002
- Sinreich R., Frieß U., Wagner T., Platt U.: Multi axis differential optical absorption spectroscopy (MAX-DOAS) of gas and aerosol distributions, *Faraday Discuss.*, 130, 153–164, doi:10.1039/B419274P, 2005
- Smirnov, A., Holben, B. N., Eck, T. F., Slutsker, I., Chatenet, B., Pinker, R. T.: Diurnal variability of aerosol optical depth observed at AERONET (Aerosol Robotic Network) sites, *Geophys. Res. Lett.*, 29, 2115, doi:10.1029/2002GL016305, 2002
- Solanki, R., Singh, N.: LiDAR observations of the vertical distribution of aerosols in free troposphere: Comparison with CALIPSO level-2 data over the central Himalayas, *Atmospheric Environment*, 99, 227-238, doi:10.1016/j.atmosenv.2014.09.083, 2014
- Solomon S., Schmeltekopf A.L., Sanders R.W.: On the interpretation of zenith sky absorption measurements, *Journal of Geophysical Research*, 92 (D7), 8311-8319, doi:10.1029/JD092ID07p08311, 1987
- Soupiona, O., Samaras, S., Ortiz-Amezcuca, P., Böckmann, C., Papayannis, A., Moreira, GA, Benavent-Oltra, J.A., Guerrero-Rascado, J.L., Bedoya-Velásquez, AE, Olmo, FJ, Román, R., Kokkalis, P., Mylonaki, M., Alados-Arboledas, L., Papanikolaou, CA, Foskinis, R.: Retrieval of optical and microphysical properties of transported Saharan dust over Athens and Granada based on multi-wavelength Raman lidar measurements: Study of the mixing processes, *Atmospheric Environment*, 214, doi.org/10.1016/j.atmosenv.2019.116824, 116824, 2019
- Stutz J., Platt U.: Numerical analysis and estimation of the statistical error of differential optical absorption spectroscopy measurements with least-squares methods, *Applied Optics*, 35 (30), 1996
- Sumner A.L., Shepson P.B., Grannas A.M., Bottenheim J.W., Anlauf K.G., Worthy D., Schroeder W.H., Steffen A., Domine F., Perrier S., Houdier S.: Atmospheric chemistry of formaldehyde in the Arctic troposphere at Polar Sunrise, and the influence of the snowpack, *Atmos. Environ.*, 36, 15-16, 2002
- Tanner R., Mong Z.: Seasonal variations in ambient atmospheric levels of formaldehyde and acetaldehyde, *Environmental Science and Technology*, 18, 723-726, doi:10.1021/es00127a017, 1984
- Theodosi C., Grivas G., Zarnpas P., Chaloulakou A., Mihalopoulos N.: Mass and chemical composition of size-segregated aerosols (PM_{10} , $PM_{2.5}$, PM_{10}) over Athens, Greece: local versus regional sources, *Atmos. Chem. Phys.*, 11, 11895-11911, doi:10.5194/acp-11-11895-2011, 2011
- Twomey, S.: Influence of pollution on the short-wave albedo of clouds, *J. Atmos. Sci.*, 34, 1149–1152, 1977
- Vandaele, A.C., Hermans, C., Simon, P.C., Carleer, M., Colin, R., Fally, S., Merienne, M., Jenouvrier, F., Coquart, B.: Measurements of the NO₂ absorption cross section from 42,000 cm⁻¹ to 10,000 cm⁻¹ (238-1000 nm) at 220 K and 294 K. *J. Quant. Spectrosc. Radiat. Transfer* 52, 171-184, 1998
- Van Dop H., Kallos G.: *Air pollution modeling and its application IX*, Springer Science & Business Media, Vol.17 Nato Challenges of Modern Society, ISBN:1461530520, 9781461530527, 2012
- Velders, G. J. M., Grainer C., Portmann R.W., Pfeilsticker K., Wenig M., Wagner T., Platt U., Richter A., Burrows J.P.: Global tropospheric NO₂ column distributions: Comparing three-dimensional model calculations with GOME measurements, *J. Geophys. Res.*, 106(D12), 12,643– 12,660, 2001

- Viras L., Siskos P.: *Air pollution by gaseous pollutants in Athens, Greece*, In: *Gaseous pollutants: Characterization and Cycling*, Edited by J.O. Nriagu, J. Wiley, 271-305, 1992
- Viras L.G., Paliatsos A.G., Fotopoulos A.G.: *Nine-year trend of air pollution by CO in Athens, Greece*, *Environmental Monitoring and Assessment*, 40, 203-216, 1996
- Volkamer R., Molina L.T., Molina M.J., Shirley T., Brune W.H.: *DOAS measurement of glyoxal as an indicator for fast VOC chemistry in urban air*. *Geophys. Res. Lett.* 32 (L08806) doi:10.1029/2005GL022616, 2005
- Voutsas D., Anthemidis A., Giakisikli G., Mitani K., Besis A., Tsolakidou A., Samara C.: *Size distribution of total and water-soluble fractions of particle-bound elements – assessment of possible risks via inhalation*, *Environmental Science and Pollution Research*, 22(17), 13412-13426, doi:10.1007/s11356-015-4559-7, 2015
- Vrekoussis M., Wittrock F., Richter A., Burrows J.P.: *Temporal and spatial variability of glyoxal as observed from space*. *Atmos. Chem. Phys.* 9, 4485e4504, 2009
- Vrekoussis M., Wittrock F., Richter A., Burrows J.P.: *GOME-2 observations of oxygenated VOCs: what can we learn from the ratio glyoxal to formaldehyde on a global scale*. *Atmos. Chem. Phys.* 10, 10145e10160, doi:org/10.5194/acp-10-10145-2010, 2010
- Vrekoussis M., Richter A., Hilboll A., Burrows J.P., Gerasopoulos E., Lelieveld J., Barrie L., Zerefos C., Mihalopoulos N. : *Economic crisis detected from space: Air quality observations over Athens/Greece*, *Geophys. Res. Lett.*, 40, doi:10.1002/grl.50118, 2013
- Wang X., Westerdahl D., Chen L.C., Wu Y., Hao J., Pan X., Guo X., Zhang K.M.: *Evaluating the air quality impacts of the 2008 Beijing Olympic Games: On-road emission factor and black carbon profiles*, *Atmospheric Environment*, 43, 4535-4543, doi:10.1016/j.atmosenv.2009.06.054, 2009
- Wagner T., von Friedeburg C., Wenig M., Otten C., Platt U.: *UV/vis observations of atmospheric O₄ absorptions using direct moon light and zenith scattered sunlight under clear and cloudy sky conditions*, *J. Geophys. Res.*, 107, 4424, doi:10.1029/2001JD001026, 2002
- Wagner T., Dix B., Friedeburg C., Frieb U., Sanghavi S., Sinreich R., Platt U. : *MAX-DOAS O₄ measurements: A new technique to derive information on atmospheric aerosols-Principles and information content*, *Journal of Geophysical Research*, Vol. 109, D22205, doi:10.1029/2004JD004904, 2004
- Wagner, T., Beirle, S., Brauers, T., Deutschmann, T., Frieß, U., Hak, C., Halla, J. D., Heue, K. P., Junkermann, W., Li, X., Platt, U., and Pundt-Gruber, I.: *Inversion of tropospheric profiles of aerosol extinction and HCHO and NO₂ mixing ratios from MAX-DOAS observations in Milano during the summer of 2003 and comparison with independent data sets*, *Atmos. Meas. Tech.*, 4, 2685–2715, doi:10.5194/amt-4-2685-2011, 2011
- Wagner, T., Ibrahim, O., Shaiganfar, R., Platt, U.: *Mobile MAX-DOAS observations of tropospheric trace gases*, *Atmos. Meas. Tech.*, 3, 129-140, 2010
- Wagner, T., Apituley, A., Beirle, S., Dörner, S., Friess, U., Remmers, J., Shaiganfar, R.: *Cloud detection and classification based on MAX-DOAS observations*, *Atmos. Meas. Tech.*, 7, 1289-1320, 2014
- Wandinger, U., Ansmann, A.: *Experimental determination of the lidar overlap profile with Raman lidar*, *Applied Optics*, 41 (3), 511-514, doi:10.1364/AO.41.000511, 2002
- Wandinger, U. and Ansmann, A.: *Experimental determination of the lidar overlap profile with Raman lidar*, *Appl. Opt.* 41, 511-514, 2002.
- Wang, S., Cuevas, C.A., Frieb, U., Saiz-Lopez, A.: *MAX-DOAS retrieval of aerosol extinction properties in Madrid, Spain*, *Atmos. Meas. Tech.*, 9, 5089-5101, doi:10.5194/amt-9-5089-2016, 2016

- Weingartner E., Saathoff H., Schnaiter M., Streit N., Bitnar B., Baltensperger U.: Absorption of light by soot particles: Determination of the absorption coefficient by means of aethalometers, *J. Aerosol Sci.*, 34, 1445-1463, doi:10.1016/S0021-8502(03)00359-8, 2003
- Wenig M., Spichtinger N., Stohl A., Held G., Beirle S., Wagner T., Jahne B., Platt U.: Intercontinental transport of nitrogen oxide pollution plumes, *Atmos. Chem. Phys.*, 3, 387–39, 2003
- Westphal D., Toon O.: Simulations of microphysical, radiative and dynamical processes in a continental-scale forest fire smoke plume, *J. Geophys. Res.*, 96(D12), 22379-22400, 1991
- Wittrock F., Oetjen H., Richter A., Fietkau S., Medeke T., Rozanov A., Burrows J.P.: MAX-DOAS measurements of atmospheric trace gases in Ny-Alesund – Radiative transfer studies and their application, *Atmos. Chem. Phys.*, 4, 955-966, 2004
- Wittrock F., Richter A., Oetjen H., Burrows J.P., Kanakidou M., Myriokefalitakis S., Volkamer R., Beirle S., Platt U., Wagner T.: Simultaneous global observations of glyoxal and formaldehyde from space. *Geophys. Res. Lett.* 33, L16804, doi:10.1029/2006gl026310, 2006
- WUP (World Urbanization Prospects): 2014 Revision, Population Division, Department of Economic and Social Affairs, United Nations.
- Yu H., Chin M., Bian H., Yuan T., Prospero J. M., Omar A. H., Remer L. A., Winker D. M., Yang Y., Zhang Y., Zhang Z.: Quantification of trans-atlantic dust transport from seven-year (2007–2013) record of calipso lidar measurements, *Remote Sensing of Environment*, 159, 232-249, doi:10.1016/j.rse.2014.12.010, 2015a
- Zerefos, C.S., Meleti, C., Eleftheratos, K., Kazadzis, S., Romanou, A., Bais, A., Ichoku, C.: Solar brightening over Thessaloniki, Greece, dimming over Beijing, China, *Tellus*, doi:10.1111/j.1600-0889.2009.00425.x, 2009
- Zieger, P., Weingartner, E., Henzing, J., Moerman, M., de Leeuw, G., Mikkilä, J., Ehn, M., Petäjä, T., Clémer, K., van Roozendaal, M., Yilmaz, S., Frieb, U., Irie, H., Wagner, T., Shaiganfar, R., Beirle, S., Apituley, A., Wilson, K., Baltensperger, U.: Comparison of ambient aerosol extinction coefficients obtained from in-situ, MAX-DOAS and LIDAR measurements at Cabauw, *Atmos. Chem. Phys.*, 11, 2603-2624, doi:10.5194/acp-11-2603-2011, 2011
- Ziomas I., Tzoumaka P., Balis D., Melas D., Zerefos C., Klemm O. : Ozone episodes in Athens, Greece. A modelling approach using data from the medcaphot-trace, *Atmosph. Environ.*, 32(12), 2313-2321, 1998
- Zyrichidou I., et al.: Satellite observations and model simulations of tropospheric NO₂ columns over south-eastern Europe, *Atmos. Chem. Phys.*, 9, 6119-6134, doi:10.5194/acp-9-6119-2009, 2009